METABOLIC FLUX ANALYSES IN DIABETIC MOUSE MODELS

By

YUJUE WANG

A dissertation submitted to the

School of Graduate Studies

Rutgers, The State University of New Jersey

In partial fulfillment of the requirements

For the degree of

Doctor of Philosophy

Graduate Program in Microbiology and Molecular Genetics

Written under the direction of

Fredric E. Wondisford

And approved by

_____

_____

_____

_____

New Brunswick, New Jersey

May 2020

ABSTRACT OF THE DISSERTATION

METABOLIC FLUX ANALYSES IN DIABETIC MOUSE MOEDLS

By YUJUE WANG

Dissertation Director:

Fredric E. Wondisford

Diabetes mellitus (DM) is a chronic disease that affects nearly 10% of the population worldwide. The most well-known symptom of DM is hyperglycemia, which causes nearly 2 million direct death each year with a series of complications including stroke, blindness and heart attack. Enhanced glucagon signaling, insulin resistance, and altered substrate availability have been offered as explanations of the elevated gluconeogenesis, but collectively their *in vivo* contributions and interactions in gluconeogenesis remain unclear. Since gluconeogenesis is a relatively complicated pathway that involves multiple substrates, enzymes and hormonal regulations, a comprehensive metabolic flux analysis (MFA) across multiple diabetic mouse models are required. The aim of this dissertation is to develop a tool for the flux analysis of gluconeogenesis and use this tool to analyze multiple diabetic models which mimics the effect of glucagon signaling, insulin resistance and high fat diet (HFD) feeding.

We first described how the gluconeogenic flux model was designed and constructed in detail (Chapter 2). Then we used this flux model to study the relative contribution of glycogen, lactate and glycerol in glucose production of male C57BL/6J-albino mice after 6, 12 and 18 hours of fasting (Chapter 3). We found that during both short and prolonged fasting, lactate served as the largest direct gluconeogenic substrate but a minor source for the net carbon contribution. In contrast, glycerol served as the second largest direct substrate and the dominant net carbon source in both short and prolonged fasting. We next used the flux model to study the effect of hepatic glucagon signaling and HFD feeding on gluconeogenesis (Chapter 4). We used constitutive protein kinase a (PKA) activation to mimic the enhanced hepatic glucagon signaling plus a classic HFD approach to model the diet-induced obesity in mice. We found that HFD feeding alone increased gluconeogenic flux from glycerol but not from lactate. In contrast, PKA activation increased gluconeogenic flux from both glycerol and lactate. Interestingly, when two effects were combined, a more than additive increase of gluconeogenesis flux from both substrates were observed. Further investigation revealed a synergistic effect of glycerol and PKA activation in up-regulating *G6pc* expression. Finally, we used the same strategy to investigate the effect of hepatic insulin resistance on gluconeogenesis under both normal chow and HFD feeding (Chapter 5). We used liver insulin receptor knockout (LIRKO) to model hepatic insulin resistance. We found LIRKO only mildly increase the gluconeogenic flux from both glycerol and lactate in normal chow fed mice. In the context of HFD feeding, LIRKO significantly decreased the flux from glycerol

but increased that from lactate compared to the HFD control mice, suggesting a shift of substrate preference from glycerol to lactate. Further investigation showed that this shift of substrate preference is related to the down-regulation of glycerol kinase (*Gyk*) caused by LIRKO.

In summary, MFA is a useful, powerful and unique tool to investigate the metabolism in complicated pathways like gluconeogenesis. Our result suggests neither enzyme activity nor substrate concentration alone is sufficient to represent the metabolic flux. To accurately quantify the metabolism *in vivo* and distinguish its changes under different conditions, MFA seems to be the only reliable solution so far. Further studies should focus on simplify the procedure of MFA experiments and make it more accessible and suitable for clinical purpose.

ACKNOWLEDGEMENTS

Finally, I would like to thank my family and friends for their love and support.

DEDICATION

This dissertation is dedicated to the following people:

My parents Hui Wang and Lusheng Wang, who taught me the importance of

persistence and provided their full support to my study and career.

My wife and soulmate Yi Zhou, who I always share the good time and bad time with.

And to my lovely daughter Sarah Wang.

TABLE OF CONTENTS

LIST OF TABLES

LIST OF FIGURES

Chapter 1 . Introduction

Diabetes mellitus – general background

Diabetes mellitus (DM), or simply diabetes, is a chronic disease characterized by high blood glucose level (i.e. hyperglycemia) over a prolonged period of time [1]. The word "diabetes" was first used by the ancient Greek physician Aretaeus to describe the excessive discharge of urine in his patients [2]. The following word "mellitus", which means "as sweet as honey" in Latin, was first introduced in late 1600s to describe the sweetness of urine in diabetes patients [3]. It should be noticed that another disease characterized by large amount of urine with non-sweet taste is named diabetes insipidus (DI), which is unrelated to DM [4].

Nowadays, diabetes has become a global challenge. According to the World Health Organization (WHO), the global incidence of diabetes had expanded from 108 million (4.7%) in 1980 to 425 million (8.5%) in 2013 and was expected to increase to 693 million by 2045 [1]. In 2013 alone, diabetes caused about 1.5 million direct death and 2.2 million indirect death from increased risks of other diseases [1]. The global economic cost of diabetes was about $850 billion in 2017 and this cost was estimated to be doubled by 2045 [5].

Diabetes occurs when the body fails to make sufficient amount of insulin, a hormone that decreases the blood glucose, or the body fails to properly respond to insulin. There

are three major types of diabetes – type 1 (T1DM), type 2 (T2DM) and gestational (GDM). T1DM (previously called insulin-dependent, juvenile or childhood-onset diabetes) is characterized as deficiency in the production of insulin; T2DM (previously called non-insulin-dependent or adult-onset diabetes) is characterized as resistance to insulin; GDM is characterized as temporary rise of blood glucose during pregnancy [1]. T2DM is the most common type of diabetes that account for 90% to 95% of the total DM cases [6].

Symptoms of diabetes include weight loss, fatigue, vision change and increase of urination, thirst and hunger. The onset of symptoms may vary with the majority of T1DM diagnosed in children and most T2DM diagnosed in adult [1]. When blood glucose is not well managed in diabetes patients, complications could develop that threaten both health and life. Acute complications including diabetic ketoacidosis, hyperosmolar coma and hypoglycemia are life threatening; chronic complications including heart disease, kidney failure, nerve damage and blindness significantly reduce the quality of life [1, 7]. In addition to the traditional complications, diabetes can also increase the risk of cognitive impairment and certain types of cancer [8, 9].

The excessive hepatic gluconeogenesis has been suggested as a major driver of hyperglycemia in both T1DM and T2DM, though the exact cause of the enhanced hepatic gluconeogenesis remains controversial [10, 11]. Three remarkable features in

diabetes have been proposed as the underlying mechanisms of enhanced hepatic gluconeogenesis: (1) increased hepatic glucagon signaling due to hyperglucagonemia [12]. (2) reduced hepatic insulin signaling due to reduced insulin secretion (T1DM) or hepatic insulin resistance (T2DM) [11, 13]. (3) increased availability of gluconeogenic substrates (e.g. glycerol) due to the chronic effect of high fat diet (HFD) [10, 14]. Although the effect of glucagon on increased gluconeogenesis is well known, the roles of the other two mechanisms are still unclear. Moreover, since multiple mechanisms appears in both types of diabetes, the interactions among these mechanisms have never been well characterized.

One major challenge to investigate these mechanisms in vivo has been the failure to study each effect separately in a tissue specific manner. For example, the reduced insulin signaling is almost always accompanied with hyperglucagonemia in diabetic mouse models. This is because the reduced insulin signaling in islet alpha cell may cause increased glucagon secretion. Moreover, the chronic effect of HFD itself includes global insulin resistance and hyperglucagonemia, both of which may increase gluconeogenesis. Such simultaneous changes in multiple pathways and multiple organs make it extremely difficult to determine the precise role of each mechanism in regulating hepatic gluconeogenesis. To overcome this problem, multiple mouse models have been developed to model the effects of glucagon, insulin and HFD. For example, the liver specific knock-down of *Prkar1α* gene have been shown to cause constitutive

activation of protein kinase a (PKA), which mimics the enhanced hepatic glucagon signaling [15]. On the other hand, the liver specific knock-down of insulin receptor have been shown to cause a complete loss of hepatic insulin signaling, which mimics the hepatic insulin resistance [16]. Finally, special diet can be applied to either wild type alone or in combination with the other two mouse models mentioned above to model the chronic effect of HFD (Fig. 1. 1).

The second major challenge in diabetic research is to properly estimate the gluconeogenic fluxes (reaction rates) from different substrates. Metabolic reactions are regulated by both the activity of enzymes and the availability of
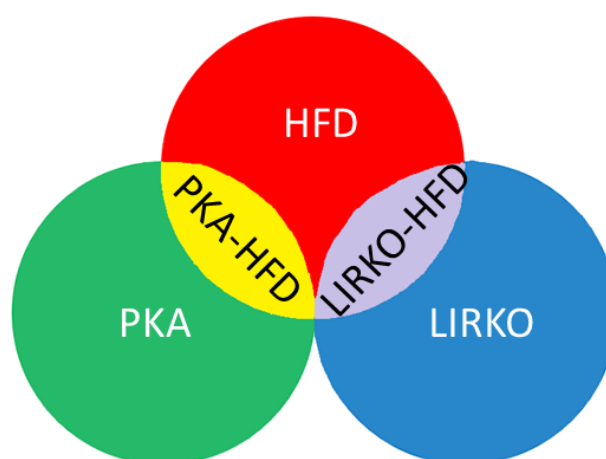
Figure 1.1 | Relationship of mouse models.

substrates (Michaelis-Menten equation, Eq. 1. 1) [17]. Omitting either of these two components could lead to a potentially biased and incomplete conclusion. For example, the most commonly used methods to estimate gluconeogenesis is through a series of tolerance tests (e.g. pyruvate tolerance test). Under these experimental settings, subjects are given a bolus injection of gluconeogenic substrates (e.g. pyruvate) and the change of blood glucose level after the injection is claimed to reflect the rate of gluconeogenesis [18]. However, what these tests truly measured is the capacity (Vmax)

of gluconeogenesis (i.e. when [S] >> K_M, V ≈ Vmax) instead of the actual flux at fasting state where the availability of substrates is usually limited. To measure the real gluconeogenic fluxes, here we introduce the method of metabolic flux analysis (MFA).

$$V = V_{max} \, [S] \, / \, (K_M + [S]) \qquad\qquad \text{[Eq. 1. 1]}$$

Metabolic Flux Analyses

Metabolism is the sum of chemical reactions in living cells and organisms, which includes the breakdown and synthesis of molecules, the generation of energy and the transduction of cell signaling. In the past few decades, the metabolic research have been rapidly expanded due to the improvement of technologies in measuring metabolites including nuclear magnetic resonance (NMR) and mass spectrometry (MS) [19]. However, the measurement of metabolite concentration (pool size) alone do not describe the activity of metabolite (flux) since metabolism is a dynamic process. For example, when glucose homeostasis is well maintained (i.e. glucose production equals consumption), the measurement of glucose concentration (pool size) tells little information about the rate of glucose being produced and consumed (flux) in the body. An analogy of the relationship between pool size and flux is the traffic. The pool size represents the density of cars on the road while the flux represents the speed of cars. Although the density of cars can be measured by taking a static picture of the road (Fig. 1. 2a), such measurement alone is insufficient to tell the speed of car, since the speed can be affected by other factors such as speed limit and the quality of road (Fig. 1. 2b).
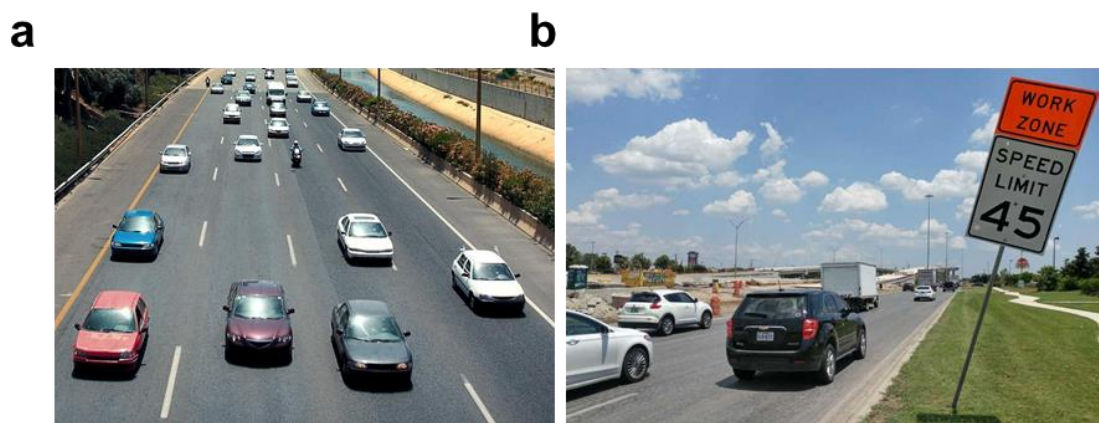
Figure 1. 2 | Difference between pool size and flux.

Unlike the concentrations of metabolites which can be directly measured by NMR and MS, the measurement of flux is not straightforward. The technique used to solve fluxes of metabolites in a biological system is referred as flux analysis [20]. There are three classes of flux analyses: flux balance analysis (FBA), stoichiometric metabolic flux analysis (stoichiometric MFA) and isotope-based flux analysis (isotope-MFA) [21]. FBA estimates fluxes by maximizing an assumed cellular objective function (e.g. cell growth) using a relatively large-scale flux model [22]. Stoichiometric MFA uses a simplified flux model and the measurement of extracellular flux rates (e.g. carbon input and output in the culture media) to calculate intracellular fluxes, which cannot be measured directly [23]. However, both FBA and stoichiometric MFA have some apparent limitations: (1) Techniques are limited to cell culture system and can hardly be applied *in vivo*. (2) The fluxes are often underdetermined (i.e. the number of measurements is less than fluxes) and therefore requires oversimplification of flux model and additional assumptions. In contrast, isotope-MFA is a more advanced

method that uses the isotope tracers, metabolite and isotopomer balancing to resolve the two limitations mentioned above [21].

An example of MFA is illustrated by the fructose bisphosphate (FBP) aldolase and triose phosphate isomerase (TPI) pathways (Fig. 1. 3a). In this metabolic network, f_{in} is the input flux; f_{out} is the output flux of GAP; f_1' and f_1 are the forward and reverse reaction of FBP aldolase; f_2' and f_2 are the forward and reverse reaction of TPI. The metabolite mass balance leads to the following equations:

$$
\begin{array}{lll}
\text{FBP:} & f_{in} + f_1 = f_1' & \\
\text{DHAP:} & f_1' + f_2 = f_1 + f_2' & \text{[Eq.1.2]} \\
\text{GAP:} & f_1' + f_2' = f_1 + f_2 + f_{out} &
\end{array}
$$

Since the network contains more fluxes (6) than non-equivalent equations (3), this network is underdetermined and need at least three additional equations (6-3=3) to solve all the fluxes. In another word, we can use at least three fluxes (i.e. free fluxes) to describe all the other fluxes (i.e. dependent fluxes). Here, we choose f_{in}, f_1 and f_2 as three free fluxes and assign f_{in} an arbitrary value: $f_{in} = 100$. Therefore, all the dependent fluxes can be expressed as a linear equation of free fluxes:

$$
\begin{array}{ll}
f_1' = f_{in} + f_1 = 100 + f_1 & \\
f_2' = f_{in} + f_2 = 100 + f_2 & \text{[Eq.1.3]} \\
f_{out} = 2*f_{in} = 200 &
\end{array}
$$

Hence, all the fluxes in the network can be described by f_1 and f_2 and the labeling pattern of all the intermediates can be described by a function of f_1 and f_2 given the labeling pattern of input (glucose). For example, when $1, 2 - {}^{13}C_2$ glucose was used as the input

substrate (Fig. 1. 3a), the labeling patterns of FBP can be predicted given any set of f_1 and f_2 (Fig. 1. 3b-d). By fitting the predicted labeling patterns with the observation (hypothetical value, Fig. 1. 3e), a best-fit value of f_1 and f_2 can be found (black dot, Fig. 1. 3f) with an area of associated confidence interval (colored, Fig. 1. 3f). The fitting progress can be achieved by graduate minimizing the square sum of residue (SSR) between the observation and simulation (Fig. 1. 4 a-e). Once the best-fit value of f_1 and f_2 is known, all the fluxes in the network can be solved (Fig. 1. 4 f).

Rationale for dissertation experiments

This dissertation aims to use MFA method to study the gluconeogenic fluxes in control and diabetic mouse models. Chapter 2 demonstrates the detailed processes of constructing the MFA model and how we tested this model using mouse primary hepatocytes. The primary hepatocytes were given gluconeogenic substrates (glycerol, lactate, and glutamine) at physiological concentrations to study the relative contribution from different substrates. We labeled each substrate with ^{13}C one at a time and examined the labeling patterns of glucose and important intermediates of the gluconeogenic pathway. The data from ^{13}C glycerol and lactate experiments were used for flux analysis and the data from ^{13}C glutamine experiment was used to verify the flux result.
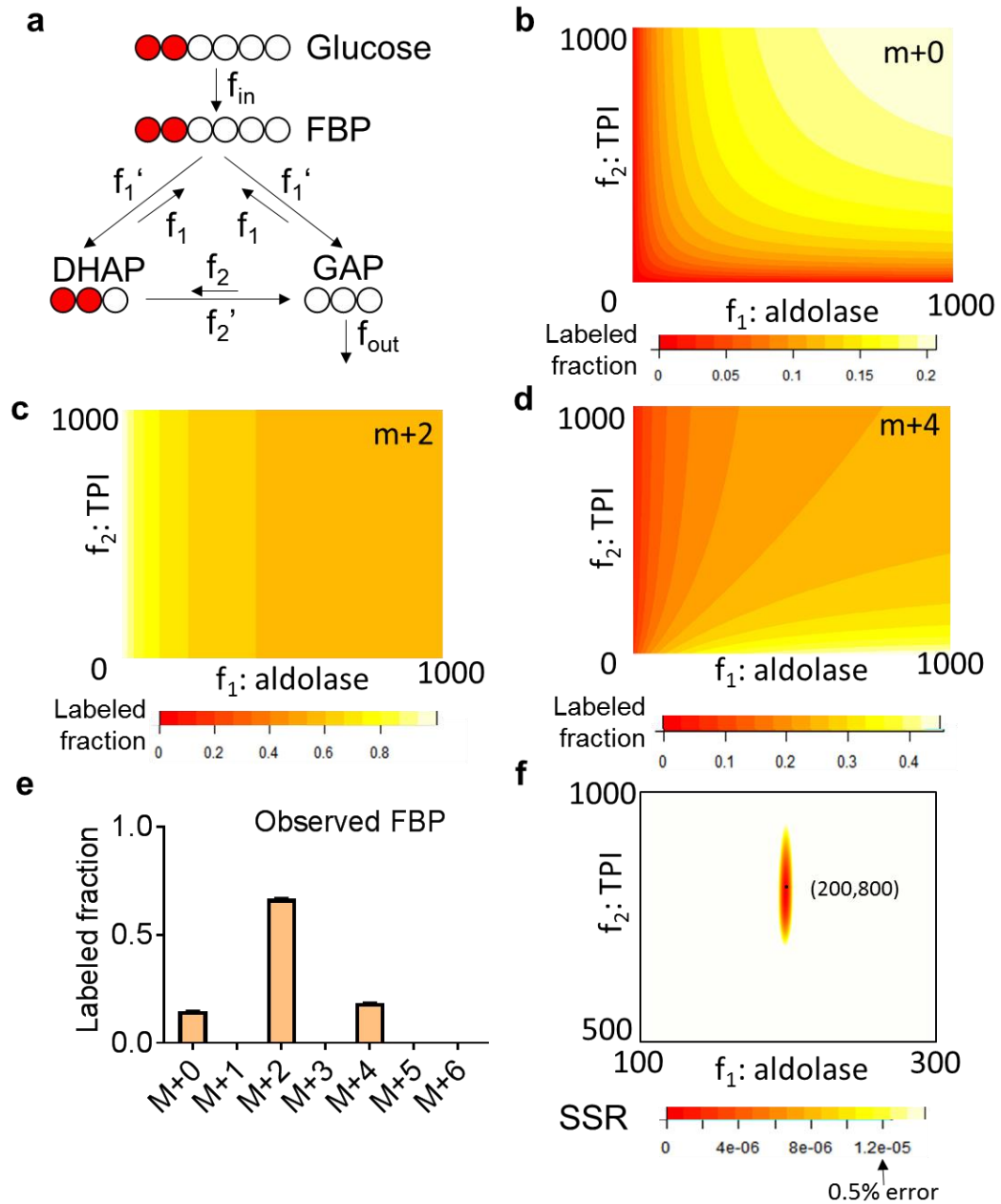
Figure 1. 3 | Example of metabolic flux analysis. a, flux network. **b-d,** predicted labeled fractions of m+0, m+2 and m+4 FBP. **e,** example of observed labeling pattern of FBP. **f,** best-fit value (black dot) with associated confidence interval (colored). FBP, fructose bisphosphate; DHAP, dihydroxyacetone phosphate; GAP, glyceraldehyde-3-phosphate; TPI, triose phosphate isomerase; SSR, sum of squared residue.

a

Iteration	f_1	f_2	SSR
1	995.0	5403.9	2.2E-02
5	232.70	2330.4	6.59E-04
10	214.91	524.30	2.49E-04
50	200.0	800.0	3.2E-13
Optimum	200.0	800.0	2.8E-22

b

c

d

e

f
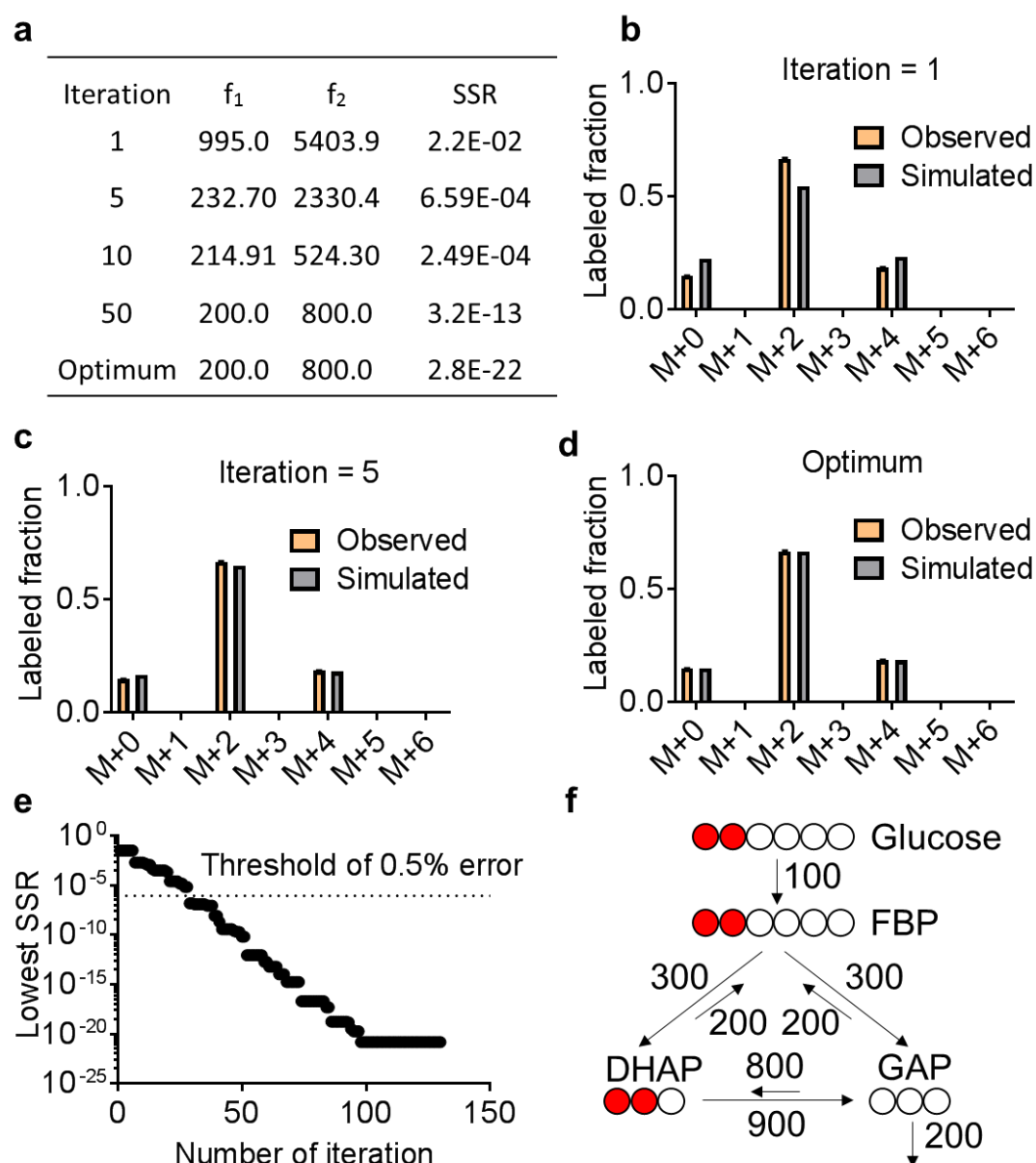
Figure 1. 4 | Fitting progress of metabolic flux analysis. a, fitting result with different iteration. **b-d,** observed and simulated labeling pattern of FBP. **e,** decrease of SSR with increased number of iteration. **f,** result of metabolic flux analysis. FBP, fructose bisphosphate; DHAP, dihydroxyacetone phosphate; GAP, glyceraldehyde-3-phosphate; SSR, sum of squared residue.

Chapter 3 start to demonstrate the application of MFA model *in vivo*. We used the flux

model to study the effect of fasting on substrate contribution in gluconeogenesis. In

this study, we fasted male C57BL/6J-albino mice for 6, 12 and 18 hours and used

non-perturbative infusions of $^{13}C_3$ lactate, $^{13}C_3$ glycerol and $^{13}C_6$ glucose to study the

relative contribution of gluconeogenic substrates under different length of fasting.

The study in Chapter 4 used the MFA model to analyze the interaction between

hepatic glucagon signaling (modeled by constitutive PKA activation) and the chronic

effect of high fat diet (HFD) feeding. We used the same non-perturbative infusion

method as described in Chapter 3 to analyze the individual and combined effect of

glucagon signaling and HFD on gluconeogenic fluxes from different substrates.

Beyond the traditional ^{13}C labeling strategy, we also used a ^{13}C-^2H double labeled

glycerol tracer in this study to investigate a proposed direct conversion from glycerol

to lactate without passing glucose.

The study in Chapter 5 investigates the interaction between the loss of hepatic insulin

signaling (modeled by insulin receptor knock-out) and the chronic effect of high fat

diet (HFD) feeding. We used similar method described above to analyze the

individual and combined effect of deficit hepatic insulin signaling and HFD on

gluconeogenic fluxes from different substrates.

Chapter 2 . Construction of Flux Model for Gluconeogenesis

Construction of the flux network

The first step to construct the flux network for gluconeogenesis (GNG) is to determine

the input, output and key-node metabolites of the network (Table 2. 1). The input

metabolites for glucose production include glycogen, glycerol, lactate, pyruvate, free

fatty acids and amino acids [24]. Since lactate must convert to pyruvate first before

entering the GNG pathway, the flux from pyruvate and lactate can be combined as one.

Similarly, some amino acids must enter GNG pathway through lactate (Fig. 2. 1) and

therefore, their input flux can be combined in the lactate/pyruvate flux. The output

metabolite of the pathway is glucose and carbon dioxide (via TCA cycle).

Table 2.1 | Metabolites in flux network.

Input	Output	Key-node metabolites
Glycogen	Glucose	Glucose-6-phosphate (G6P)
Glycerol	CO_2	Dihydroxyacetone phosphate (DHAP)
Lactate/Pyruvate		Phosphoenolpyruvate (PEP)
Free fatty acids		Pyruvate (in mitochondria)
Amino acids (TCA)		Oxaloacetate (Oxa)
		Acetyl-CoA (Ac-CoA)
		Succinate (Suc)
		Citrate (Cit)
		a-ketoglutarate (aKG)
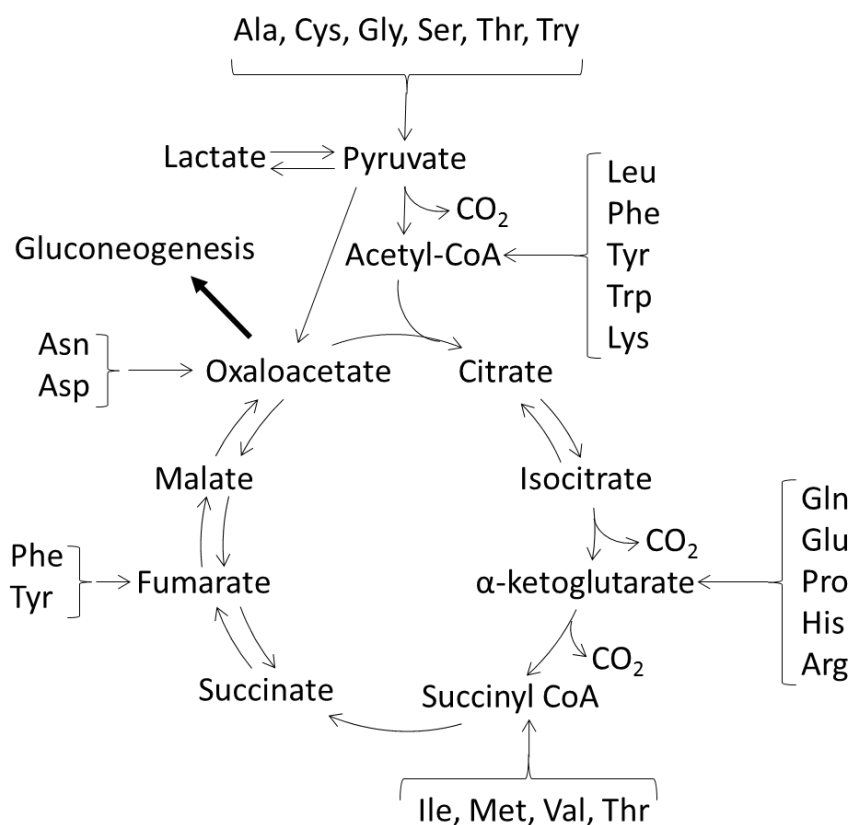
Figure 2.1 | Entrance of gluconeogenic substrates.

The key-node metabolites are metabolites that connect the input and output metabolites in the network (Table 2. 1). For example, glucose-6-phosphate (G6P) and dihydroxyacetone phosphate (DHAP) are entrance metabolites of glycogen and glycerol in the GNG network respectively. Except glycogen and glycerol, all the other input metabolites enter GNG via the tricarboxylic acid (TCA) cycle. There are five entrance metabolites (Fig. 2. 1) in the TCA cycle: 1. Oxaloacetate (e.g. pyruvate and lactate); 2. Fumarate (Phe and Tyr); 3. Succinyl CoA (e.g. Ile and Met); 4. α-ketoglutarate (e.g. Glu and Gln); 5. Citrate (acetyl CoA). Since there is no atom transition between fumarate and succinyl CoA, these two entrances can be further

combined into one (represented as succinate). Besides these entrance metabolites, metabolites that participate in atom transitions are also key-node metabolites. For example, phosphoenolpyruvate (PEP) participated in the atom transition from oxaloacetate (4 carbons) to DHAP (3 carbons) in which process one carbon atom is lost as CO_2.

After determined all the input, output and key-node metabolites in the network (Table 2. 1), the next step is to connect all the metabolites with fluxes (Fig. 2. 2). Most reactions
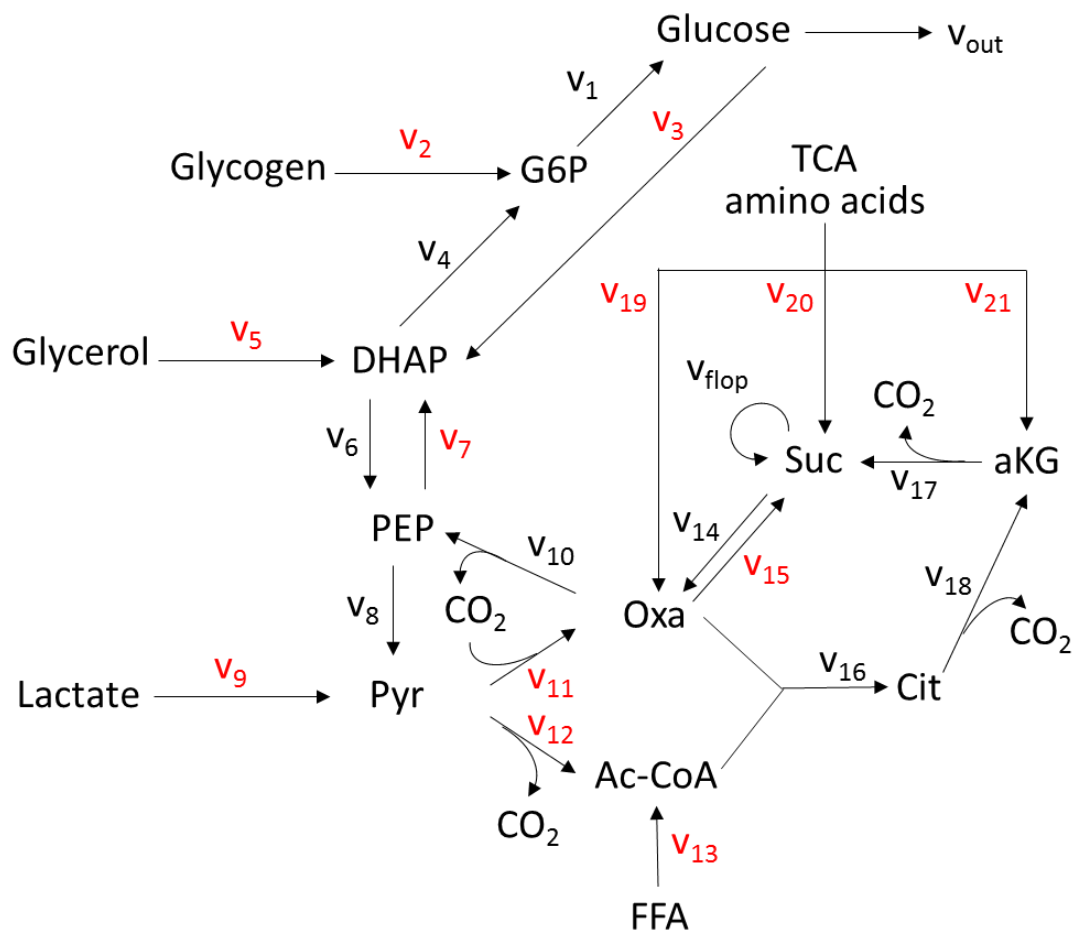
Figure 2. 2 | Flux network of gluconeogenesis. Free fluxes and dependent fluxes are shown in red and black respectively. G6P, glucose-6-phosphate; TCA, tricarboxylic acid; AA, amino acids; PEP, phosphoenolpyruvate; DHAP, dihydroxyacetone phosphate; Pyr, pyruvate; Ac-CoA, acetyl CoA; Oxa, oxaloacetate; Suc, succinate; Cit, citrate; aKG, α-ketoglutarate; FFA, free fatty acids.

in the network are unidirectional with two exceptions: the enolase flux (between DHAP

and PEP) and the succinate dehydrogenase flux (between succinate and oxaloacetate)

which are bidirectional and represented as two separate fluxes (Fig. 2. 2). Some

metabolites in the network are achiral (e.g. succinate), therefore, an infinitely large flop

flux is added to those metabolites to reflect their achiral property.

<u>Determination of stoichiometric functions and free fluxes</u>

After the flux network is constructed, the next step is to determine the stoichiometric

functions. The stoichiometric functions are based on the fact the pool size of all the

metabolites do not change at steady state. In another word, the sum of influx equals the

sum of outflux for all metabolites. Therefore, the following stoichiometric equations

can be obtained (Eq. 2. 1):

Glucose:	$V_1 - 0.5*V_3 = V_{out}$	
G6P:	$V_1 - V_4 = V_2$	
DHAP:	$2*V_4 + V_6 - V_3 - V_7 = V_5$	
PEP:	$V_7 + V_8 - V_6 - V_{10} = 0$	
Pyr:	$V_{11} + V_{12} - V_8 = V_9$	
Oxa:	$V_{16} + V_{10} + V_{15} - V_{11} - V_{14} = V_{19}$	[Eq.2. 1]
Ac-CoA:	$V_{16} - V_{12} = V_{13}$	
Suc:	$V_{14} - V_{15} - V_{17} = V_{20}$	
Cit:	$V_{16} - V_{18} = 0$	
aKG:	$V_{17} - V_{18} = V_{21}$	

Since the network contains more fluxes (22) than non-equivalent equations (10), this

network is underdetermined and need at least 12 additional equations (22-10=12) to

solve all the fluxes. In another word, we can use at least 12 fluxes (i.e. free fluxes) to

describe all the other fluxes (i.e. dependent fluxes). The assignment of free fluxes is

arbitrary though several rules need to be followed to obtain an ideal result:

1. Prioritize the input fluxes and fluxes with the most significance of study.

2. When both forward and reverse flux exist, choose the relatively smaller flux as

   a free flux.

3. When one flux equals the sum of several smaller fluxes, prioritize those smaller

   fluxes.

Following these rules, V_2, V_3, V_5, V_7, V_9, V_{11}, V_{12}, V_{13}, V_{15}, V_{19}, V_{20} and V_{21} are

assigned as free fluxes and can describe all the other fluxes in the network (Eq. 2. 2):

$$V_1 = 0.5*(V_3 + V_5 + V_9 + V_{19} + V_{20} + V_{21} - V_{12}) + V_2$$
$$V_4 = 0.5*(V_3 + V_5 + V_9 + V_{19} + V_{20} + V_{21} - V_{12})$$
$$V_6 = V_7 + V_{12} - V_9 - (V_{19} + V_{20} + V_{21})$$
$$V_8 = V_{11} + V_{12} - V_9$$
$$V_{10} = V_{19} + V_{20} + V_{21} + V_{11} \qquad \text{[Eq.2. 2]}$$
$$V_{14} = V_{15} + V_{12} + V_{13} + V_{19} + V_{20} + V_{21}$$
$$V_{16} = V_{12} + V_{13}$$
$$V_{17} = V_{12} + V_{13} + 0.45*V_{19}$$
$$V_{18} = V_{12} + V_{13}$$
$$V_{out} = 0.5*(V_5 + V_9 + V_{19} + V_{20} + V_{21} - V_{12}) + V_2$$

Determination of EMU and atom transition matrices

After all the free fluxes are determined, the next step is to model the atom transition

between metabolites. There are many different ways to model the atom transition in the

network. For example, one could track how individual carbon atom is transferred

between different molecules. However, because there are 62 distinct atoms (from 16

metabolites) in total and the relationship between any two atoms need to be described, totally 3844 parameters (62 atoms * 62 atoms) is required to describe all the atom transitions. An alternative approach is to use elementary metabolite units (EMU) to model the atom transition.

In the example of glycolysis (Fig. 1. 3), instead of describing atoms individually, we grouped all the atoms into six small subsets (Glucose [1-3], Glucose [4-6], FBP [1-3], FBP [4-6], DHAP, GAP). This is because atoms within the same subset always stay together during atom transition and therefore can be described together. Thus, we only need 36 parameters (6 subsets * 6 subsets) instead of 324 (18 atoms * 18 atoms) to describe all the atom transition information.

Similarly, we can identify the EMU in gluconeogenesis network using a designed algorithm (Fig. 2. 3). The "fitting EMU" are the metabolites whose labeling patterns will be used to fit the observation. For example, in this network, we will use the labeling pattern of glucose, citrate and pyruvate to fit the observation. Therefore, Glucose [1-6], Citrate [1-6] and Pyruvate [1-3] are the fitting EMU in this process. The aim of this algorithm is to find all the EMU that are responsible for the production of the fitting EMU. We totally identified 96 EMU that are responsible for making glucose, citrate and pyruvate (Table 2. 2)
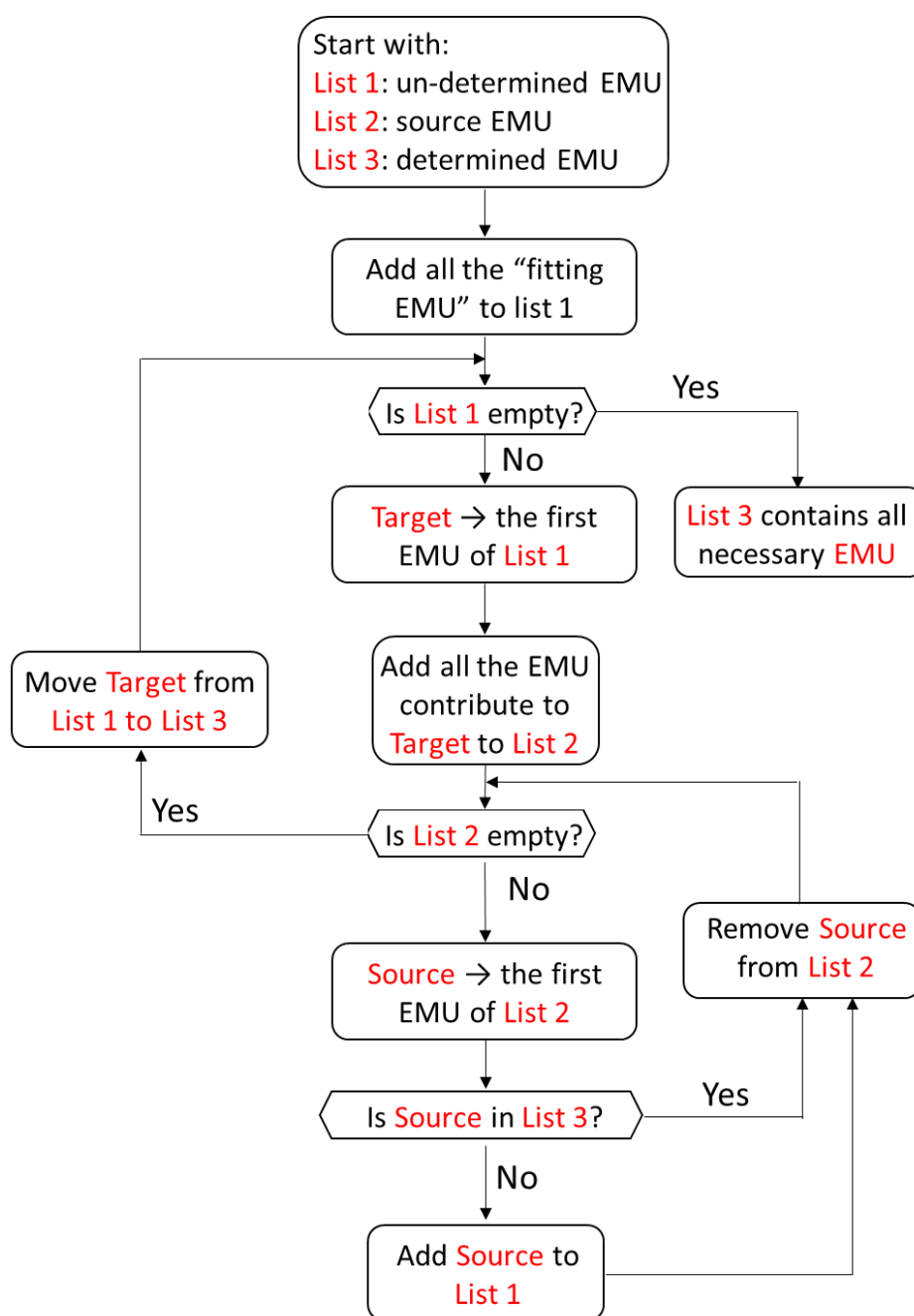
Figure 2.3 | Algorithm to determine all the necessary elementary metabolite unit (EMU) responsible for atom transition.

Table 2.2 | List of elementary metabolite unit (EMU) responsible for making glucose, citrate and pyruvate.

Size	EMU	Size	EMU	Size	EMU	Size	EMU
1	AcCoA[1]	1	Glycerol[3]	2	PEP[2-3]	3	Oxa[4-2]
1	aKG[2]	1	Glycogen[1]	2	PEP[3-2]	3	PEP[1-3]
1	aKG[3]	1	Lactate[2]	2	Pyr[2-3]	3	Suc[1-3]
1	Cit[2]	1	Lactate[3]	2	Pyr[3-2]	3	Suc[4-2]
1	Cit[3]	1	Protein[1]	2	Suc[2-3]	3	Pyr[1-3]
1	DHAP[2]	1	FFA[1]	2	Suc[3-2]	3	Glycerol[1-3]
1	DHAP[3]	1	Glutamine[1]	2	Glycerol[2-3]	3	Glycogen[1-3]
1	G6P[2]	2	AcCoA[1-2]	2	Glycerol[3-2]	3	Lactate[1-3]
1	G6P[3]	2	aKG[2-3]	2	Glycogen[1-2]	3	Protein[1-3]
1	G6P[4]	2	aKG[3-2]	2	Lactate[2-3]	3	Glutamine[1-3]
1	G6P[5]	2	Cit[2-3]	2	Lactate[3-2]	4	Suc[1-4]
1	Glucose[2]	2	Cit[3-2]	2	FFA[1-2]	4	aKG[1-4]
1	Glucose[3]	2	DHAP[2-3]	2	Protein[1-2]	4	Cit[1-4]
1	Glucose[4]	2	DHAP[3-2]	2	Glutamine[1-2]	4	Oxa[1-4]
1	Glucose[5]	2	G6P[2-3]	3	aKG[1-3]	4	Protein[1-4]
1	Oxa[2]	2	G6P[3-2]	3	aKG[4-2]	4	Glutamine[1-4]
1	Oxa[3]	2	G6P[4-5]	3	Cit[1-3]	5	aKG[1-5]
1	PEP[2]	2	G6P[5-4]	3	Cit[4-2]	5	Cit[1-5]
1	PEP[3]	2	Glucose[2-3]	3	DHAP[1-3]	5	Protein[1-5]
1	Pyr[2]	2	Glucose[3-2]	3	G6P[1-3]	5	Glutamine[1-5]
1	Pyr[3]	2	Glucose[4-5]	3	G6P[6-4]	6	Glucose [1-6]
1	Suc[2]	2	Glucose[5-4]	3	Glucose[1-3]	6	G6P[1-6]
1	Suc[3]	2	Oxa[2-3]	3	Glucose[6-4]	6	Cit[1-6]
1	Glycerol[2]	2	Oxa[3-2]	3	Oxa[1-3]	6	Glycogen[1-6]

After determined all the EMU responsible for making glucose and pyruvate, the next step is to use them to construct the atom transition matrices. An example of the matrix has been shown in Fig. 2. 4. These matrices describe how unknown EMU is solved by known EMU. In this example, the unknown EMU with the size of 6 carbons are Glucose [1-6], G6P [1-6] and Cit [1-6]. The EMU with known labeling patterns are DHAP [1-3], Glycogen [1-6], Oxa [1-4] and AcCoA [1-2]. By re-writing equations of Fig. 2. 4a

in the form of matrices, we grouped all the unknown EMU on the left and all the known

EMU on the right of the equation (Fig. 2. 4b). Meanwhile, we obtained two atom

transition matrices (left and right) whose values are solely determined by fluxes. Thus,

the unknown EMU can be solved by multiplying both sides by the inverse of the left

matrix (Fig. 2. 4c). Using an R code (Supplementary Fig. A2. 1), we are able to generate

the transition matrices for all sizes of unknown EMU.

a

$$\text{G6P [1-6]} * V_1 = \text{Glucose [1-6]} * V_1 \tag{1}$$

$$\text{G6P [1-6]} * (V_2 + V_4) = (\text{DHAP [1-3]} \times \text{DHAP [1-3]}) * V_4 + \text{Glycogen [1-6]} * V_2 \tag{2}$$

$$\text{Cit [1-6]} * V_{16} = (\text{Oxa [1-4]} \times \text{AcCoA [1-2]}) * V_{16} \tag{3}$$

b

$$\begin{pmatrix} -V_1 & V_1 & 0 \\ 0 & V_2+V_4 & 0 \\ 0 & 0 & V_{16} \end{pmatrix} * \begin{pmatrix} \text{Glucose [1-6]} \\ \text{G6P [1-6]} \\ \text{Cit [1-6]} \end{pmatrix} = \begin{pmatrix} 0 & 0 & 0 \\ V_4 & V_2 & 0 \\ 0 & 0 & V_{16} \end{pmatrix} * \begin{pmatrix} \text{DHAP [1-3]} \times \text{DHAP [1-3]} \\ \text{Glycogen [1-6]} \\ \text{Oxa [1-4]} \times \text{AcCoA [1-2]} \end{pmatrix}$$

Left matrix   Unknown EMU   right matrix   Known EMU

c

$$\begin{pmatrix} \text{Glucose [1-6]} \\ \text{G6P [1-6]} \\ \text{Cit [1-6]} \end{pmatrix} = \begin{pmatrix} 0 & 0 & 0 \\ V_4 & V_2 & 0 \\ 0 & 0 & V_{16} \end{pmatrix} * \begin{pmatrix} \text{DHAP [1-3]} \times \text{DHAP [1-3]} \\ \text{Glycogen [1-6]} \\ \text{Oxa [1-4]} \times \text{AcCoA [1-2]} \end{pmatrix} * \begin{pmatrix} -V_1 & V_1 & 0 \\ 0 & V_2+V_4 & 0 \\ 0 & 0 & V_{16} \end{pmatrix}^{-1}$$

Unknown EMU   right matrix   Known EMU   Inverse of Left matrix

Figure 2. 4 | Example of atom transition matrix. The isotopic balance equation (a) can be re-written in the form of EMU matrices where all the unknown and known EMU are grouped together (b). The unknown EMU can be solved by multiplying both sides of equation by the inverse of the left matrix (c).

Calculation of free fluxes and confidence intervals

After all the atom transition matrices are determined, the next step is to enumerate

different combinations of free fluxes and simulate the labeling patterns of glucose and

pyruvate. An R code was written for this purpose (Supplementary Fig. A2. 2). The

simulated labeling patterns are then compared to the observed ones with equal weight.

The combination whose labeling patterns are most similar to the observed ones are the

best-fit fluxes. The best-fit fluxes can be obtained by graduate minimizing the sum of

squared residues (SSR) between the simulated and observed labeling patterns. An

example of the fitting process have been shown in Fig. 2. 5.

Once the best-fit fluxes are found, the next step is to determine the confidence interval

associated with the best-fit fluxes. The confidence interval describes how reliable the

estimation is for each individual flux. If a flux can be well determined in the system, a

small change of this flux would have a large effect on the SSR and therefore its

confidence interval would be narrow. In contrast, if a flux cannot be determined well,

its confidence interval would be wide and the change of this flux would have a small

effect on the SSR. The confidence interval is calculated by (1) move one target flux

away from the best-fit value by a small step; (2) choose a combination of other fluxes

that minimize the increase of SSR; (3) calculate the new SSR and repeat step (1) to (3)

until the new SSR reached the cutoff for confidence interval, which is determined by

the X^2 (df = 1) value. For example, cutoff for the 95% confidence interval is $X^2_{0.95}$ (df

= 1) = 3.841459, which is equivalent to an increase of SSR value for 0.000384.

The confidence interval is strongly affected by the tracers and measurable metabolites in the experiment. Generally, the more tracers and measurable metabolites, the narrower the confidence interval would be. An example has been shown in Fig. 2. 6.

a

Iterations	flux1	flux2	flux3	flux4	flux5	flux6	flux7	flux8	flux9
1	1	1	1	1	1	1	1	1	1
10	12	49	26	146	65	35	41	273	19
100	7	37	26	135	52	64	26	340	20
1000	14	37	23	18	63	63	45	82	19

b

c
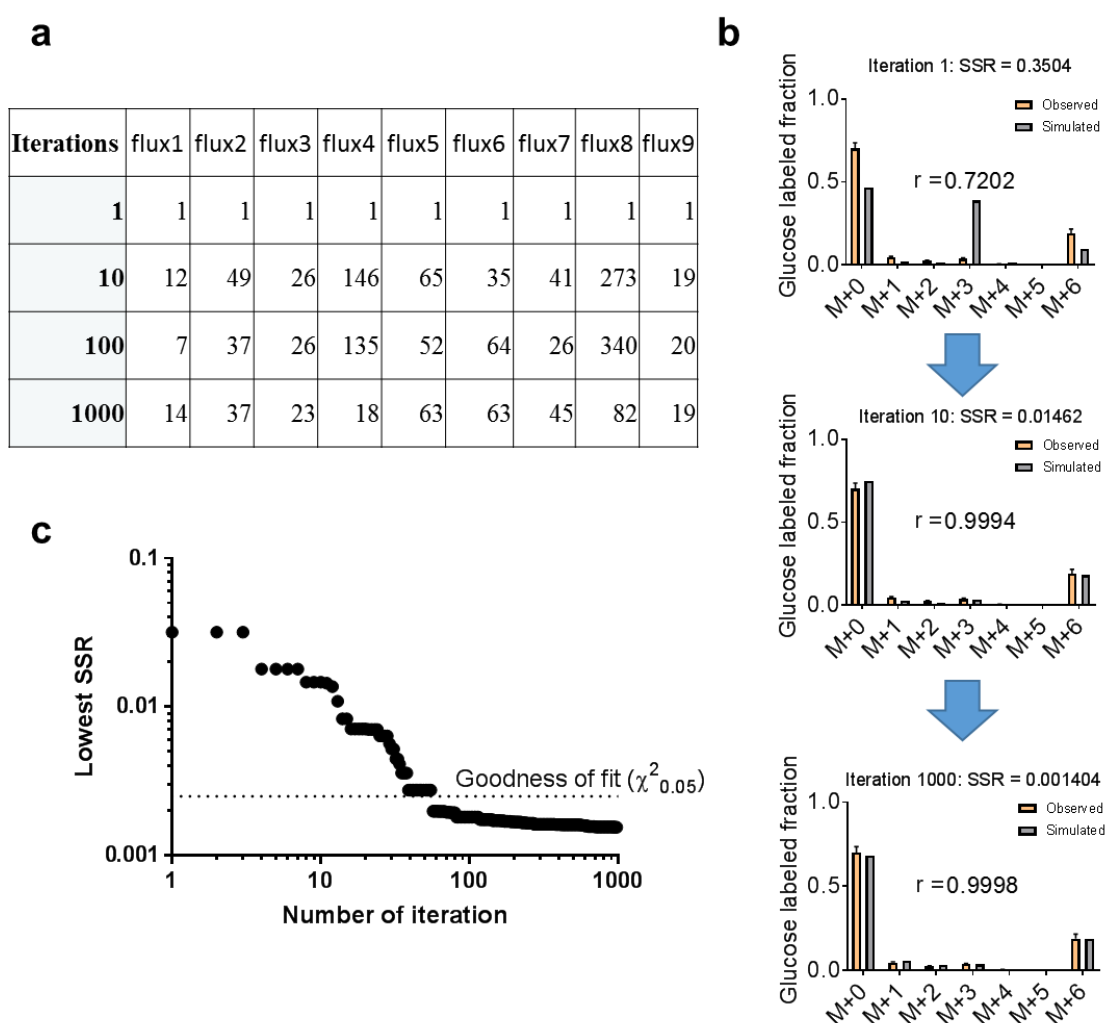
Figure 2. 5 | Example of how to find the best-fit fluxes. In each iteration, a combination of flux values are enumerated (a) and the labeling pattern of metabolite associated with this combination is simulated and compared to the observed one (b). After a large number of iterations, the best-fit combination whose labeling pattern is the most similar to the observed ones can be obtained (c).
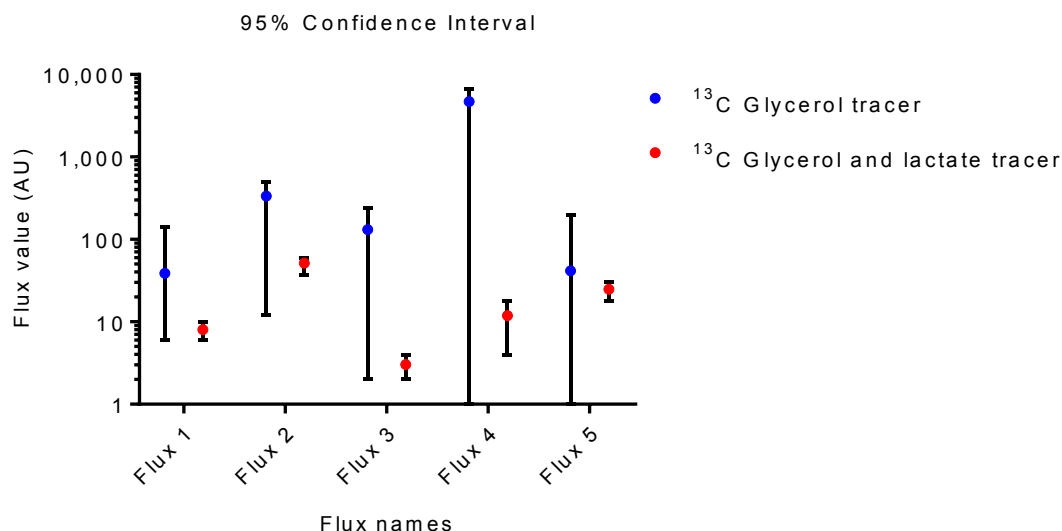
Figure 2.6 | Example of how confidence interval is improved by the number of tracers used in the experiment.

Validation of flux model

After constructed the flux model, we used primary hepatocytes to verify the model. The primary hepatocytes are isolated from mouse and recovered in the Petri dish for 24 hours and starved with serum free media for 3 hours before experiments. Cells were treated with three different media with each medium contains 2.5 mM lactate with 0.25 mM pyruvate, 0.45 mM glycerol and 0.40 mM glutamine but only one substrate was labeled at a time (Fig. 2. 7). The labeling patterns of glucose, glucose-6-phosphate (G6P), phosphoenolpyruvate (PEP), succinate and pyruvate were used as the "fitting metabolites". Labeling patterns generated from $^{13}C_3$ pyruvate/lactate and glycerol (Fig. 2. 7b-c) was used to obtain the best-fit fluxes. The best-fit fluxes was then used to predict the labeling patterns in the third data set where ^{13}C glutamine is used as tracer (Fig. 2. 7d). We found the model accurately estimated all the fluxes as the predicted

labeling patterns match the observed ones well (Fig. 2. 7d). In consistent with these

findings, the 95% confidence interval of glutamine flux (TCA AA; Fig. 2. 8) is narrow,

indicating the accuracy of the estimation.
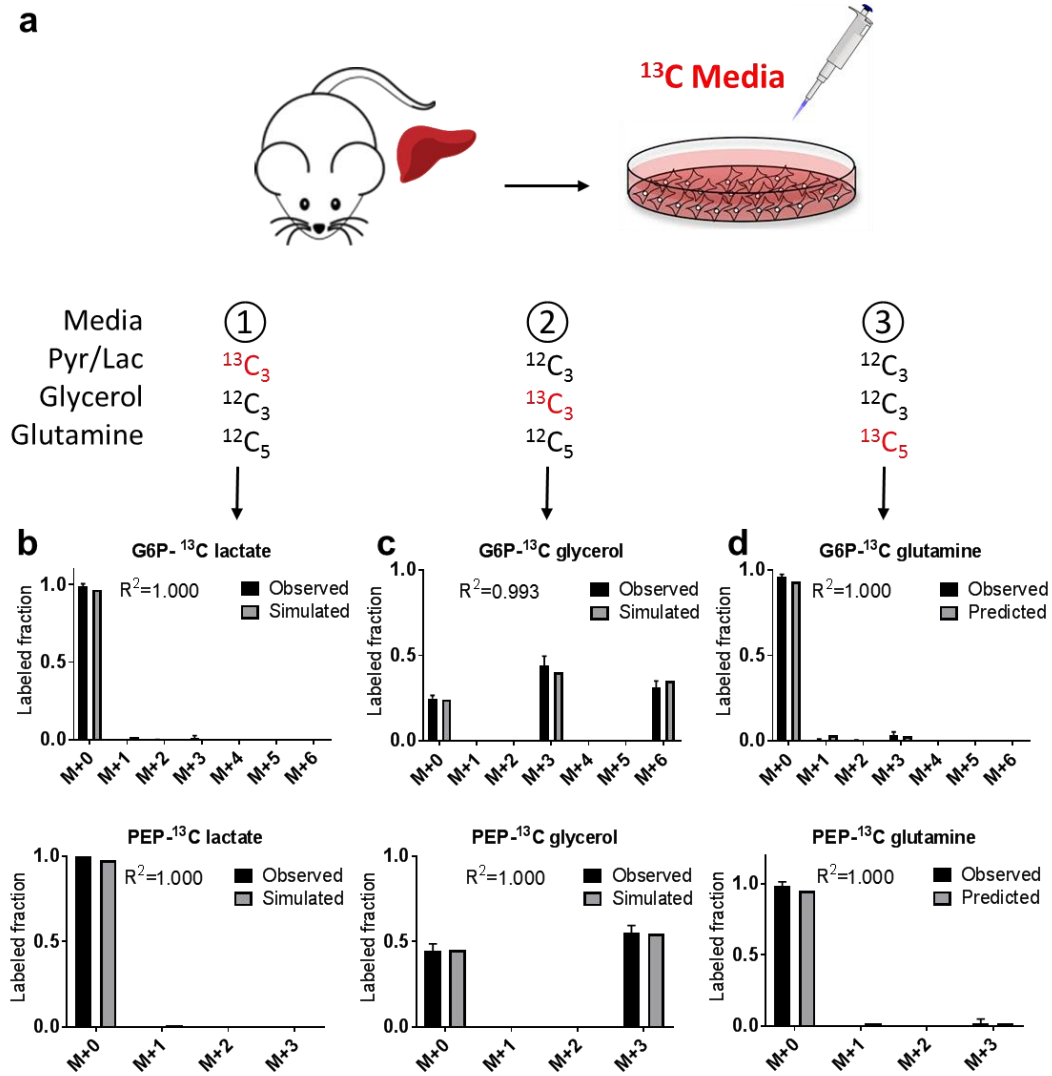
Figure 2. 7 | Verification of flux model using primary hepatocytes. a, Experimental scheme. **b-c,** simulated and observed labeling pattern of G6P and PEP. **d,** predicted and observed labeling pattern of G6P and PEP. G6P, glucose-6-phosphate; PEP, phosphoenolpyruvate.
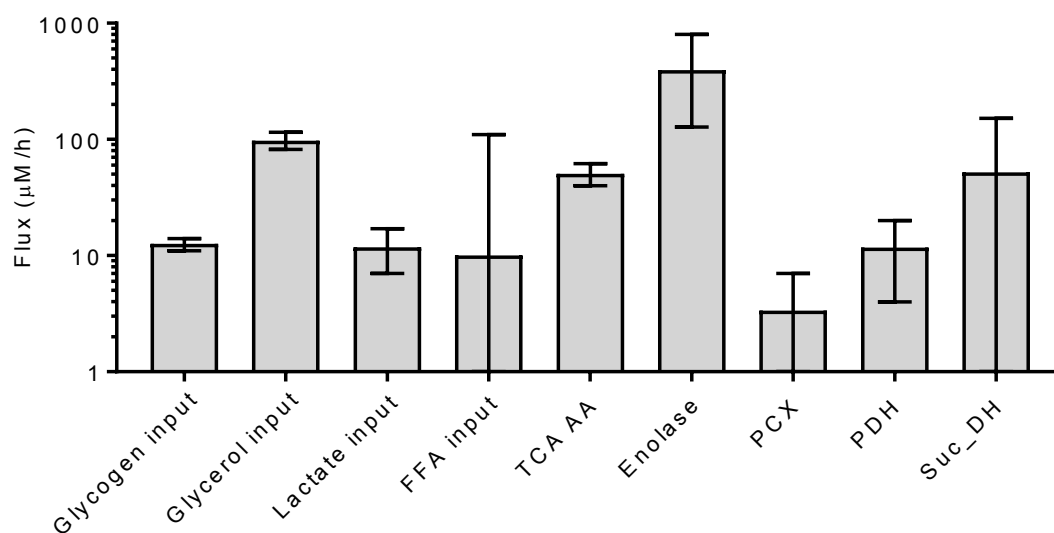
Figure 2. 8 | Best-fit value of all free fluxes with 95% confidence intervals. FFA, free fatty acids; PCX, pyruvate carboxylase. PDH, pyruvate dehydrogenase; Suc_DH, succinate dehydrogenase.

Chapter 3 . Effect of Fasting on Substrate Contribution in Gluconeogenesis

Yujue Wang, Hyok Joon Kwon, Xiaoyang Su, Fredric E. Wondisford

Department of Medicine, Rutgers-Robert Wood Johnson Medical School, New Brunswick, NJ 08901, USA.

Published in Molecular Metabolism in the title of 'Glycerol not lactate is the major net carbon source for gluconeogenesis in mice during both short and prolonged fasting'

Abstract

Fasting results in major metabolic changes including a switch from glycogenolysis to gluconeogenesis to maintain glucose homeostasis. However, the relationship between the length of fasting and the relative contribution of gluconeogenic substrates remains unclear. Here, we investigated the relative contribution of glycogen, lactate and glycerol in glucose production of male C57BL/6J-albino mice after 6, 12 and 18 hours of fasting. We used non-perturbative infusions of $^{13}C_3$ lactate, $^{13}C_3$ glycerol and $^{13}C_6$ glucose combined with liquid chromatography mass spectrometry and metabolic flux analysis to study the contribution of substrates in gluconeogenesis (GNG). During infusion studies, both lactate and glycerol significantly labels about 60% and 30-50% glucose carbon respectively, but glucose labels much more lactate (~90%) than glycerol carbon (~10%). Our analyses indicate that lactate, but not glycerol is largely recycled during all fasting periods such that lactate is the largest direct contributor to GNG via the Cori cycle but a minor source of new glucose carbon (overall contribution). In contrast, glycerol is not only a significant direct contributor to GNG but also the largest overall contributor to GNG regardless of fasting length. Prolonged fasting decreases both the whole body turnover rate of glucose and lactate but increases that of glycerol, indicating that the usage of glycerol in GNG become more significant with longer fasting. Collectively, these findings suggest that glycerol is the dominant overall contributor of net glucose carbon in GNG during both short and prolonged fasting.

Introduction

Elevated fasting glucose is commonly used to diagnose diabetes mellitus (DM) [25], and enhanced hepatic glucose production is the major cause of fasting hyperglycemia in DM [26-29]. At an early stage of fasting, glycogen is the major carbon source of glucose; yet as fasting persists, the major carbon source for glucose switches to gluconeogenesis (GNG) which produces glucose from small metabolites such as lactate, glycerol and amino acids [29-31]. The relationship between the length of fasting and the relative contribution of different substrates in GNG, however, remains unclear.

It is believed that lactate is the major substrate contributing to GNG through a process commonly known as the Cori cycle. The dominate role of lactate in GNG is evidenced by experiments showing that enrichment of circulating glucose at steady state is more than half of the enrichment of a circulating lactate tracer [32-35]. However, this conclusion is confounded by the fact that lactate is largely generated from glucose and resynthesized to glucose via the Cori cycle, making lactate the largest direct contributor to glucose carbon but not necessarily a good source for new carbon entering GNG, which we refer to as an overall contribution. On the other hand, GNG substrates such as glycerol and amino acids are much less recyclable from glucose during fasting [36, 37], making them better candidates to increase overall net contribution of glucose carbon during GNG. Several studies have emphasized the critical roles of glycerol and amino acids in increased GNG found in patients with DM [29, 38-40]. Therefore, a

better understanding of substrate usage in GNG during normal fasting is necessary.

In this study, we fasted mice for 6, 12 and 18 hours to study the relative contribution of different GNG substrates under different fasting conditions. We show that prolonged fasting clearly shifts the metabolomic profiles of circulating metabolites to one enriched in carboxylic acids without significantly affecting the circulating concentration of important GNG substrates. By performing a comprehensive flux analysis, we demonstrate that lactate is the dominant direct contributor but a minor overall contributor to GNG under all three fasted conditions. On the other hand, glycerol was the second largest direct contributor and the dominant overall contributor to GNG in all three fasting periods. We also showed that the GNG flux of lactate decreased while that of glycerol remained stable with prolonged fasting. Together, glycerol is the dominant net carbon source for GNG during short and prolonged fasting.

Methods

Animals

All mice were maintained on a C57BL/6J-albino background (Jackson Laboratories; B6(Cg)-Tyr^{c-2J}/J). The glucose homeostasis varies throughout the estrous cycle in female mice [41]. To avoid the variation caused by estrous cycles, only male mice were used in this study. Mice were housed in a pathogen-free barrier facility maintained on a 12-hour light/dark cycle. At 3-4 month of age, mice were catheterized on the right

jugular vein [42] and recovered for more than 7 days before experiments. All animal studies were approved by the Institutional Animal Care and Use Committees of Rutgers-Robert Wood Johnson Medical School.

Tracer infusion studies

Catheterized mice were kept in dark phase with food for at least 6 hours before the fasting experiment. All mice were transferred to new cages to fast 0, 6 and 12 hours followed by 6 hours infusion of tracer without food. For the mouse infusion, a tether and swivel system were used to allow mice free movement in the cage (Instech Laboratories). Water-soluble isotope-labelled metabolites tracers (Cambridge Isotope Laboratories) were prepared as solutions in sterile normal saline and infused via the catheter at a constant rate (0.1 µl/g body weight/min). 200 mM $^{13}C_6$ glucose, 150 mM $^{13}C_3$ glycerol or 40 mM $^{13}C_3$ sodium pyruvate with 360 mM $^{13}C_3$ lactate were prepared as the infusate. The purpose of using a mixture of $^{13}C_3$ sodium pyruvate and lactate is to maintain their physiological ratio (1:9) in the serum. About 30 µl blood were collected by tail vein bleeding after 5 and 6 hour of infusion, placed at room temperature in the absence of anticoagulant for 30 minutes and centrifuged at 4 °C to prepare serum. At the end of the last tracer infusion experiment, the mice were euthanized by cervical dislocation and quickly dissected liver was snap frozen in liquid nitrogen. Serum and tissue samples were kept at −80 °C until further analysis.

Glycerol derivatization for LC-MS Analysis

Due to the poor ionization of glycerol, an enzymatic derivatization is required to detect glycerol in liquid chromatography mass spectrometry (LC-MS) [43]. Samples containing glycerol were added into 10× volume of reaction buffer containing 25 mM Tris (pH 8.0), 10 mM Mg^{2+}, 50 mM NaCl, 5 mM ATP and 2 U/ml glycerol kinase (Sigma-Aldrich) and incubated for 10 minutes at room temperature. The reaction was quenched with 40:40:20 methanol:acetonitrile:water solution with 0.1% formic acid, and later neutralized with NH_4HCO_3 solution. The same reaction was also performed on blank to remove background. The ion counts of glycerol-3-phosphate in blank was subtracted from that of the derivatized sample.

LC-MS analysis

Serum samples were mixed with -20 °C 40:40:20 methanol:acetonitrile:water solution with 0.1% formic acid, followed by vortexing for 10 sec, incubation at 4 °C for 10 min, and centrifugation at 4 °C and ×16,000g for 10 min. The volume of the extraction solution was 25× the volume of serum. The supernatant was transferred to a clean tube, and neutralized with NH_4HCO_3 solution. The mixture was centrifuged again at 4 °C and ×16,000g for 10 min. The supernatant was then transferred to another clean tube for LC-MS analysis.

LC separation was achieved on a XBridge BEH Amide column (2.1 mm × 150 mm,

2.5 μm particle size, 130 Å pore size; Waters) using a gradient of solvent A (20 mM ammonium acetate + 20 mM ammonium hydroxide in 95:5 water:acetonitrile, pH 9.4) and solvent B (20 mM ammonium acetate + 20 mM ammonium hydroxide in 20:80 water:acetonitrile, pH 9.4). Flow rate was 300 μl min^{-1}. Samples were running using an isocratic method lasting for 6 min, 73% B. The autosampler temperature was set to 4 °C and the injection volume was 5 μL. For a better metabolome coverage, the m/z scan range was set to 72 to 1000 m/z at a resolution of 70,000 under negative polarity with AGC target of 3×10^6 and a maximum IT of 500 ms. The derivatized glycerol-3-phosphate is eluted at 1.9 min (m/z 171.0063). Data were analyzed using MAVEN [44]. The isotope natural abundances were corrected using AccuCor [45].

Liver glycogen measurement

Liver glycogen content were measured using the Glycogen Assay Kit (Sigma-Aldrich).

Metabolomic analyses

All the heatmaps and principle component analyses were performed on the serum samples after 0, 6 and 12 hours fasting followed by 6 hour infusion of $^{13}C_6$ glucose. The graphs were generated using R and GraphPad Prism software.

F$_{circ}$ calculation

The calculation of F$_{circ}$ (turnover rate of metabolites) is based on the labelled fraction

of tracers and the infusion rate at steady state using the following equation:

$$\text{F}_{circ} = \text{ Infusion rate} * \left(\frac{1}{labelled\ fraction\ of\ tracer} - 1 \right) \quad \text{[Eq.3. 1]}$$

Flux modeling

The relative contributions from substrates were calculated by an elementary metabolite

units (EMU) based method [46]. In brief, a flux network was constructed

(Supplementary Fig. A2. 1a; Supplementary Table A2. 1; Supplementary Fig. A2. 2).

All fluxes were calculated in the unit of nmol product/g/min. All fluxes occur in the

liver except V_{out}, V_{glc}, V_3, V_5, V_6 and V_9 which occur in the periphery. V_2, V_5, V_9, V_{13}

and V_{19} are input fluxes from glycogen, glycerol (from triglycerides), lactate (including

alanine and pyruvate), free fatty acid (FFA) and amino acids (via TCA cycle)

respectively. V_{glc} represents the infusion flux from $^{13}C_6$ glucose tracer. V_{11} is pyruvate

carboxylase flux that incorporates carbon dioxide. V_{10}, V_{12}, V_{17} and V_{18} are

decarboxylase fluxes that release carbon dioxide. V_{flop} is an infinitely large flux to

account for the achirality of metabolites. V_3 represents the glycolysis process in

peripheral tissue. V_6 represents glycerol synthesis from glucose. V_1 is the endogenous

glucose production (EGP) flux which equals to the sum of the glucose recycled via the

Cori cycle (V_3), glycerol synthesis (V_6) and the net production of glucose (V_{out} - V_{glc}).

Therefore, the absolute value of V_1 can be measured as the steady-state glucose turnover

rate (F_{circ}) in circulation.

The contribution of amino acids through TCA cycle consists of three components: 1. via oxaloacetate (Asp, Asn); 2. via fumarate or succinyl CoA (Phe, Tyr, Ile, Met, Val, Thr); 3. via α-ketoglutarate (Gln, Glu, Pro, His, Arg). The average physiological concentrations of amino acids are 13.5 μM Asp, 35.9 μM Asn, 54.1 μM Phe, 46.7 μM Tyr, 73.1 μM Ile, 52.4 μM Met, 178.7 μM Val, 126.2 μM Thr, 25.1 μM Glu, 397.0 μM Gln, 67.4 μM Pro, 49.6 μM His and 93.4 μM Arg [47]. Therefore, the total substrate concentration in the three possible pathways are 49.4, 531.2 and 632.5 μM respectively. Assuming proportional contribution by the three routes, the three sub-fluxes to oxaloacetate, succinate and α-ketoglutarate are 4%, 44% and 52% of V_{19} respectively. The metabolite mass balance leads to the following equations:

Glucose:	$V_1 - 0.5V_3 - 0.5V_6 + V_{glc} = V_{out}$	
G6P:	$V_1 - V_4 = V_2$	
DHAP:	$2V_4 - V_7 = V_8$	
Glycerol:	$V_8 - V_6 = V_5$	
PEP:	$V_7 - V_{10} = 0$	
Pyr:	$V_{11} + V_{12} - V_3 = V_9$	[Eq.3. 2]
Oxa:	$V_{10} + V_{15} + V_{16} - V_{11} - V_{14} = 0.04V_{19}$	
Ac-CoA:	$V_{16} - V_{12} = V_{13}$	
Suc:	$V_{14} - V_{15} - V_{17} = 0.44V_{19}$	
Cit:	$V_{16} - V_{18} = 0$	
aKG:	$V_{17} - V_{18} = 0.52V_{19}$	

Balance of input and output mass leads to the following equation:

$$6V_{out} = 6V_2 + 6V_{glc} + 3V_5 + 3V_9 + 2V_{13} + 4.52V_{19}$$
$$- V_{12} - V_{10} - V_{17} - V_{18} + V_{11}$$

[Eq.3. 3]

Nine fluxes were designated free fluxes: V_2, V_3, V_5, V_9, V_{12}, V_{13}, V_{15}, V_{19} and V_{glc}. All other fluxes can be expressed using the free fluxes or known constants ([Eq. 3. 4]).

$$V_1 = EGP = F_{circ}$$

$$V_4 = F_{circ} - V_2$$

$$V_6 = 2F_{circ} - 2V_2 - V_3 - V_5 - V_9 + V_{12} - V_{19}$$

$$V_7 = V_3 + V_9 - V_{12} + V_{19}$$

$$V_8 = 2F_{circ} - 2V_2 - V_3 - V_9 + V_{12} - V_{19}$$

$$V_{10} = V_3 + V_9 - V_{12} + V_{19}$$

$$V_{11} = V_3 + V_9 - V_{12}$$

[Eq. 3. 4]

$$V_{14} = V_{12} + V_{13} + V_{15} + 0.96V_{19}$$

$$V_{16} = V_{12} + V_{13}$$

$$V_{17} = V_{12} + V_{13} + 0.52V_{19}$$

$$V_{18} = V_{12} + V_{13}$$

$$V_{out} = 0.5*(V_5 + V_9 + V_{19} - V_{12}) + V_2 + V_{glc}$$

$$V_{flop} = Infinite$$

Since the labeling patterns of all the input molecules are known (either unlabeled or fully labeled as tracer), the steady-state labeling patterns of all metabolites in the system can be calculated using the EMU approach given any set of the nine fluxes. The

calculated labeling patterns were compared to the measured ones with equal weight. The best estimated flux set was obtained by minimizing the sum of squared residues (SSR) between the calculated and measured labeling patterns. The measured labeling patterns of glucose, glycerol and pyruvate under three tracers ($^{13}C_3$ glycerol, $^{13}C_3$ lactate and $^{13}C_6$ glucose) were used in this process. The numerical simulation of labeling patterns was achieved in R software and the optimization was achieved with DEoptim package [48]. 95% confidence intervals were calculated by (1) move one target flux away from the best-fit value by a small step (2) choose a combination of the other fluxes that minimize the increase of SSR, (3) calculate the new SSR and repeat step (1) to (3) until the new SSR reached the cutoff for 95% confidence interval [49]. The goodness of fit was tested by chi-square test, $X^2_{0.05}$ (df=15) = 24.996, which is equivalent to an SSR value of 0.0024996. The 15 degrees of freedom are based on 24 measurements (labeling fractions of three metabolites under three tracers) and having 9 unknown fluxes; 24 - 9 = 15.

Five-pool network

To illustrate the direct and overall contribution better, we simplified the pathways into the 5-pool network (Supplementary Fig. A2. 1b). For convenience, all units of fluxes were normalized to nmol C/g/min. U_1 and U_2 are input fluxes from glycerol and lactate respectively. U_5 and U_6 represent fluxes that glucose making the glycerol and lactate respectively. U_7 , U_8 , U_3 and U_4 represent the fluxes that glycerol, lactate, glycogen

and TCA amino acids making glucose respectively. U_9 represents the pyruvate dehydrogenase (PDH) flux that consumes lactate in TCA cycle. U_{out} is the glucose output which equals to the net production of glucose. By definition, all fluxes can be represented by the equivalent fluxes in the EMU model:

$$U_1 = 3V_5; \quad U_2 = 3V_9; \quad U_3 = 6V_2; \quad U_4 = 3V_{19}; \quad U_5 = 3V_6;$$
$$U_6 = 3V_3; \quad U_7 = 3V_8; \quad U_8 = 3V_{11}; \quad U_9 = 3V_{12}; \quad U_{out} = 6(V_{out} - V_{glc})$$

[Eq. 3. 5]

The direct contributions from glycerol, lactate, glycogen and TCA amino acids were calculated as the relative ratio of U_7, U_8, U_3 and U_4 respectively (green arrows; supplementary Fig. A2. 1b). The overall contributions from glycerol, lactate, glycogen and TCA amino acids were calculated as the relative ratio of U_1, U_2, U_3 and U_4 respectively (purple arrows; supplementary Fig. A2. 1b).

Substrate specific flux calculation

The substrate specific flux of gluconeogenesis was calculated by multiplying the overall contribution to glucose by the glucose F_{circ} measured from the $^{13}C_6$ glucose infusion experiment.

Statistical analyses

Statistical analyses were performed using the GraphPad Prism software, version 7.04.

Results

Prolonged fasting increases serum carboxylic acid levels but has little effect on GNG substrates

To investigate the effects of fasting on concentrations of serum metabolites, we generated the serum metabolomic profiles of mice after 6, 12 or 18 hours of fasting (Fig. 3. 1a). In general, the serum profiles of 12 and 18 hour fasted mice were similar, while the serum profile from 6 hour fasted mice was clearly different. Consistent with these findings, the principle component analysis (PCA) showed a significant separation of samples prepared from the three fasting conditions with 12 and 18 hour samples appearing closer to each other and separated from 6 hour samples (Fig. 3. 1b). We then identified all serum metabolites that showed significantly different concentrations in 6 and 18 hour fasted mice and found the majority of the metabolites increased after 18 hour of fasting are carboxylic acids (red; Fig. 3. 1c, Supplementary Table A2. 2). Glucose and pantothenate/vitamin B_5, a precursor for coenzyme A, are the only metabolites found to be significantly decreased after 18 hours of fasting. Interestingly, none of the GNG substrates including pyruvate, lactate, glycerol and amino acids showed significant changes between the 6 and 18 hours of fasting (green; Fig. 3. 1c, Supplementary Table A2. 2), suggesting prolonged fasting has little impact on the pool size of GNG substrates.
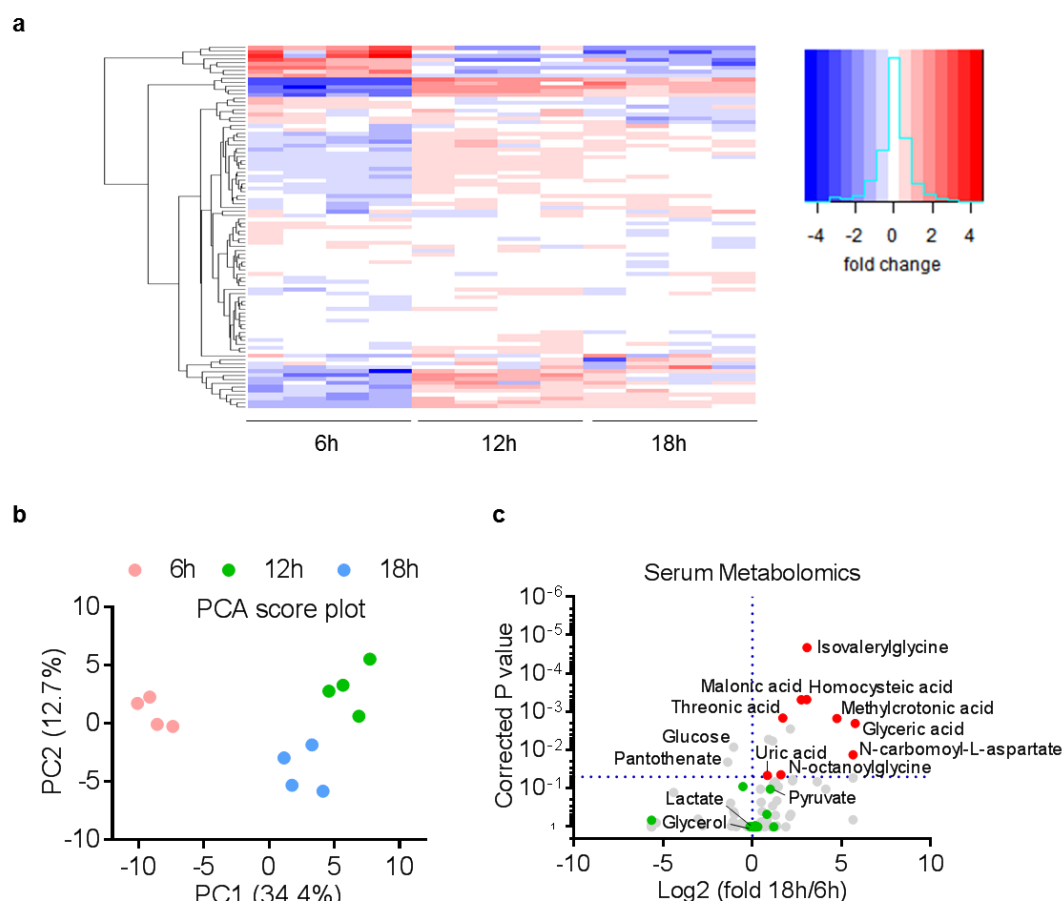
Figure 3. 1 | Metabolomic profiles after short and prolonged fasting. a, Heatmap of serum metabolite clusters. Each column represents one mouse and each row represents one metabolites. **b,** Principle component analysis (PCA) of metabolomic profile. Each dot represents one mouse. PC1 and PC2 are the two component explained the highest variance. **c,** Volcano plot of serum metabolomic fold changes between mice fasted for 6 and 18 hours. Each dot represents a metabolite: red, carboxylic acids with significant changes; green, gluconeogenic substrates. P values were calculated using two-sided Student's t-test and corrected for multiple comparisons using the Holm-Sidak method. $P<0.05$ is considered significant. n= 4 mice for each group. See also Supplementary Table A2. 1.
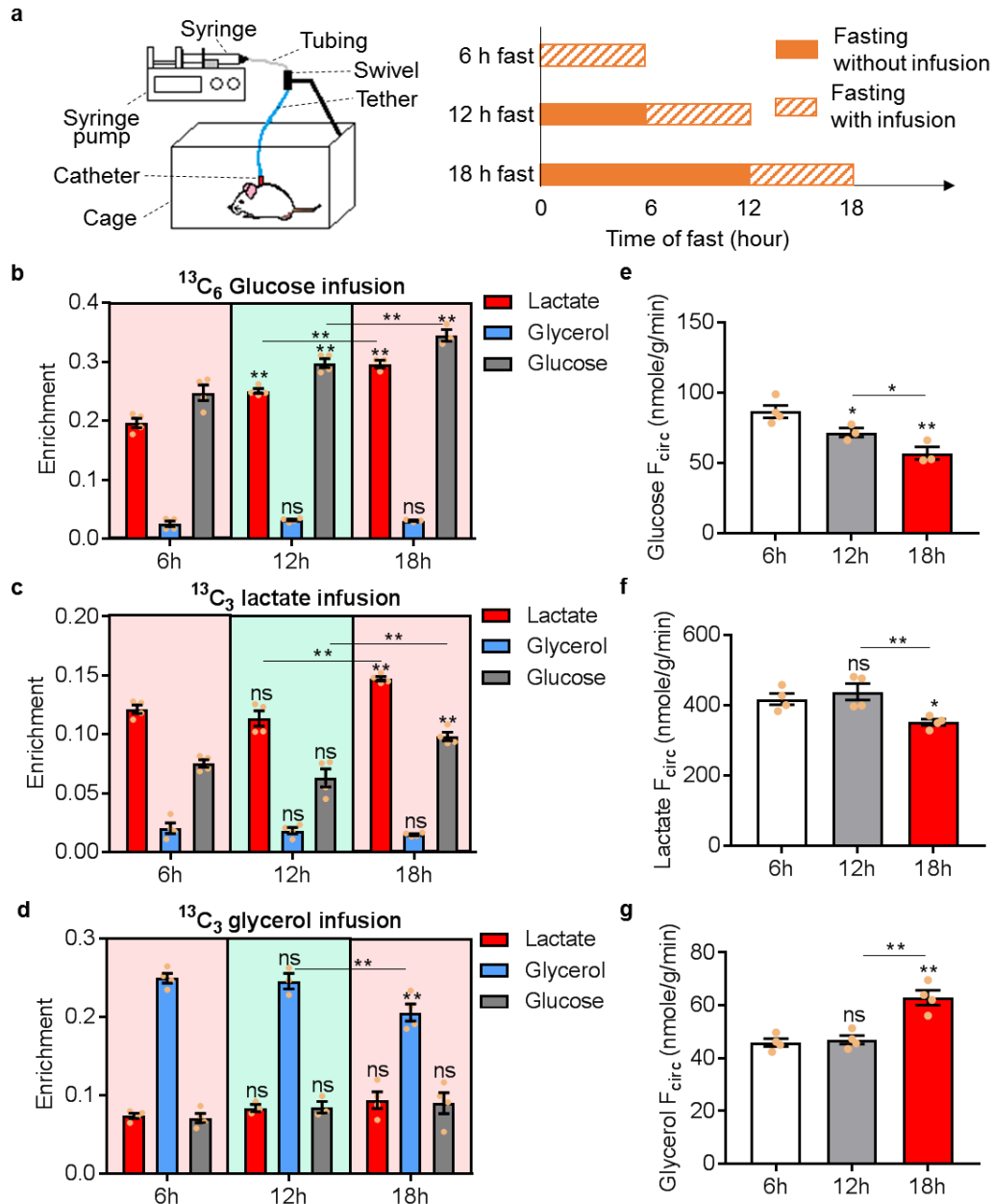
Figure 3. 2 | Prolonged fasting increases glycerol turnover and decreases lactate and glucose turnover. a, Experimental scheme of ^{13}C tracer infusions. **b-d,** [13]C average carbon enrichment of serum metabolites at steady state infused with [13]C_6 glucose, [13]C_3 lactate or [13]C_3 glycerol tracers. **e-g,** Turnover rate (F_{circ}) of circulating glucose, lactate and glycerol. For all experiment, n=3 or 4 for each group. All data are expressed as mean ± s.e.m. **P<0.01; *P<0.05; ns = not significant by one-way ANOVA. All comparisons are against 6 h data unless indicated otherwise.

Prolonged fasting increases glycerol turnover but decreases lactate and glucose turnover

To investigate the kinetics of GNG substrates during short and prolonged fasting, we fasted mice as described above and infused one of three tracers ($^{13}C_3$ lactate, $^{13}C_3$ glycerol or $^{13}C_6$ glucose) for 6 hours before blood sampling (Fig. 3. 2a), which is sufficient to achieve isotopic steady states for all three tracers [50] (Supplementary Fig. A2. 3a-b). No significant difference of glucose or insulin level was found across different tracer usage (Supplementary Fig. A2. 3c-d), suggesting similar physiological conditions under different tracers. We then calculated the average carbon enrichment (Fig. 3. 2b-d). When we infused $^{13}C_6$ glucose or $^{13}C_3$ lactate, enrichment in lactate or glucose was enhanced, respectively, without significant enrichment in glycerol, suggesting that glucose and lactate are interconvertible (Fig. 3. 2b-c). In contrast, when we infused $^{13}C_3$ glycerol, both glucose and lactate showed substantial enrichment (30-50% of the $^{13}C_3$ glycerol tracer), indicating that glycerol is converted to both glucose and lactate efficiently (Fig. 3. 2d) but little glucose is converted to glycerol (Fig. 3. 2b). Next, we calculated endogenous turnover rates (F_{circ}, Fig. 3. 2e-g) of circulating glucose, lactate and glycerol. The turnover rate of glucose continuously decreased from 6 to 18 hours (Fig. 3. 2e), suggesting a decrease in total glucose production with prolonged fasting. In contrast, lactate and glycerol exhibit no significant changes between 6 and 12 hours of fasting, but showed a significant decrease and increase, respectively at 18 hours of fasting (Fig. 3. 2f -g).

Glycerol is less recyclable glucose precursor than lactate

Because only one tracer was used at a time and that tracer was the only ^{13}C source in

all of the three ^{13}C tracer infusion studies, the relative contribution from the tracer to

other metabolites can be estimated using the following equation:

$$\text{Relative contribution} = \frac{\text{Enrichment of metabolite}}{\text{Enrichment of tracer}} \qquad \text{[Eq. 3.6]}$$

For example, in the $^{13}C_3$ lactate infusion, the relative contribution of glucose from

lactate can be estimated by the enrichment ratio of glucose versus lactate. Using this

method, we compared the interconversion between lactate and glucose (Fig. 3. 3a) and

between glycerol and glucose (Fig. 3. 3b). In all three fasting conditions, lactate

contributed about 60% of glucose carbon while glucose contributed about 90% of

lactate carbon (Fig. 3. 3a). In addition, the fraction of glucose from lactate are

significantly lower than the fraction of lactate from glucose in all three fasting

conditions. In contrast, glycerol contribution to glucose increased from 30% to 50%

with prolonged fasting while glucose contribution to glycerol remained at about 10%

(Fig 3. 3b). In all three fasting conditions, the fraction of glucose from glycerol are

significantly higher than the fraction of glycerol from glucose. Overall, these data

suggest glycerol is a much less recyclable glucose precursor than lactate under fasting

conditions since about 90% of lactate is recycled from glucose while only 10% of

glycerol is recycled from glucose.
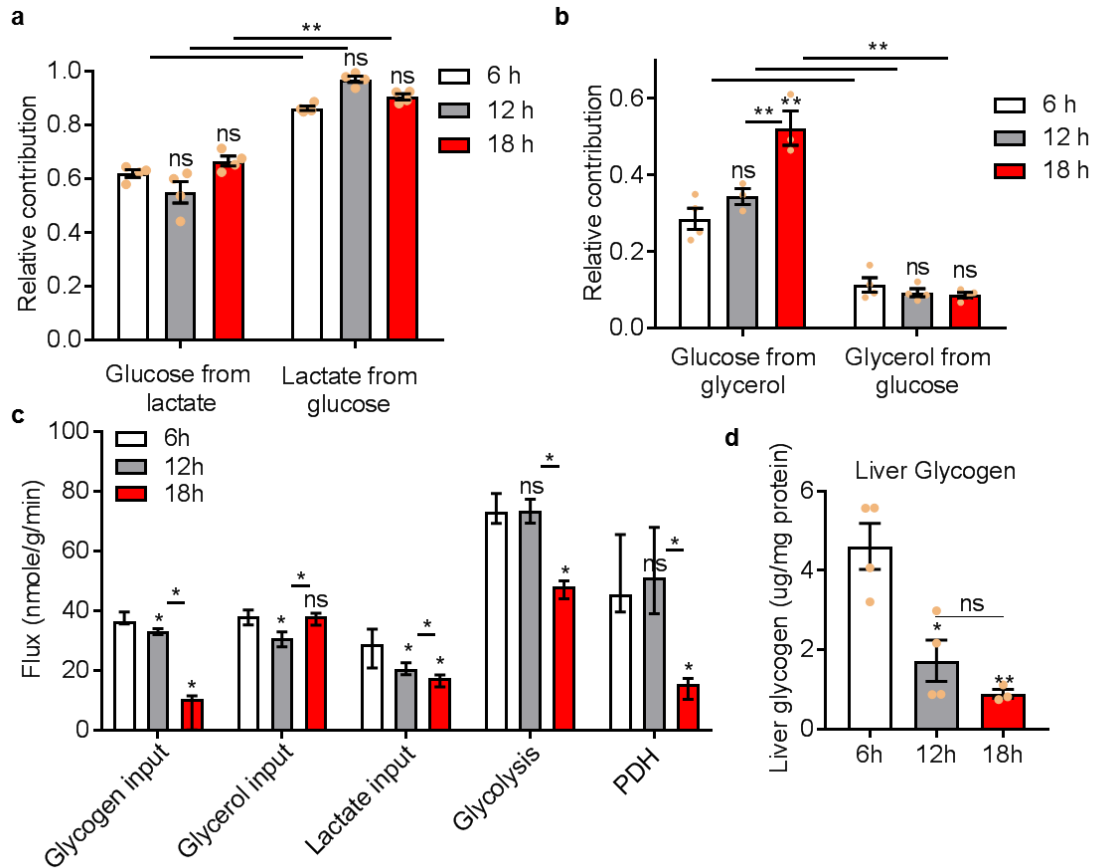
Figure 3. 3 | Estimate fluxes in glucose GNG. a-b, Relative contribution of gluconeogenic substrate and product represented by the ratio of ^{13}C enrichment (metabolite versus tracer). **c,** Estimated fluxes in gluconeogenesis pathway. **d,** Liver glycogen content. Data are mean ± s.e.m in **a**, **b** and **d** and best-fit value ± 95% confidence interval in **c**. n= 3 to 4 mice in each group, **P<0.01; *P<0.05; ns, not significant by one-way ANOVA. All comparisons are against 6 h data unless indicated otherwise. PDH, pyruvate dehydrogenase; See also Supplementary Fig. A2. 1 and Supplementary Fig. A2. 3

Prolonged fasting has significant impacts on gluconeogenic fluxes

The enrichment ratio method is only a rough estimation of the relative contribution because it assumes all non-tracer metabolites are un-labeled and therefore overestimates contributions from the tracer. To accurately evaluate the relative contribution from different substrates, we developed a mathematical model which

enumerates different flux combinations and simulates the labeling pattern of metabolites associated with each combination (Supplementary Fig. A2. 4). The best-fit flux is the one associated with the least residue between simulated and observed labelling patterns. Using this method, we are able to estimate all the essential fluxes in GNG pathway (Fig. 3. 3c; Supplementary Fig. A2. 1a). The input fluxes of glycogen and lactate showed continuous and significant decreases with prolonged fasting. In contrast, the input flux of glycerol remained relatively stable between 6 and 18 hours. The fluxes of glycolysis and PDH also decreased from 12 to 18 hour. Interestingly, the change of the glycogen flux over time is not in the same pattern as the liver glycogen content (Fig. 3. 3d). For example, between 6 and 12 hour fasting, the liver glycogen content was reduced by 63% while the glycogen flux was only reduced by 10%. Our analyses have also tested the possibility of a pathway that directly convert glycerol to lactate/pyruvate without passing through glucose (Supplementary Fig. A2. 5). However, in all three fasting conditions, the 95% confidence interval of this flux included 0, suggesting whether this pathway exist or not is inconclusive.

Lactate is the major direct contributor while glycerol is the major overall contributor to GNG

To illustrate the contribution of substrates better, we summarized all the fluxes into a 5-pool network (Fig. 3. 4a-c, Supplementary Table A2. 3) and calculated the direct and overall contributions from all substrates (Fig. 3. 4d and 3. 4e). The direct contribution

is the relative ratio of the four fluxes directly making glucose (green arrows, Fig. 3. 4a-c) while the overall contribution is the relative ratio of the four overall input fluxes (purple arrows, Fig. 3. 4a-c). In all three fasting conditions, lactate exhibits the highest direct contribution to GNG (non-glycogen glucose production) (Fig. 3. 4d). However, such a high direct contribution is largely due to the recyclable property of lactate because in terms of the overall contribution, the majority of GNG carbon is ultimately from glycerol (Fig. 3. 4e). Interestingly, when glycogen contribution was high (6 and 12 hour fast), the contribution from TCA amino acids was negligible. Only when glycogen contribution was diminished at 18 hours did the contribution from TCA amino acids start to appear.

Based on the overall contribution data, we next calculated the absolute GNG fluxes specific to each substrate (Fig. 3. 4f). Unlike the lactate input flux which showed continuous decrease with prolonged fasting (Fig. 3. 3c), the GNG specific flux from lactate only decreased from 6 to 12 hours and remained relatively stable between 12 and 18 hours. This is because between 12 and 18 hours, the decrease of PDH flux (Fig. 3. 3c) directed more lactate towards glucose rather than acetyl CoA, which overcame the decrease of total lactate input. In contrast, the GNG specific flux from glycerol (Fig. 3. 4f) remained relatively stable across different fasting periods. In all three fasting conditions, the gluconeogenic flux from glycerol dominates the other substrates.
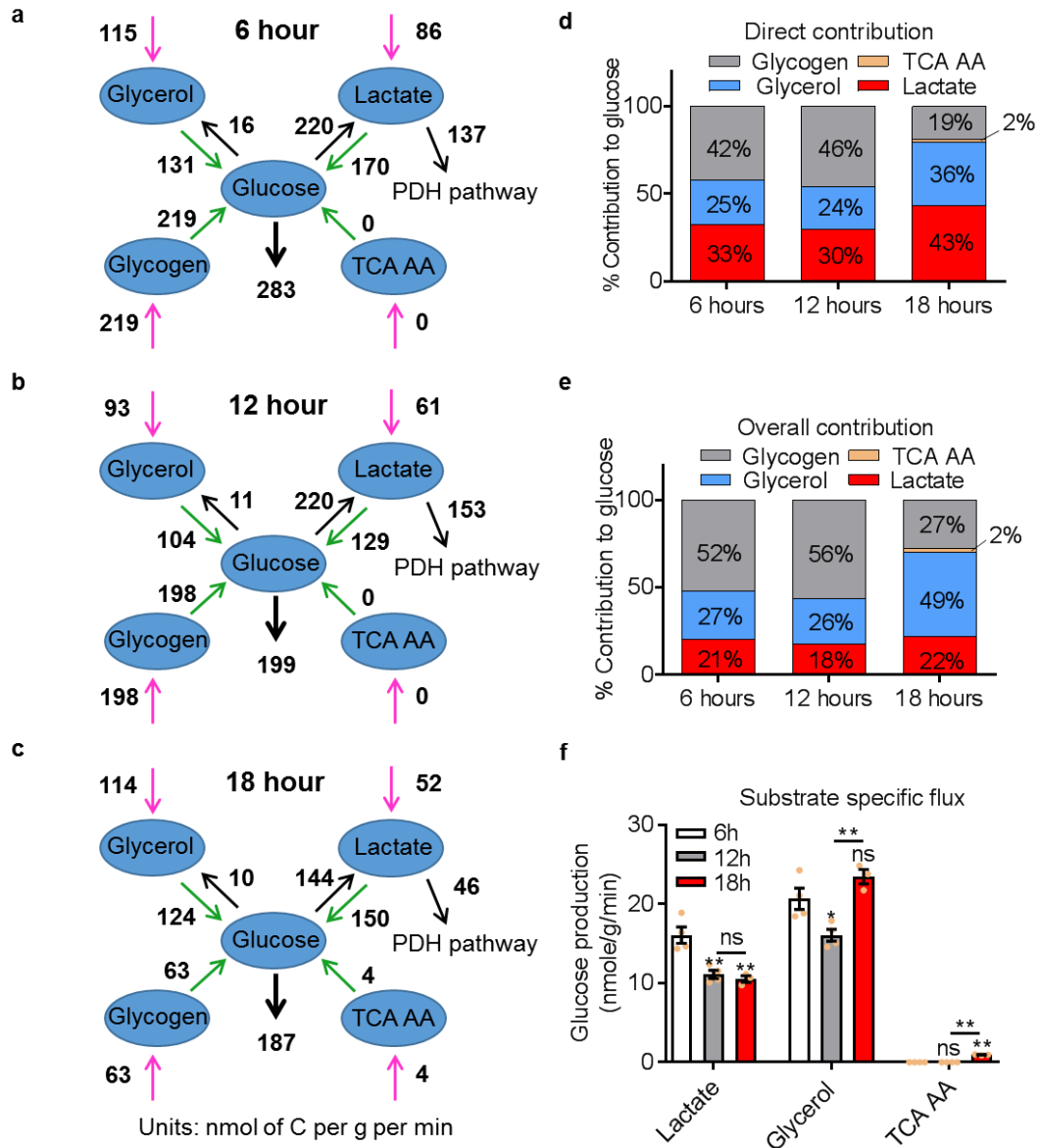
Figure 3. 4 | Gluconeogenic contribution. a-c, glucose production network after 6 (**a**), 12 (**b**) and 18 (**c**) hours of fasting. All fluxes are normalized to nmole carbon per gram body weight per minute. The best-fit value are shown for each flux. Fluxes involved in the direct and overall contribution are shown in green and purple respectively. For convenience, all numbers are rounded to the nearest whole number. **d-e,** Direct and overall contribution from lactate, glycerol, glycogen and TCA amino acids. **f,** Substrate specific gluconeogenic fluxes from lactate, glycerol and TCA amino acids. Data are mean ± s.e.m.; for all data, n= 3 to 4 mice per group, **P<0.01; *P<0.05; ns = not significant by one-way ANOVA. All comparisons are against 6 h data unless indicated otherwise. PDH, pyruvate dehydrogenase; TCA AA, amino acids that enter gluconeogenesis through TCA intermediates. See also Supplementary Table A2. 3 for confidence intervals of flux.

Discussion

This study re-evaluated the roles of lactate and glycerol as direct and overall (net carbon) GNG substrate sources during different fasting conditions. Lactate is known as the dominant substrate of GNG based on its high turnover and knowledge that lactate is recycled (Cori cycle). The Cori cycle, however, is not a net glucose producer unless lactate is derived from substrates other than existing circulating glucose such as new glucose from glycogenolysis or from GNG substrates such as pyruvate, alanine and glycerol. Consistent with this view, our analysis indicates that although lactate serves as the dominant direct GNG substrate (Fig 3. 4d), its net carbon contribution is too small to account for the total glucose consumption flux. In fact, glycerol through both direct synthesis (Fig. 3. 4d) and by labeling a fraction of circulating lactate that subsequently is used in GNG contributes the majority of the net carbon to GNG during all fasting periods (Fig 3. 4e).

Our results demonstrate both the direct and indirect pathway used by glycerol to form glucose based on different labelling patterns of glycerol and lactate-derived glucose (Supplementary Fig. A2. 3). $^{13}C_3$-labeled glycerol makes glucose that is mainly M+3, suggesting that the glycerol carbon backbone is preserved in the newly made glucose (direct glycerol pathway). In contrast, $^{13}C_3$-lactate generates a significant portion of M+1 and M+2 glucose, suggesting extensive carbon shuffling in the TCA cycle of lactate entering at the beginning of the GNG pathway. Thus the major glycerol to

glucose pathway is direct and does not involve lactate as an intermediate. However, some of the glucose derived from glycerol has an M+1 pattern indicating entry as lactate (Supplementary Fig. A2. 3).

Lactate turnover flux during fasting is reported to be more than twice of that of glucose [33]. One potential consumer of serum lactate in a fasting animal is the Cori cycle; but as Hui and colleagues have recently shown, another more important consumer of lactate is the TCA cycle in most peripheral tissues except the brain [33]. Knowing that much of circulating lactate is completely metabolized in the TCA cycle makes it now unnecessary to assume that it must be regenerated to glucose in the Cori cycle. In fact, our data suggest a large proportion of lactate was consumed in the TCA cycle through PDH pathway instead of entering GNG (Fig. 3. 4a-c). Moreover, assuming these flux data are correct, another source of lactate production beyond glycolysis must be present to support the high lactate flux. Given that glycerol tracer labels about 30-50% of circulating lactate, it remains possible that peripheral glycerol metabolism contributes to lactate production.

A review of the tracer enrichment data suggest this pathway may exist (Fig. 3. 2b-d). Assuming that the Cori cycle is responsible for generating lactate from glucose and glucose from lactate, then at equilibrium the enrichment fractions of both glucose and lactate should be similar. However, in the $^{13}C_6$-glucose infusion, the lactate

enrichment is lower than glucose enrichment, suggesting entry of unlabeled lactate into the cycle in the periphery. In contrast, in the $^{13}C_3$-glycerol infusion, the ^{13}C enrichment gap between glucose and lactate disappeared, suggesting that glycerol contributes to lactate production independent of glucose production. Therefore, we adapted our flux model to include a direct pathway from glycerol to lactate without a glucose intermediate (Supplementary Fig. A2.5). Due to uncertainty in estimating flux in the new model, we were unable to establish this direct pathway, but the relatively high upper boundary of 95% confidence interval suggests that it could potentially account for up to 40% of the total glycerol input flux. Uncertainty is mainly due to high recycling of ^{13}C labeling between glucose and lactate, making it difficult to distinguish a direct (glycerol → lactate) versus indirect (glycerol → glucose → lactate) pathway for lactate generation. To solve this issue, a tracer that is non-recyclable between lactate and glucose seems necessary.

Several limitations of this study are noted. First, the contribution from glycogen and TCA amino acids might be overestimated since our model assumes both glycogen and TCA amino acids are non-recyclable from glucose during fasting. However, this limitation is expected to have limited impact on our conclusions since the contribution from glycogen is excluded when calculating the GNG rate and the overall contribution from TCA amino acids is not dominant in all three fasting conditions. Second, our current flux model assumes TCA amino acids contribute to GNG via a universal pool

of TCA intermediates, though in reality liver and peripheral tissues may functionally use two separate pools. Future studies will investigate the effect of tissue compartmentalization on flux analyses. Third, a relatively high infusion rate of $^{13}C_6$ glucose tracer was used in this study to obtain accurate enrichment values. Consequently, the glucose consumption rate might be increased during $^{13}C_6$ glucose infusion, although no significant difference was found in glucose or insulin levels during fasting comparing to the use of the other two tracers (Supplementary Fig. A2. 3c and A2. 3d). Finally, this study is unable to distinguish the contribution from pyruvate, lactate and alanine due to the high interconversion rate among these three metabolites *in vivo*. Consequently, the lactate flux we referred in this study also included the contribution from other metabolites (including pyruvate and alanine), which enters GNG via lactate.

It should be noted that mice have faster metabolic rates than humans, and therefore it would take longer time for humans to reach the same fasting state as described in this study [51]. A rough translation can be achieved based on the fact that it takes 36 to 40 hours of fasting in human subjects to deplete liver glycogen storage [52] while it only takes 12 to 18 hours in mice (Fig. 3. 3d). Therefore, fasting for 6, 12 and 18 hours in mice is roughly 15, 30 and 45 hours in humans respectively. Future studies should be necessary to investigate the direct and overall contribution in human subjects and diabetic mouse models at different fasting states.

Conclusions

The direct contribution of substrates to GNG have been determined by several authors, but none have investigated the net carbon contribution of these substrates in GNG [32, 34, 35, 53-55]. Our findings suggest that glycerol is the major net carbon contributor in GNG during both short and prolonged fasting. Elevated glycerol is an important biomarker for the development of hyperglycemia and type 2 DM [56], and patients with type 2 DM also show significantly increased gluconeogenic flux from glycerol [10, 57]. Given the importance of glycerol as the dominant ultimate carbon source of gluconeogenesis, the glycerol metabolic pathway is a potentially important therapeutic target in patients with DM.

Chapter 4 . Effect of Hepatic Glucagon Signaling and High Fat Diet Feeding on Gluconeogenesis

Yujue Wang,[1,5] Sara M. McMillin,[1,2,5] Katarzyna Kalemba,[1] Hyokjoon Kwon,[1] Wenyun Lu,[3] Huiting Xu,[1] Aditya V. Chauhan,[1] Nathaniel E. White,[1] Keith R. Anacker,[1] Joshua D. Rabinowitz,[3,4] Xiaoyang Su,[1,4,*] and Fredric E. Wondisford[1,4*]

[1]Department of Medicine, Rutgers-Robert Wood Johnson Medical School, New Brunswick, NJ 08901, USA. [2]Fred Wilson School of Pharmacy, High Point University, High Point, NC 27268, USA. [3]Department of Chemistry and Lewis-Sigler Institute for Integrative Genomics, Princeton University, Princeton, NJ 08544, USA. [4]Rutgers Cancer Institute of New Jersey, New Brunswick, NJ 08903, USA. [5]These authors contributed equally: Yujue Wang, Sara M. McMillin.

Abstract

Fasting hyperglycemia in diabetes mellitus (DM) involves excessive gluconeogenesis (GNG). Enhanced glucagon signaling, insulin resistance, and altered substrate availability all play a role, but how they interact *in vivo* remains incompletely understood. To explore this question, mouse models of enhanced hepatic glucagon signaling fed a normal or high fat diet (HFD) were studied. Glucagon signaling increased gluconeogenic enzyme expression and HFD increased glycerol availability and decreased peripheral insulin sensitivity. Strikingly, however, glycerol from a HFD and glucagon signaling together augmented G6pc expression, GNG and fasting hyperglycemia, while preserving insulin sensitivity. During fasting, in vivo isotope tracing demonstrated that glycerol was the origin of most GNG carbon, and glucagon signaling promoted a further increase in hepatic glycerol flux to glucose. Hepatic *Gyk* knockdown in HFD reversed hyperglycemia and G6pc induction. Thus, glycerol metabolism is an important and previously underappreciated pathway that could be targeted in treatment strategies for patients with DM.

Introduction

Diabetes mellitus is currently a global health epidemic that affects nearly 10% of the population worldwide [58, 59]. In both type 1 (T1DM) and type 2 diabetes mellitus (T2DM), enhanced gluconeogenesis is the major contributor to fasting hyperglycemia [26-29]. During prolonged fasting, gluconeogenesis is the major contributor to glucose

production [29-31]. Relatively early on, breakdown of glycogen and glycolysis in muscle and other peripheral organs produces circulating lactate, which has sometimes been assumed to be the dominant source of gluconeogenic carbon [31]. Longer fasting, however, depletes glycogen stores, and breakdown of fat and protein become the ultimate providers of gluconeogenic carbon, in the form of glycerol and amino acids. Several studies have emphasized the role of gluconeogenic amino acids and glycerol in gluconeogenesis in diabetic patients [29, 38, 39].

Gluconeogenesis takes place substantially in the liver, where multiple hormones and substrates control the overall pathway [29]. While defects in insulin signaling are central to diabetes pathogenesis, the effects of insulin signaling on acute hepatic glucose production appear to be largely indirect [60-63]. Glucagon, in contrast, is a major endocrine hormone that directly regulates glucose production by its action on hepatocytes [11, 64]. The secretion of glucagon is suppressed by insulin signaling in pancreatic α-cells, and the loss of this paracrine regulation mechanism markedly increases glucagon levels in poorly controlled T1DM as well as the late stage of T2DM [65, 66]. Even in patients with early stage T2DM where glucagon levels may not be elevated, glucagon levels are nonetheless inappropriate given the setting of hyperglycemia [67]. Hyperglucagonemia promotes increased hepatic glucose production by activation of the glucagon receptor expressed on the surface of hepatocytes [11, 64, 68]. The signaling cascade activated by glucagon ultimately leads

to the activation of protein kinase A (PKA), which mediates intracellular signaling pathways that enhance hepatic gluconeogenesis [69-71].

In addition to increased glucagon signaling, dietary excess also contributes to dysregulated hepatic gluconeogenesis. For example, provision of additional substrates may increase gluconeogenesis by a 'substrate push' mechanism [72] or by allosteric regulation of gluconeogenic enzymes [61]. It has been reported that increased glucagon signaling and fat availability found in obese T1DM and late stage T2DM patients worsen metabolic regulation [73-76]. Mechanisms by which high fat diet (HFD)-induced obesity and enhanced glucagon signaling collaborate to activate gluconeogenesis remain unstudied.

Here, we utilized constitutive PKA activation in the liver [77] to mimic hyperglucagonemia plus a classic HFD approach to model the combined role of high glucagon signaling and diet-induced obesity in gluconeogenesis of mice. By performing metabolomic and enzymatic analyses, we show that glucagon signaling and HFD feeding work in concert to activate hepatic gluconeogenesis, leading to a severe hyperglycemia. Glycerol plays two roles in this process: (1) it is the origin of most gluconeogenic carbon, especially in high fat diet conditions. (2) it also enhances the PKA-mediated up-regulation of *G6pc* promoting glucose synthesis from both glycerol as well as from pyruvate/lactate.

Methods

Animals and Diets

All mice were maintained on a C57BL6/J-albino background (Jackson Labs; B6(Cg)-Tyrc-2J/J). The glucose homeostasis varies throughout the estrous cycle in female mice [41]. To avoid the variation caused by estrous cycles, only male mice were used in this study. To generate the L-PKA and the L-GFP mice, mice homozygous for the floxed PKA $R1\alpha$ allele [77] were maintained on a normal chow for 11 weeks after weaning and then injected with either Ad5-CMV-CRE or Ad5-CMV-eGFP (3×10^9 pfu/mouse; University of Iowa Viral Vector Core) via the tail vein and allowed to recover for 7 days. To generate the L-PKA-HFD and L-GFP-HFD, mice homozygous for the floxed PKA $R1\alpha$ allele were maintained on a high fat diet for 11 weeks after weaning and then injected with Ad5-CMV-CRE or Ad5-CMV-eGFP, as described above. For Gyk knockdown experiments, Ad-U6-m-Gk-shRNA or Ad-U6-shRNA-mCherry (2×10^9 pfu/mouse; Vector Biolabs) were injected at the same time with Ad5-CMV-CRE. Mice were housed in a pathogen-free barrier facility maintained on a 12-hour light/dark cycle. All animal studies were approved by the Animal Care and Use Committees of Johns Hopkins University Medical School and Robert Wood Johnson Medical School.

Protein Extraction and Western Blotting

All protein preparations were conducted using tissue samples that had been immediately snap frozen in liquid nitrogen following the sacrifice of the animal. For

protein preparations, tissues were mechanically homogenized in ice-cold RIPA buffer (Sigma) with 1 × protease inhibitor (Roche) and 1 × phosphatase inhibitor (Thermo Scientific) using a handheld tissue homogenizer (E-Z Grind; Denville Scientific). The homogenate was then centrifuged at 16,000 × g at 4 degrees and the supernatant was collected. Protein concentrations were measured using the Pierce BCA assay (Thermo Scientific). Western blotting was performed using standard procedures utilizing the standard V3 Western Workflow (Bio-Rad). All standard western blotting reagents were obtained from Bio-Rad. Antibodies were obtained from Cell Signaling Technology (PRKAR1α, AKT, AKT pSer473), Bio-Rad (HRP-conjugated anti-mouse IgG) or Sigma (Cyclophilin).

Metabolic Tests

All in vivo metabolic tests presented herein were performed within 3 weeks after the injection of virus. Blood glucose measurements were obtained via a small nick in the lateral tail vein using a glucometer (Bayer Contour). For the pyruvate and glycerol tolerance tests, mice were fasted overnight (12 hours) and then injected i.p. with sodium pyruvate or glycerol (9.1 mmole/kg; Sigma). For the insulin tolerance tests, mice were fasted for 6 hours and then injected i.p. with human insulin (0.5 U/kg; Novo Nordisk). For refed-glucose measurements, mice were fasted for 12 hours and refed for 2 hours before measurement.

RNA Analysis

Total RNA was obtained from mouse tissue samples that had been snap frozen in liquid nitrogen immediately after sacrificing the animal. RNA was extracted using the RNeasy Plus Mini Kit (Qiagen). Complementary DNA (cDNA) was generated from 1 µg total RNA using the iScript cDNA Synthesis kit (Bio-Rad). Primers were designed with NCBI Primer-BLAST [78]. Quantitative PCR (qPCR) reactions were conducted using the SYBR green PCR master mix (Applied Biosystems) in CFX96 Touch Real-Time PCR Detection System (Bio-Rad). CT values were normalized to beta actin (*Actb*) mRNA and interpreted as fold changes to the L-GFP control group.

Insulin Response Test

Mice were fasted for 6 hours and then injected i.p. with human insulin (Novo Nordisk). Ten minutes after the injection, mice were sacrificed by cervical dislocation to harvest livers and other organs. All samples were snap frozen in liquid nitrogen and stored at -80 °C before analyses.

Insulin, Glycerol, Glycogen and Triglycerides Measurements

Serum insulin levels were measured using the Ultra-Sensitive Mouse Insulin ELISA Kit (Crystal Chem). Serum glycerol levels were measured using the Glycerol Assay Kit (Sigma). Liver glycerol levels were calculated by subtracting the endogenous glycerol-3-phosphate level (measured using the Sigma Glycerol Assay Kit without the addition

of ATP) from the sum of glycerol-3-phosphate and liver glycerol (measured using the Sigma Glycerol Assay Kit with the addition of ATP). Liver glycogen levels were measured using Glycogen Assay Kit (Sigma). Liver triglyceride levels were measured using the triglyceride quantification kit (Sigma).

In vivo Isotope Labeling Studies

For continuous infusion experiments, approximately four mice from each group (L-GFP, L-GFP-HFD, L-PKA, and L-PKA-HFD) were catheterized on the right jugular vein [42] and recovered more than 6 days. Catheterized mice were fasted for 12 h and then transferred to new cages without food and infused for 6 h. During infusion, a tether and swivel system were used to allow mice free movement in the cage (Instech Laboratories). Water-soluble isotope-labelled metabolites tracers (Cambridge Isotope Laboratories) were prepared as solutions in sterile normal saline and infused via the catheter at a constant rate (0.1 µl/g body weight/min). 200 mM 6, 6-^{2}H$_2$-glucose, 200 mM ^{13}C$_6$ glucose, 150 mM ^{13}C$_3$ glycerol, 150 mM ^{13}C$_3$-^{2}H$_8$ glycerol or 40 mM ^{13}C$_3$ sodium pyruvate with 360 mM ^{13}C$_3$ lactate were infused. About 30 µl blood were collected by tail vein bleeding at each time point, placed on room temperature in the absence of anticoagulant for 30 minutes and centrifuged at 4 °C to prepare serum. At the end of the last infusion experiment, the mouse was euthanized by cervical dislocation and quickly dissected liver was snap frozen in liquid nitrogen with pre-cooled Wollenberger clamp [79]. Serum and tissue samples were kept at −80 °C until

further extraction.

Frozen liver pieces were ground using a Cryomill (Retsch) and stored at -80° C until extraction. Tissue powder (25 mg each) or serum (10 µl each) was mixed with −20 °C 40:40:20 methanol:acetonitrile:water solution with 0.1% formic acid, followed by vortexing for 10 s, incubation at 4 °C for 10 min, and centrifugation at 4 °C and 16,000 × g for 10 min. The volume of the extraction solution (in µl) was 40× the weight of tissue (in mg) or 25× the volume of serum. The supernatant was transferred to a clean tube, and neutralized with NH_4HCO_3 solution. The mixture was centrifuged again at 4 °C and 16,000 × g for 10 min. The supernatant was then transferred to another clean tube for mass spectrometry (LC-MS) analysis.

Hyperinsulinemic-euglycemic clamp

Catheterized mice were fasted for 3 hours and then administered an initial bolus of 6, 6-$^2H_2$-glucose (10 mg/kg), followed by continuous infusion of 6, 6-$^2H_2$-glucose (728 µg/kg/min) throughout the entire experiment. Isotopic steady-state of glucose was achieved 3 hours after the onset of infusion, and the first blood samples were collected at this time (t = 0 hour). Immediately after blood collection, insulin was constantly infused at the rate of 8 mU/kg/min. Glucose (50% w/v) was infused at various rates until the blood glucose concentration reached a euglycemia (100 ± 10 mg/dL). Blood samples were taken at t = 3 hour. Serum was prepared for LC-MS as described above.

Glycerol derivatization for LC-MS Analysis

Due to poor ionization of glycerol, an enzymatic derivatization is required to detect

glycerol in LC-MS [43]. Samples containing glycerol were added into 10× volume of

reaction buffer containing 25 mM Tris (pH 8.0), 10 mM Mg^{2+}, 50 mM NaCl, 5 mM

ATP and 2 U/ml glycerol kinase (Sigma-Aldrich G6278) and incubated for 10 minutes

at room temperature. The reaction was quenched with 40:40:20

methanol:acetonitrile:water solution with 0.1% formic acid, and later neutralized with

NH_4HCO_3 solution. The same reaction was also performed on blank to remove

background. The ion counts of glycerol-3-phosphate in blank was subtracted from that

of the derivatized sample.

LC-MS Analysis

The LC-MS method used reversed-phase ion-pairing chromatography coupled with

negative mode electrospray ionization to a stand-alone orbitrap mass spectrometer

(Thermo Scientific) scanning from m/z 85-1,000 at 1 Hz at 100,000 resolution with LC

separation on a Synergi Hydro RP column (150 mm × 2 mm, 2.4 μm particle size,

Phenomenex) using a gradient of solvent A (97%:3% H2O:MeOH with 10 mM

tributylamine and 15 mM acetic acid), and solvent B (100% MeOH). The gradient was

0 min, 0% B; 5 min, 0% B; 7 min, 20% B; 17 min, 80% B; 20 min, 100% B; 23.5 min,

100% B; 24 min, 0% B; 30 min, 0% B. The flow rate was 0 min, 200 μl min^{-1}; 20 min,

200 μl min^{-1}; 20.5 min, 300 μl min^{-1}; 29.5 min, 300 μl min^{-1}; 30 min, 200 μl min^{-1}.

Injection volume was 10 μl and column temperature 25 °C. For phosphate-containing

gluconeogenic intermediates, the extract was dried down under Nitrogen gas and

reconstituted in 100 μl of water for LC-MS analysis. For other metabolites, the extract

was directly transferred to LC-MS sample vial for analysis, which involves a

quadrupole-orbitrap mass spectrometer (Q Exactive Plus, Thermo Fisher Scientific)

operating in negative ion mode coupled to hydrophilic interaction chromatography

via electrospray ionization scanning from m/z 72 to 1,000 at 2 Hz and 70,000

resolution. LC separation was achieved on a XBridge BEH Amide column

(2.1 mm × 150 mm, 2.5 μm particle size, 130 Å pore size; Waters) using a gradient of

solvent A (20 mM ammonium acetate + 20mM ammonium hydroxide in 95:5

water:acetonitrile, pH 9.4) and solvent B (20 mM ammonium acetate + 20mM

ammonium hydroxide in 20:80 water:acetonitrile, pH 9.4). Flow rate was 300 μl

min^{-1}. The gradient was: 0 min, 100% B; 3 min, 100% B; 3.2 min, 90% B; 6.2 min,

90% B; 6.5 min, 80% B; 10.5 min, 80% B; 10.7 min, 70% B; 13.5 min, 70% B;

13.7 min, 45% B; 16 min, 45% B; 16.5 min, 100% B; 22 min, 100% B. Data were

analyzed using the MAVEN software [44]. The ^{13}C isotope natural abundances were

corrected using AccuCor [45].

Metabolomic Analyses

All the heatmaps and principle component analyses were performed on the liver

samples after 12 hours fasting followed by 6 hour infusion of $^{13}C_3$ lactate/pyruvate. The graphs were generated using R and GraphPad Prism software.

Metabolic Flux Analyses

For the calculation of F_{circ} (turnover rate of metabolites), the calculation is based on the enrichment of tracers and the infusion rate at steady state using the following equation:

$$F_{circ} = \text{Infusion rate} * \left(\frac{1}{labeled\ fraction\ of\ tracer} - 1\right) \quad [\text{Eq. 4.1}]$$

The flux modeling is modified from a previously described method [80]. In brief, a flux network is constructed (Supplementary Fig. A3.5a) with the following assumptions:

1. At steady state, all labeled and non-labeled metabolites are completely mixed.

2. The labeled and unlabeled metabolites react identically (i.e. there is no isotope discrimination).

3. All glycerol and lactate that makes glucose are from blood circulation.

4. The state of animal is the same when infused with different tracers.

5. The infusion does not alter the normal physiology of mice.

6. Glycogen, free fatty acid and TCA amino acids are non-recyclable from glucose during fasting.

7. TCA amino acids contribute to GNG via a universal pool of TCA intermediates.

8. Due to the high interconversion rate among pyruvate, lactate and alanine in vivo, the total contribution of these three metabolites can be calculated together as lactate contribution.

Fluxes were calculated in the unit of 10^{-2} nmol product/min. All fluxes occur in the liver except V_{out}, V_{glc}, V_3, V_5, V_6, V_9 and V_{20} which occur in the periphery. V_2, V_5, V_9, V_{13} and V_{19} are input fluxes from glycogen, glycerol (from triglycerides), lactate (including alanine and pyruvate), free fatty acid (FFA) and amino acids (via TCA cycle) respectively. V_{glc} represents the infusion flux from $^{13}C_6$ glucose tracer. V_{11} is pyruvate carboxylase flux that incorporates carbon dioxide. V_{10}, V_{12}, V_{17} and V_{18} are decarboxylase fluxes that release carbon dioxide. V_{flop} is an infinitely large flux to account for the achirality of metabolites. V_3 represents the glycolysis process in peripheral tissue. V_6 represents glycerol synthesis from glucose. V_{20} represents the direct conversion from glycerol to lactate. V_1 is the endogenous glucose production (EGP) flux which equals to the sum of the glucose recycled via the Cori cycle (V_3), glycerol synthesis (V_6) and the net production of glucose (V_{out} - V_{glc}). Therefore, the absolute value of V_1 can be measured as the steady-state glucose turnover rate (F_{circ}) in circulation.

The contribution of amino acids through TCA cycle consists of three components: 1. via oxaloacetate (Asp, Asn); 2. via fumarate or succinyl CoA (Phe, Tyr, Ile, Met, Val,

Thr); 3. via α-ketoglutarate (Gln, Glu, Pro, His, Arg). The average physiological concentrations of amino acids are 13.5 μM Asp, 35.9 μM Asn, 54.1 μM Phe, 46.7 μM Tyr, 73.1 μM Ile, 52.4 μM Met, 178.7 μM Val, 126.2 μM Thr, 25.1 μM Glu, 397.0 μM Gln, 67.4 μM Pro, 49.6 μM His and 93.4 μM Arg [47]. Therefore, the total substrate concentration in the three possible pathways are 49.4, 531.2 and 632.5 μM respectively. Assuming proportional contribution by the three routes, the three sub-fluxes to oxaloacetate, succinate and α-ketoglutarate are 4%, 44% and 52% of V_{19} respectively. The metabolite mass balance leads to the following equations:

$$
\begin{array}{lll}
\text{Glucose:} & V_1 - 0.5V_3 - 0.5V_6 + V_{glc} = V_{out} & \\
\text{G6P:} & V_1 - V_4 = V_2 & \\
\text{DHAP:} & 2V_4 - V_7 = V_8 & \\
\text{Glycerol:} & V_{20} + V_8 - V_6 = V_5 & \\
\text{PEP:} & V_7 - V_{10} = 0 & \\
\text{Pyr:} & V_{11} + V_{12} - V_3 - V_{20} = V_9 & \text{[Eq. 4.2]} \\
\text{Oxa:} & V_{10} + V_{15} + V_{16} - V_{11} - V_{14} = 0.04V_{19} & \\
\text{Ac-CoA:} & V_{16} - V_{12} = V_{13} & \\
\text{Suc:} & V_{14} - V_{15} - V_{17} = 0.44V_{19} & \\
\text{Cit:} & V_{16} - V_{18} = 0 & \\
\text{aKG:} & V_{17} - V_{18} = 0.52V_{19} & \\
\end{array}
$$

Balance of input and output mass leads to the following equation:

$$
\begin{aligned}
6V_{out} = &\ 6V_2 + 6V_{glc} + 3V_5 + 3V_9 + 2V_{13} + 4.52V_{19} \\
&\ - V_{12} - V_{10} - V_{17} - V_{18} + V_{11}
\end{aligned}
\qquad \text{[Eq. 4.3]}
$$

Ten fluxes are designated free fluxes: V_2, V_5, V_8, V_9, V_{12}, V_{13}, V_{15}, V_{19}, V_{20} and V_{glc}.

All other fluxes can be expressed using the free fluxes or known constants ([Eq. 4.4]).

$$
\begin{aligned}
&V_1 = EGP = F_{circ} \\
&V_3 = 2F_{circ} - 2V_2 - V_9 + V_{12} - V_{19} - V_{20} - V_8 \\
&V_4 = F_{circ} - V_2 \\
&V_6 = V_{20} + V_8 - V_5 \\
&V_7 = 2F_{circ} - 2V_2 - V_8 \\
&V_{10} = V_3 + V_9 - V_{12} + V_{19} + V_{20} \\
&V_{11} = V_3 + V_9 - V_{12} + V_{20} \qquad\qquad\text{[Eq. 4.4]} \\
&V_{14} = V_{12} + V_{13} + V_{15} + 0.96V_{19} \\
&V_{16} = V_{12} + V_{13} \\
&V_{17} = V_{12} + V_{13} + 0.52V_{19} \\
&V_{18} = V_{12} + V_{13} \\
&V_{out} = 0.5*(V_5 + V_9 + V_{19} - V_{12}) + V_2 + V_{glc} \\
&V_{flop} = \text{Infinite}
\end{aligned}
$$

Since the labeling patterns of all the input molecules are known (either unlabeled or fully labeled as tracers), the steady-state labeling patterns of all metabolites in the system can be calculated using the EMU approach given any set of the ten fluxes. For $^{13}C_3$-$^2H_8$ glycerol infusion data, only $^{13}C_3$-$^2H_1$ and $^{13}C_3$-$^2H_2$ lactate is calculated using the following equation:

$$
\begin{aligned}
&^{13}C_3\text{-}^2H_1\ \text{lactate} = 0.5V_8*V_3 / (V_1 + V_{glc}) \\
&^{13}C_3\text{-}^2H_2\ \text{lactate} = 0.5V_8*V_3 / (V_1 + V_{glc}) + V_{20} \qquad\text{[Eq. 4.5]} \\
&\text{Fraction of } ^{13}C_3\text{-}^2H_1\ \text{lactate} = ^{13}C_3\text{-}^2H_1\ \text{lactate} / (^{13}C_3\text{-}^2H_1\ \text{lactate} + {}^{13}C_3\text{-}^2H_2\ \text{lactate}) \\
&\text{Fraction of } ^{13}C_3\text{-}^2H_2\ \text{lactate} = ^{13}C_3\text{-}^2H_2\ \text{lactate} / (^{13}C_3\text{-}^2H_1\ \text{lactate} + {}^{13}C_3\text{-}^2H_2\ \text{lactate})
\end{aligned}
$$

The calculated labeling patterns were compared to the measured ones with equal weight. The best estimated flux set was obtained by minimizing the sum of squared residues (SSR) between the calculated and measured labeling patterns. The measured labeling patterns of glucose, glycerol and pyruvate under four tracers ($^{13}C_3$ glycerol, $^{13}C_3$-$^2H_8$ glycerol, $^{13}C_3$ lactate and $^{13}C_6$ glucose) were used in this process. The numerical simulation of labeling patterns was achieved in R software and the optimization was achieved with DEoptim package [48]. 95% confidence intervals were calculated by (1) move one target flux away from the best-fit value by a small step (2) choose a combination of the other fluxes that minimize the increase of SSR, (3) calculate the new SSR and repeat step (1) to (3) until the new SSR reached the cutoff for 95% confidence interval [49]. The goodness of fit was tested by chi-square test, $X^2_{0.05}$ (df = 18) = 28.8693, which is equivalent to an SSR value of 0.00288693. The 18 degrees of freedom are based on 28 measurements (labeling fractions of three metabolites under four tracers) and having 10 unknown fluxes; 28 - 10 = 18.

To illustrate the direct contribution and origin of carbon better, we simplified the pathways into the 4-pool network (Supplementary Fig. A3.5b). For convenience, all units of fluxes were normalized to 10^{-2} nmol C/min. U_1 and U_2 are input fluxes from glycerol and lactate respectively. U_5 and U_6 represent fluxes that glucose making the glycerol and lactate respectively. U_7, U_8 and U_3 represent the fluxes that glycerol, lactate and glycogen making glucose respectively. U_9 represents the pyruvate

dehydrogenase (PDH) flux that consumes lactate in TCA cycle. U_{10} represents the flux

glycerol directly making lactate. U_4 is the glucose output which equals to the net

production of glucose. By definition, all fluxes can be represented by the equivalent

fluxes in the EMU model:

The direct contribution from glycerol and lactate are calculated as the relative ratio of

U_7 and U_8 (green arrows; supplementary Fig. A3.5b). The origin of carbon from

glycerol and lactate are calculated as the relative ratio of U_1 and U_2 (purple arrows;

supplementary Fig. A3.5b).

$$
\begin{array}{lllll}
U_1 = 3V_5 & U_2 = 3V_9 & U_3 = 6V_2 & U_4 = 6(V_{out} - V_{glc}) & U_5 = 3V_6 \\
U_6 = 3V_3 & U_7 = 3V_8 & U_8 = 3V_{11} & U_9 = 3V_{12} & U_{10} = 3V_{20}
\end{array}
\qquad \text{[Eq. 4.6]}
$$

G6PC Activity Assay

The procedure of G6PC activity assay was previously described [81]. In brief, frozen

liver samples were homogenized in buffers containing 10 mM HEPES and 0.25 M

sucrose, pH 7.4 (8 μl/mg tissue) by Bullet Blender (Next Advance, Inc., NY). Total

phosphatase activity was assayed in homogenates by providing G6P (20 mM, Sigma)

as a substrate and allowing the reaction to proceed for 10 minutes at 30°C, pH 7.3. Non-

specific phosphatase activity was assayed by providing β-glycerophosphate (20 mM,

Sigma) as substrate. Released Pi was determined by colorimetric assay. The specific

activity of G6PC was obtained by subtracting the non-specific basal phosphatase

activity to the total activity.

In vivo Induction of *G6pc* by Glycerol

All mice were fasted overnight (12 hours) and then injected i.p. with a bolus of glycerol (9.1 mmole/kg; Sigma) or saline. One hour after the injection, mice were sacrificed and livers were snap frozen and kept at -80 ° C until RNA extraction.

Human Primary Hepatocyte Studies

Fresh human primary hepatocytes (Lonza) were obtained and cultured following the manufacture's recommendation. Cells were starved for 3 hours in an insulin free Hepatocyte Maintenance Media (Lonza) and then treated with forskolin (20 μM) and/or glycerol (10 mM) for 6 hours. Cells were then harvested and proceed for RNA analysis.

Statistical Analysis

Statistical analyses were performed using the GraphPad Prism software, version 6.07.

Data and Code availability

All data and computer code are available from the authors upon reasonable request.

Results

L-PKA mice exhibit increased fasting glucose and expression of gluconeogenic genes

In order to model activation of hepatic gluconeogenesis through the glucagon signaling pathway [15], we knocked-down the *Prkar1α* gene, which encodes the regulatory subunit type 1α of cAMP-dependent protein kinase, in the liver using adenoviral CRE recombinase (Ad-CRE). As others have shown, this results in constitutive hepatic PKA activity [77, 83]. Compared to control mice injected with an adenovirus encoding GFP (L-GFP), mice injected with an adenovirus encoding CRE recombinase (L-PKA) had significantly reduced PRKAR1α (R1α) expression in the liver but not in skeletal muscle (Supplementary Fig. A3.1a). The L-PKA mice also showed elevated blood glucose levels in the fasted and refed state (Fig. 4.1a), which mimicked the phenotype of hyperglucagonemia.

HFD treatment further enhance fasting blood glucose and endogenous glucose production in L-PKA mice

To obtain a model of both diet-induced obesity and elevated glucagon signaling, we first placed male *Prkar1a*$^{fl/fl}$ mice on either a normal chow or a HFD (60% kcal fat) at 4 weeks of age. After 11 weeks of these diets, mice were treated with either Ad-CRE or control Ad-GFP virus to generate four experimental groups: normal glucagon signaling with normal chow or HFD (L-GFP and L-GFP-HFD, respectively) and PKA activation

groups with normal chow or HFD (L-PKA and L-PKA-HFD, respectively) (Supplementary Fig. A3.1b). Both HFD groups displayed similar increases in body weight and epididymal fat mass (Supplementary Fig. A3.1c and d).

Interestingly, the L-PKA-HFD group displayed a more than additive increase in fasting glucose levels compared to either L-GFP-HFD or L-PKA group (Fig. 4.1a), demonstrating that PKA activation and HFD work together to elevate fasting glucose levels. We hypothesized that the higher fasting glucose level in L-PKA-HFD mice was caused by increased glucose production. To test this possibility, we first measured the liver glycogen level after overnight fasting (Supplementary Fig. A3.1e). Though L-GFP-HFD mice showed higher glycogen level than L-GFP mice, both L-PKA and L-PKA-HFD mice showed similar glycogen levels when compared to L-GFP mice, suggesting the enhanced fasting glucose level in L-PKA-HFD mice is unlikely due to increased glycogen levels.
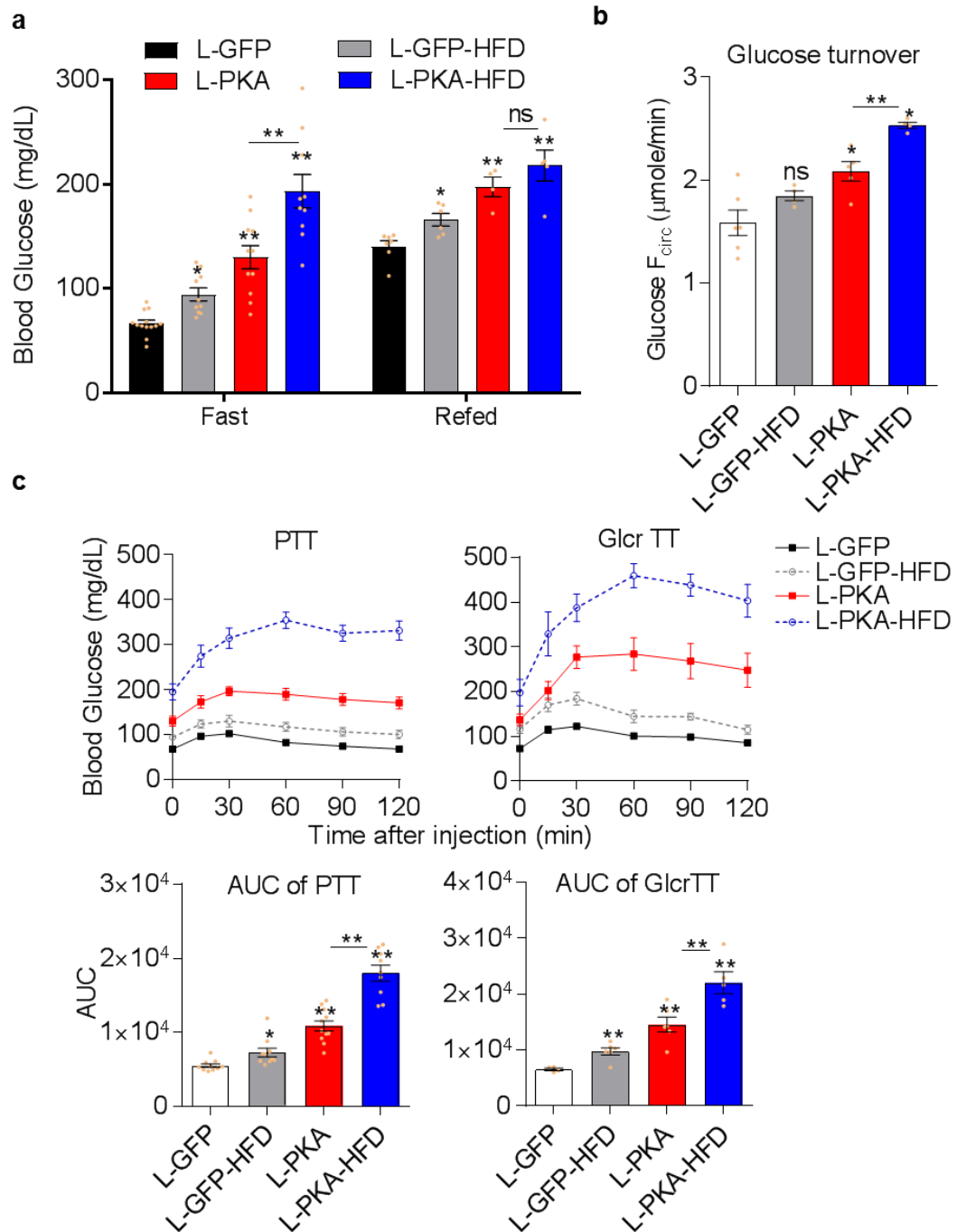
Figure 4.1 | L-PKA-HFD mice have increased fasting glucose and endogenous glucose production. a, Glucose level after 12-hour fasting (fast) or 12-hour fasting followed by 2-hour refeeding (refed); n = 10-13 for fasting and n = 4-7 for refeeding. **b,** Endogenous production rate (F_{circ}) of glucose after 12-hour fasting; n= 4-6. **c,** glucose level following pyruvate or glycerol bolus injection (i.p., 9.1 mmole/kg body weight); For pyruvate, n= 9-11; For glycerol, n = 4-6; graphs of area under the curve (AUC) are used to compare among groups. In all figures, data are mean ± s.e.m.; n = number of mice, **P<0.01; *P<0.05; ns, not significant by one-way ANOVA. All comparisons are against L-GFP in the same condition unless indicated otherwise.

We next measured the endogenous glucose production rate (EGPR or, in the fasted state, equivalently F_{circ}) after overnight fasting using a non-perturbative infusion of 6,6-^{2}H$_2$-glucose [84]. 6,6-^{2}H$_2$-glucose is a reliable tracer for measuring EGPR because it is a non-recyclable substrate, which by entering the TCA cycle loses the ^{2}H labeling through tautomerization and only generates unlabeled glucose through gluconeogenesis [84]. Therefore, when isotope labeling steady state is achieved, the EGPR of glucose can be determined from the infusion rate (Supplementary Fig. A3.2a) and the fraction of 6,6-^{2}H$_2$-glucose in the serum (Supplementary Fig. A3.2b). We found that the L-PKA mice showed an increased EGPR (F_{circ}) compared to the L-GFP mice (Fig. 4.1b; Supplementary Fig. A3.2c), demonstrating higher gluconeogenic fluxes when PKA is activated. In the HFD groups, F_{circ} measurements are complicated by obesity, which results in alterations in body weight and composition. Accordingly, although F_{circ} does not increase on a per gram basis in the L-PKA-HFD versus the L-PKA group (Supplementary Fig. A3.2c), it does so on a per mouse basis (Fig. 4.1b), which we consider most relevant as liver weight is not different among the groups (Supplementary Fig. A3.2d). Consistent with these findings, the L-PKA-HFD mice also showed the highest glucose production after intraperitoneal (i.p.) injection of pyruvate or glycerol (Fig. 4.1c).

Both L-PKA and L-PKA-HFD mice are insulin sensitive

HFD feeding could cause chronic hyperinsulinemia and induce insulin resistance [85].

To test whether the elevated gluconeogenesis in L-PKA-HFD mice was caused by insulin resistance, we investigated insulin signaling in all four groups of mice. After overnight fasting, L-GFP-HFD, L-PKA, and L-PKA-HFD mice all showed increased insulin levels compared to the L-GFP group (Supplementary Fig. A3.1f), suggesting all three groups produced more insulin in response to elevated fasting glucose levels. Unlike L-GFP-HFD mice that showed significant insulin resistance as shown in insulin tolerance test (ITT, Fig. 4.2a; Supplementary Fig. A3.1g) and AKT phosphorylation studies (Fig. 4.2b&c), both L-PKA and L-PKA-HFD mice showed similar insulin sensitivity compared to L-GFP mice (Fig. 4.2a-c).

To confirm these findings, we performed a hyperinsulinemic-euglycemic clamp with 6,6-^{2}H$_2$-glucose infused simultaneously [86, 87]. Neither L-PKA nor L-PKA-HFD mice showed significant difference in the glucose infusion rate compared to L-GFP group (Fig. 4.2d), suggesting preserved insulin sensitivity. Interestingly, the EGPR measurements revealed that the endogenous glucose production in L-PKA and L-PKA-HFD was elevated basally and not suppressed by hyperinsulinemia (Fig. 4.2e), suggesting that PKA activation was unaffected by insulin signaling in the liver of L-PKA and L-PKA-HFD mice. Together, these data indicated that L-PKA and L-PKA-HFD mice were insulin sensitive in peripheral tissues, while endogenous glucose production was unaffected by hyperinsulinemia. Therefore, changes in insulin sensitivity did not explain the difference between L-PKA and L-PKA-HFD mice.
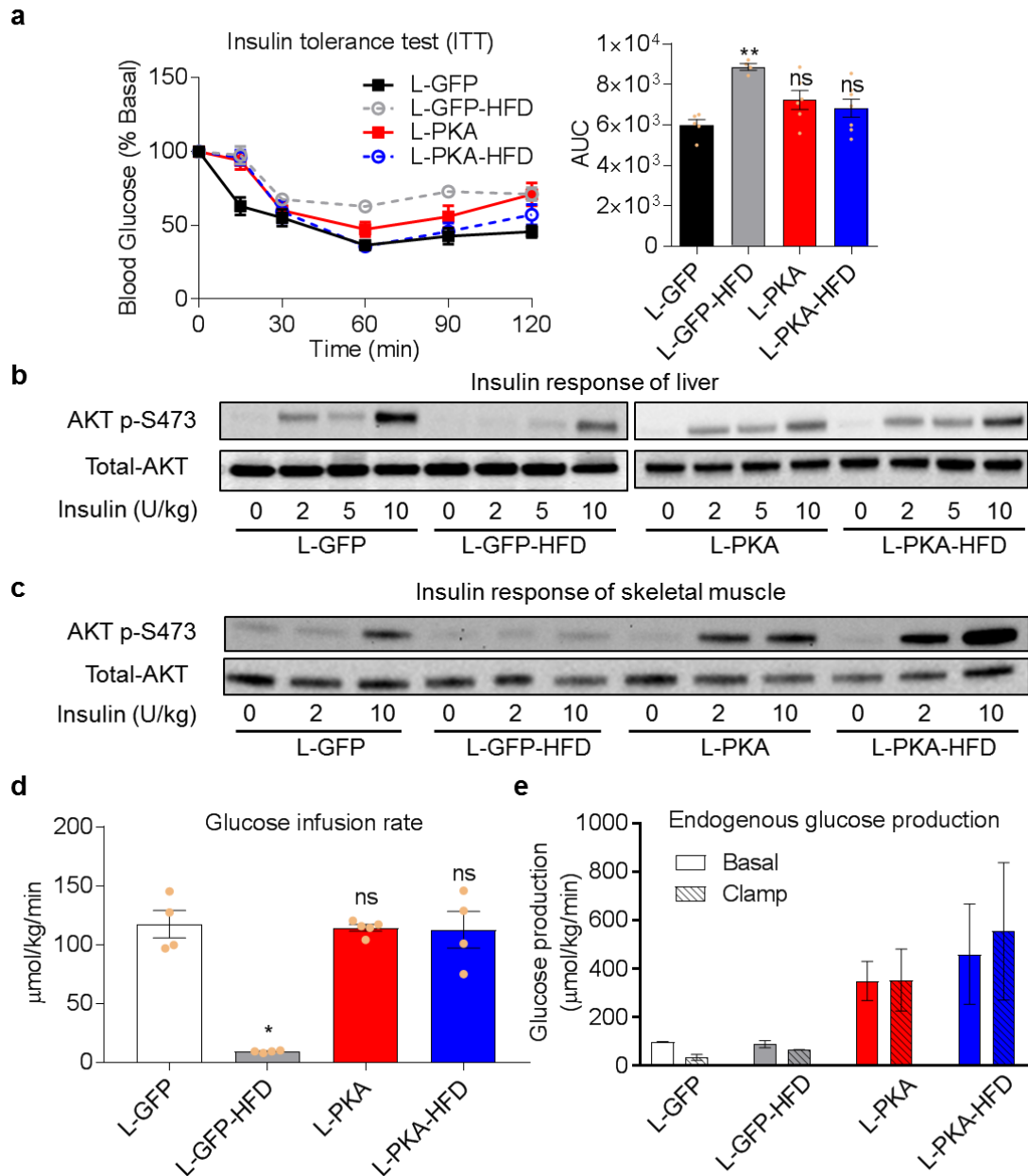
Figure 4.2 | HFD does not induce insulin resistance in L-PKA mice. a, Insulin tolerance test; n = 5-7; Graphs of area under the curve (AUC) are used to compare among groups. **b-c,** Western blot images showing levels of AKT p-S473 and total AKT in livers (**b**) and skeletal muscle (**c**) of the indicated groups 10 minutes following an injection (i.p.) with different dosages of insulin. **d-e,** Hyperinsulinemic-euglycemic clamp (n = 4). **d,** Glucose infusion rate under hyperinsulinemic clamp. **e,** Endogenous glucose production rate. All mice were fasted for 6 hours before experiments. Data are mean ± s.e.m.; n= number of mice; **P<0.01; *P<0.05; ns, not significant by one-way ANOVA. All comparisons are against L-GFP.

L-PKA-HFD mice exhibit increased glycerol levels compared to L-PKA mice

Availability of gluconeogenic substrates is one mechanism regulating gluconeogenesis as reviewed by Petersen *et al.* [29]. To test whether substrate availability might explain our results, we generated the liver metabolomic profiles in all four groups of mice after overnight fasting (Fig. 4.3a). Liver samples from the same genetic groups were clustered together (Fig. 4.3a), suggesting that the presence of activated PKA had the greatest impact on the liver metabolome. To investigate these findings further, we performed a principal component analysis (PCA). On the score plot of PCA (Fig. 4.3b), the four sample groups showed separation along the first principal component (PC1, x-axis), which suggest that HFD shifted the metabolome in the same direction as PKA activation did. Meanwhile, the effect of PKA was greater than that of diet. The PCA loading plot helped us uncover the metabolites that caused the separation of the four groups on the score plot (Supplementary Fig. A3.3a). We observed a general trend that the TCA cycle intermediates had positive loading and gluconeogenic substrates including glycerol, pyruvate and amino acids had negative loading, which suggest HFD feeding and PKA activation increased the levels of TCA intermediates and decreased the levels of gluconeogenic substrates.
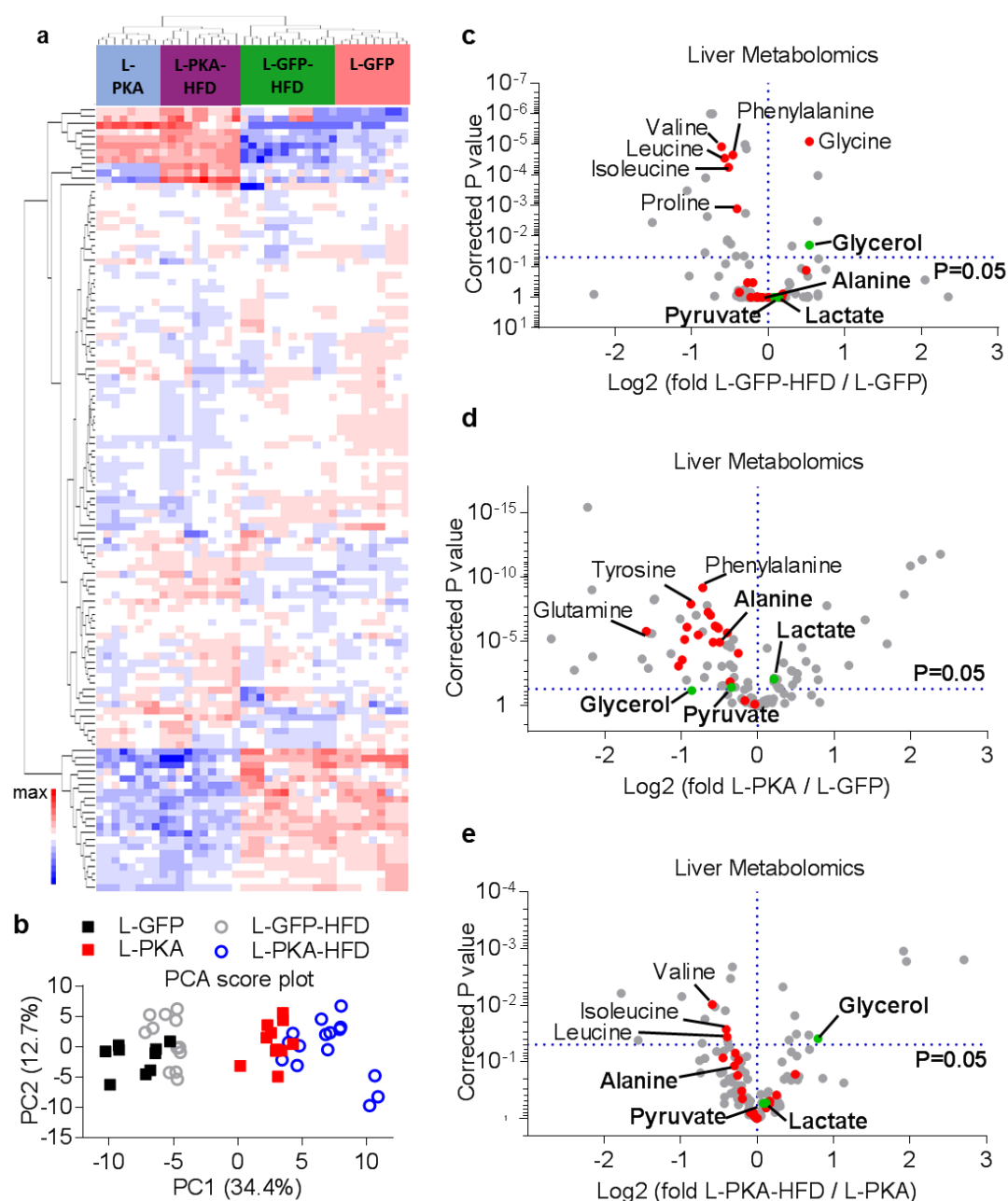
Figure 4.3 | Comparison of metabolomic profiles. a, Heat-map of liver metabolite clusters. Each column represents one liver sample and each row represents one metabolites. **b,** Principle component analysis (PCA) of metabolomic profile. Each dot represents one liver sample. **c-e,** Volcano plot of liver metabolomic fold changes. Each dot represents one metabolite: red, amino acids; green, non-amino acid gluconeogenic substrates. P values were calculated using two-sided Student's t-test and corrected for multiple comparisons using the Holm-Sidak method. P<0.05 is considered significant. n= 3-5 mice, 2-3 liver samples per mice.

We then identified all liver metabolites that showed significantly different concentrations between different group pairs (Fig. 4.3c-e). Consistent with the PCA analysis, both HFD feeding and PKA activation decreased most gluconeogenic substrates with two exceptions: 1) HFD increased the concentration of glycine and glycerol (Fig. 4.3c), and 2) PKA slightly increased the concentration of lactate (Fig. 4.3d). Interestingly, the L-PKA-HFD group also showed increased glycerol level when compared to L-PKA group. To confirm this finding, we measured the glycerol level in both liver and serum using a colorimetric method and found the same trend as measured using mass spectrometry (Supplementary Fig. A3.3b&c). Together, these findings suggest substrate availability – especially glycerol and lactate – may play important roles in the gluconeogenesis of L-PKA-HFD mice.

PKA activation changes the destination of glycerol

Given that metabolomic profiling identified glycerol and lactate as potentially important gluconeogenic substrates in L-PKA-HFD mice, we studied their relative contributions to gluconeogenesis *in vivo* using non-perturbative $^{13}C_3$-glycerol or $^{13}C_3$-sodium lactate (mixed with $^{13}C_3$-sodium pyruvate in physiological ratio to maintain NAD/NADH balance) infusion in mice after a 12-hour fast (Fig. 4.4). After infusion for 6 hours, all isotopologues of serum glucose reached steady state from both tracers (Supplementary Fig. A3.4).
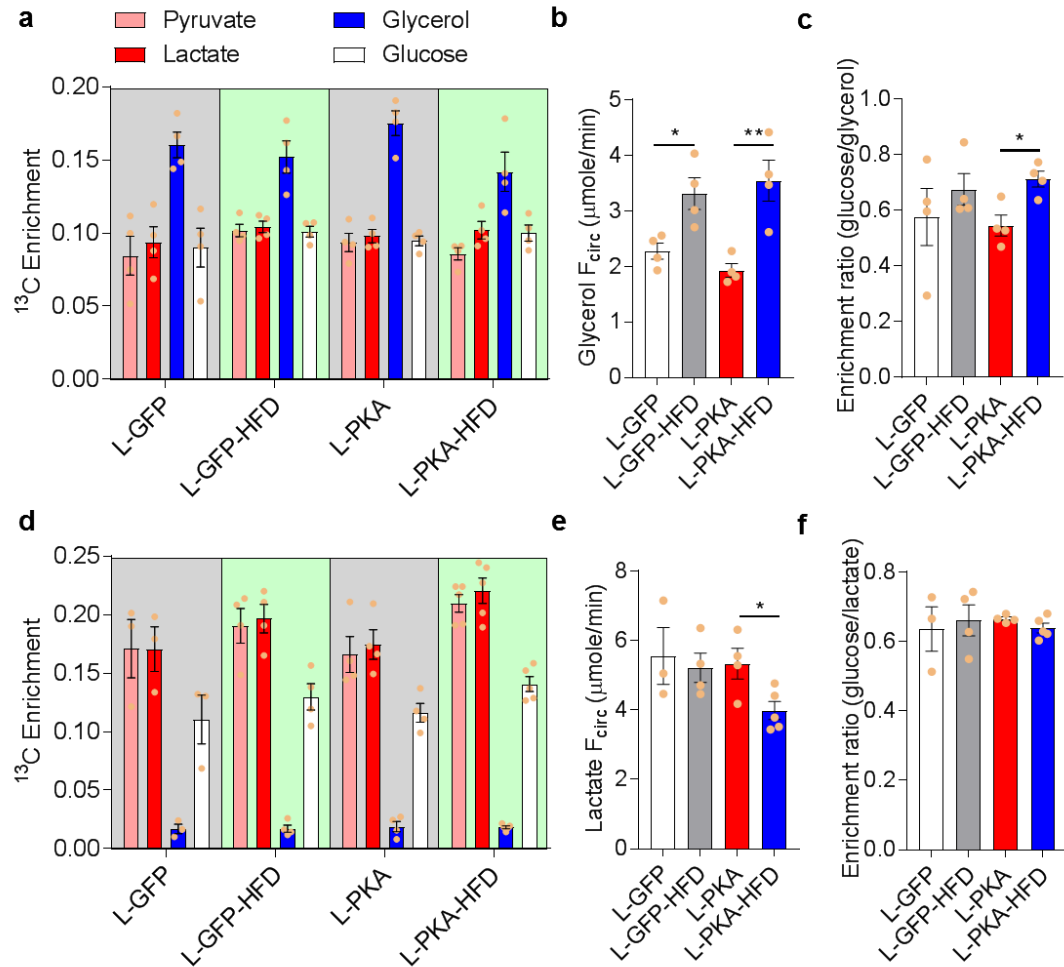
Figure 4.4 | Glycerol and lactate as two major gluconeogenic carbon source at fasting. a-c, Infusion of $^{13}C_3$ glycerol. **a,** ^{13}C enrichment of serum metabolites at steady state. **b,** Turnover rate of circulating glycerol (F_{circ}). **c,** Ratio of ^{13}C enrichment (glucose over glycerol). **d-f,** Infusion of $^{13}C_3$ sodium pyruvate and $^{13}C_3$ sodium lactate mixed in physiological ratio. **d,** ^{13}C enrichment of serum metabolite **e,** Turnover rate of circulating lactate (F_{circ}). **f,** Ratio of ^{13}C enrichment (glucose over lactate). All animals were fasted for 12 hours followed by a 6-hour infusion to reach steady state. For glycerol infusion, n = 4. For lactate infusion, n = 3-5. All data are expressed as mean ± s.e.m. **P<0.01; *P<0.01; *P<0.05 by one-way ANOVA. n= number of mice.

Both L-GFP-HFD and L-PKA-HFD mice showed higher glycerol turnover rate (F_{circ}) than their corresponding non-HFD control (Fig. 4.4b), indicating a potentially important role for glycerol in supporting a higher gluconeogenic flux in HFD mice. Because glycerol was the only ^{13}C source at steady state conditions, the fractional

contribution of glycerol to glucose production can be roughly estimated based on the relative average carbon enrichment in circulating glucose versus glycerol (Fig. 4.4c). We found that glycerol contributed approximately 55-70% of glucose carbon. The fractional contribution of glycerol to gluconeogenesis tended to be higher in L-GFP-HFD compared to L-GFP mice and was significantly increased in L-PKA-HFD compared to L-PKA mice.

Such high gluconeogenic contribution from glycerol was unexpected, since lactate/pyruvate have been previously described as the major substrates for gluconeogenesis [31, 32]. Indeed, lactate contributed around 65% of glucose carbon and this fraction did not differ significantly across groups (Fig. 4.4f), although a decrease of lactate F_{circ} was observed in L-PKA-HFD group (Fig. 4.4e). How can both lactate/pyruvate and glycerol contribute more than half of glucose carbon? Because circulating lactate/pyruvate can be labeled from glycerol too (Fig. 4.4a). Thus, a significant proportion of the lactate that being used to drive gluconeogenesis is originally from glycerol (Fig. 4.5a). In contrast, minimal glycerol was labeled by lactate/pyruvate tracer (Fig. 4.4d), suggesting carbon flow from glycerol to lactate is significantly higher than in the opposite direction.
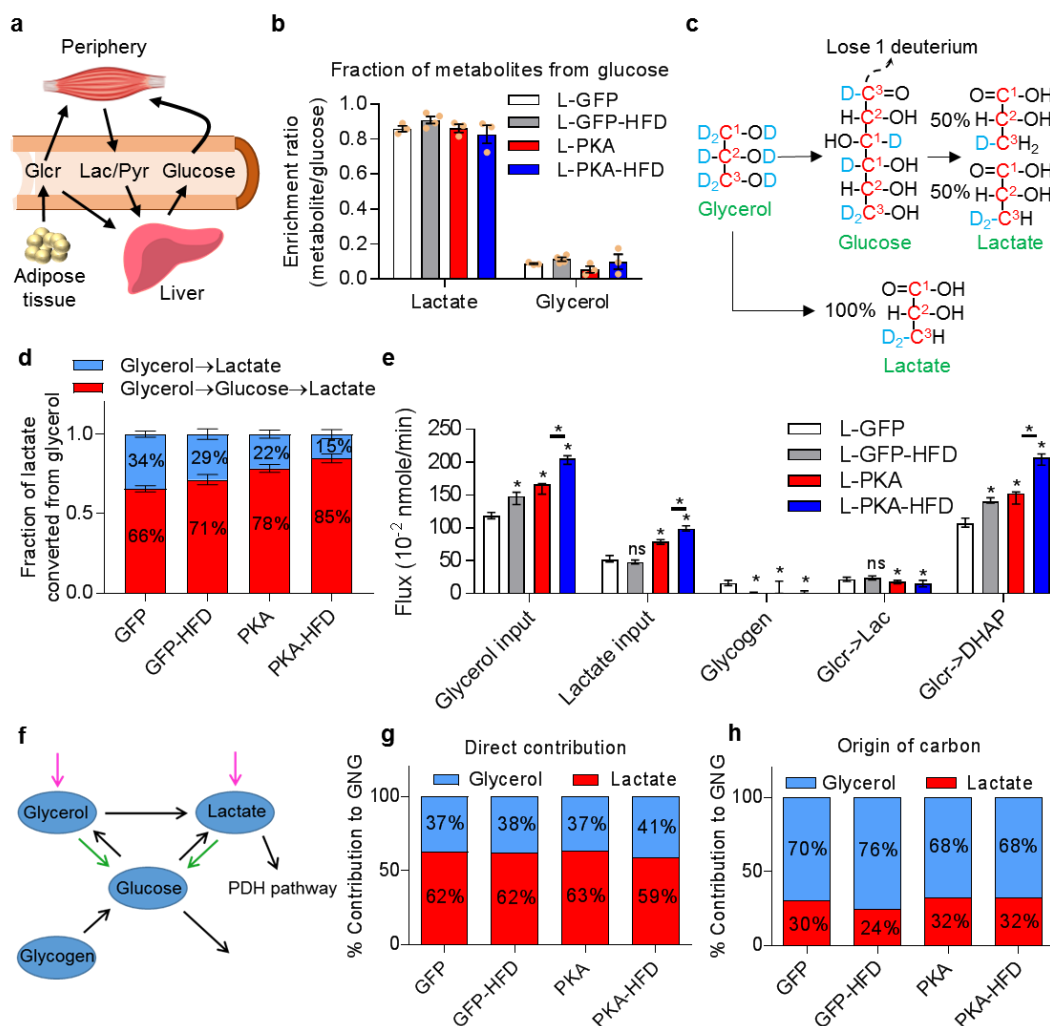
Figure 4.5 | L-PKA and L-PKA-HFD mice exhibit increase in gluconeogenic flux from both glycerol and lactate. a, Illustration of the roles of lactate/pyruvate (Lac/Pyr) and glycerol (Glcr) in gluconeogenesis. **b,** Fraction of lactate and glycerol from glucose measured as enrichment ratio (metabolite/glucose) after $^{13}C_6$ glucose infusion; n = 3-4. **c,** $^{13}C_3$-$^2H_8$ glycerol take direct and indirect paths to make different lactate isotopologues. ^{13}C and deuterium (^2H) atoms are shown in red and blue respectively. **d,** Fraction of lactate converted from glycerol measured by $^{13}C_3$-$^2H_8$ glycerol infusion experiment; n = 3-5. **e,** Estimated fluxes in gluconeogenesis pathway. **f,** Summarized gluconeogenic network; the direct and overall contribution fluxes are shown in green and purple respectively. **g,** Direct gluconeogenic contribution from glycerol and lactate. **h,** Origin of carbon from glycerol and lactate. Data are mean ± s.e.m in **b&d** and best-fit value ± 95% confidence interval in **e**. *P<0.05; ns, not significant. All comparisons are against L-GFP unless indicated otherwise. PDH, pyruvate dehydrogenase; DHAP, dihydroxyacetone phosphate. See also Supplementary Fig. A3.5&A3.6

One possible pathway by which glycerol enters gluconeogenesis is through lactate. In peripheral tissues, glycerol is phosphorylated and oxidized to dihydroxyacetone phosphate (DHAP), which then enters glycolysis to become pyruvate and lactate. However, glucose produced from $^{13}C_3$ glycerol and $^{13}C_3$ lactate/pyruvate showed different labeling patterns. Glucose generated from the $^{13}C_3$ lactate/pyruvate tracer showed mixed labeling fractions of M+3/M+2/M+1 (Supplementary Fig. A3.4b). The partial labeling comes from the fact that lactate and pyruvate enter the TCA cycle and undergo extensive carbon shuffling [88]. On the other hand, glucose generated from the $^{13}C_3$ glycerol tracer was mainly M+3 labeled (Supplementary Fig. A3.4a). If glycerol contributes to gluconeogenesis mainly through lactate, the $^{13}C_3$ glycerol tracer would have generated similar labeling patterns as that generated from $^{13}C_3$ lactate/pyruvate tracer. In fact, the dominant M+3 labeled fraction suggests glycerol can synthesize glucose independently from lactate and TCA cycle carbon shuffling. Given that glycerol largely keeps its 3-carbon backbone intact, direct glucose production from glycerol is suggested.

We next aimed to quantitatively investigate the glycerol contribution to glucose production, either through a direct pathway in liver or through an indirect lactate production in peripheral tissues. Unfortunately, ^{13}C tracers are insufficient to accurately quantify these two pathways because the carbon labeling patterns are preserved in Cori cycle (glucose→lactate→glucose, Fig. 4.4f & Fig. 4.5b) [80]. To solve this problem,

we used a $^{13}C_3$-$^2H_8$-glycerol tracer to investigate the direct and indirect glucose production pathways. The ^2H labeling pattern provided additional information beyond that provided by the ^{13}C tracer. Lactate generated from the glycerol $\rightarrow$ glucose $\rightarrow$ lactate pathway would yield 50% $^{13}C_3$-$^2H_2$ and 50% $^{13}C_3$-$^2H_1$ labeling, since one deuterium is lost on C-1 of glucose (Fig. 4.5c). In contrast, lactate generated from the glycerol $\rightarrow$ lactate pathway would yield 100% $^{13}C_3$-$^2H_2$ labeling. Therefore, by analyzing the ratio of $^{13}C_3$-$^2H_2$ and $^{13}C_3$-$^2H_1$ labeled lactate, we can calculate the relative contribution of these two pathways (Fig. 4.5d). Our analysis suggests in the fasting state, the glycerol $\rightarrow$ glucose $\rightarrow$ lactate pathway yielded 66% of the lactate made from glycerol and this proportion increased to 71%, 78% and 85% in L-GFP-HFD, L-PKA and L-PKA-HFD mice respectively. In all four groups, the glycerol $\rightarrow$ glucose $\rightarrow$ lactate pathway is the preferred pathway.

L-PKA and L-PKA-HFD mice exhibit increase in gluconeogenic flux from both glycerol and lactate

Knowing this information, we established the gluconeogenic contribution from different substrates using a modified metabolic flux analysis (MFA) model we recently published [80]. An MFA seeks the combination of metabolic fluxes which generates metabolite labeling patterns that best fit experimental observations [89-91] (Supplementary Fig. A3.5a). Using this method, we estimated the critical fluxes in gluconeogenic pathway (Fig. 4.5e; Supplementary Fig. A3.5a). L-GFP-HFD mice

showed increased glycerol input flux with unchanged lactate input flux when compared to L-GFP mice. In contrast, L-PKA mice showed increases in both glycerol and lactate input flux when compared to L-GFP mice. Interestingly, L-PKA-HFD mice showed a further increase in not only glycerol but also lactate input flux when compared to L-PKA mice. Both L-PKA and L-PKA-HFD mice showed a decrease in the glycerol → lactate flux, suggesting PKA activation directs more glycerol to glucose in the liver rather than to lactate.

To illustrate substrate contribution better, we summarized all the fluxes into a 4-pool network (Fig. 4.5f; Supplementary Fig. A3.5b & A3.6) and calculated the direct contribution and the origin of carbon from all substrates (Fig. 4.5g&h). To assess gluconeogenesis only, the glycogen flux is excluded from the calculation. The direct contribution is the relative ratio of the two fluxes directly making glucose (green arrows, Fig. 4.5f; Supplementary Fig. A3.6) while the origin of carbon is the relative ratio of the two original input fluxes (purple arrows, Fig. 4.5f; Supplementary Fig. A3.6). In all four groups, lactate exhibited the highest direct contribution to gluconeogenesis (Fig. 4.5g) but more of the gluconeogenic carbon originated from glycerol (Fig. 4.5h). Consistent with the flux data, glycerol but not lactate input flux increased in L-GFP-HFD mice (Fig. 4.5e) and the origin of carbon in L-GFP-HFD mice favored glycerol (Fig. 4.5h). In contrast, L-PKA mice demonstrated increases in both glycerol and lactate flux, causing almost no change in relative contributions compared to L-GFP mice.

Similarly, when L-PKA-HFD mice were compared with L-PKA mice, both glycerol

and lactate fluxes increased proportionally, although in absolute terms the glycerol flux

increased much more than the lactate flux.
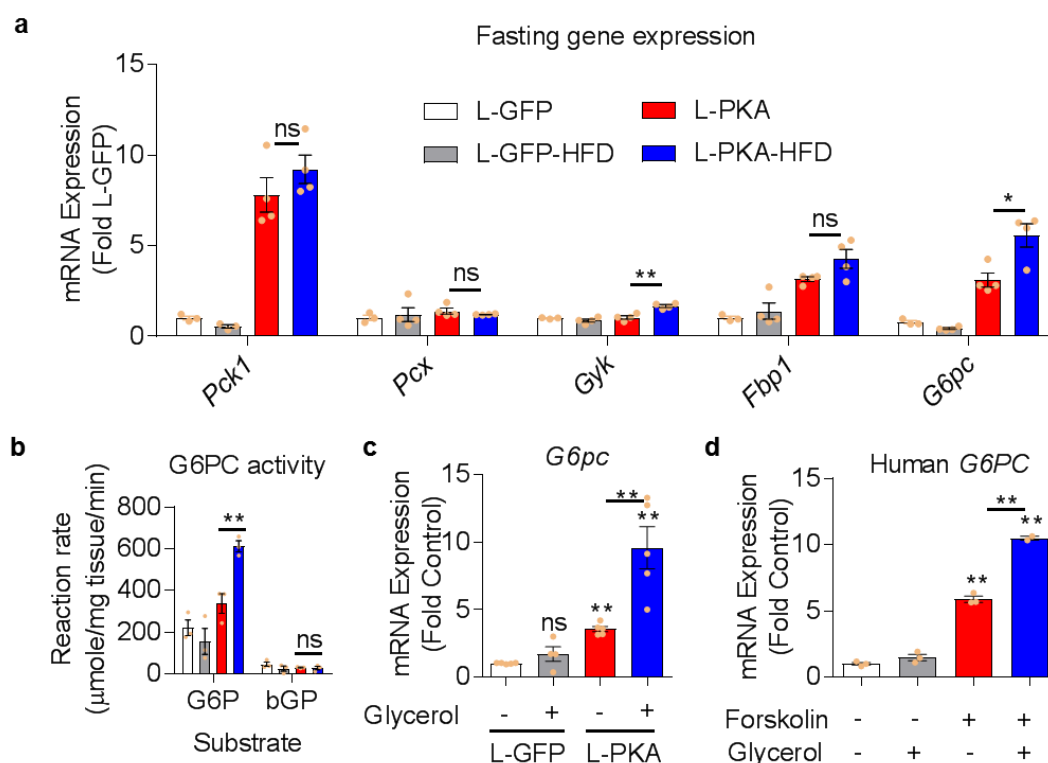
Figure 4.6 | *G6pc* gene expression is further induced by glycerol in L-PKA-HFD mice. a, Fasting gene expression of *Pck1*, *Pcx*, *Gyk*, *Fbp1* and *G6pc* in the liver; n = 3-4; Expression levels are normalized to beta actin and expressed as fold change to L-GFP controls. **b,** In vitro G6PC activity assay of liver extract; G6P or β-glycerophosphate (bGP) were provided as substrates to measure the specific and non-specific phosphatase activity of G6PC respectively; n=3 mice per group. **c,** Gene expression of *G6pc* one hour after the injection of glycerol or saline; n = 4-5; Expression levels are normalized to beta actin and expressed as fold change to L-GFP controls injected with saline. **d,** Gene expression of *G6PC* in human primary hepatocytes after 6-hour treatment of forskolin and/or glycerol; n= 2-3 cell population per group. In all figures, data are mean ± s.e.m.; **P<0.01; *P<0.05; ns, not significant by one-way ANOVA. All comparisons are against the control group (without glycerol or PKA activation) unless indicated otherwise.

G6pc gene expression is further induced by glycerol metabolism in L-PKA-HFD mice

To explore further the mechanism responsible for higher gluconeogenesis in L-PKA-HFD mice, we characterized the expression patterns of major gluconeogenic genes under fasting conditions (Fig. 4.6a). When L-PKA-HFD and L-PKA mice were compared, we observed no significant differences in the expression of genes relevant to pyruvate metabolism such as *Pck1* and *Pcx*. In contrast L-PKA-HFD mice exhibited an increase of ~60% and ~100% in *Gyk* and *G6pc* expression, respectively, compared to L-PKA mice. Since G6PC is a rate-limiting enzyme in gluconeogenesis, we hypothesized that increased *G6pc* expression contributes to the elevated hepatic glucose production. To test this hypothesis, we performed a G6PC activity assay in liver lysates and found that L-PKA-HFD mice had significantly higher G6PC activity when compared to those of L-PKA mice (Fig. 4.6b). These data are consistent with the result from pyruvate and glycerol tolerance tests (Fig. 4.1c) showing that L-PKA-HFD mice had a higher capacity for glucose production than L-PKA mice. Interestingly, increased glycerol metabolism has been shown to upregulate *G6pc* expression in primary hepatocytes [82]. Since G6PC is primarily regulated at the transcriptional level [92] and L-PKA-HFD mice showed significantly higher hepatic glycerol levels than L-PKA mice (Fig. 4.3e; Supplementary Fig. A3.3b&c), we hypothesized that the increased *G6pc* expression observed in the L-PKA-HFD was caused by the stimulatory effect of glycerol on *G6pc* expression. To test this hypothesis, we injected fasting L-GFP and L-

PKA mice with glycerol; and one hour following the injection, the livers of L-PKA mice exhibited a robust elevation in *G6pc* gene expression (Fig. 4.6c). This effect was not seen in similarly injected L-GFP mice, suggesting that PKA activation and glycerol work together to increase *G6pc* expression. The effect was also observed in human primary hepatocytes treated with forskolin and/or glycerol (Fig. 4.6d). Together, these results confirmed that glycerol metabolism regulates *G6pc* preferentially in the presence of increased PKA activity.

Hepatic *Gyk* knockdown reduces hyperglycemia in L-GFP-HFD and L-PKA-HFD mice

After establishing glycerol's critical role in hepatic gluconeogenesis, we tested whether blocking glycerol metabolism in the liver would correct hyperglycemia and activated gluconeogenesis in L-GFP-HFD and L-PKA-HFD mice. We injected either a control (sh-NC) or *Gyk* adenoviral shRNA (sh-Gyk) and found that knockdown of hepatic *Gyk* successfully neutralized the HFD effect on fasting glucose level (Fig. 4.7a) and *G6pc* expression (Fig. 4.7b). Interestingly, the decreased *G6pc* expression in L-PKA-HFD with *Gyk* knock down was associated with increased glycerol (Supplementary Fig. A3.7a), suggesting it was not glycerol itself but the metabolism of glycerol that upregulated *G6pc*. In addition, *Gyk* expression in muscle and kidney was not affected by the knock-down (Supplementary Fig. A3.7b). Moreover, hepatic *Gyk* knockdown normalized glucose production from glycerol in both L-GFP-HFD and L-PKA-HFD

background (Fig. 4.7c). Importantly, hepatic *Gyk* knockdown also reduced glucose production from pyruvate in L-PKA-HFD mice, which suggests a central role of glycerol metabolism in regulating gluconeogenesis via regulation of *G6pc*.
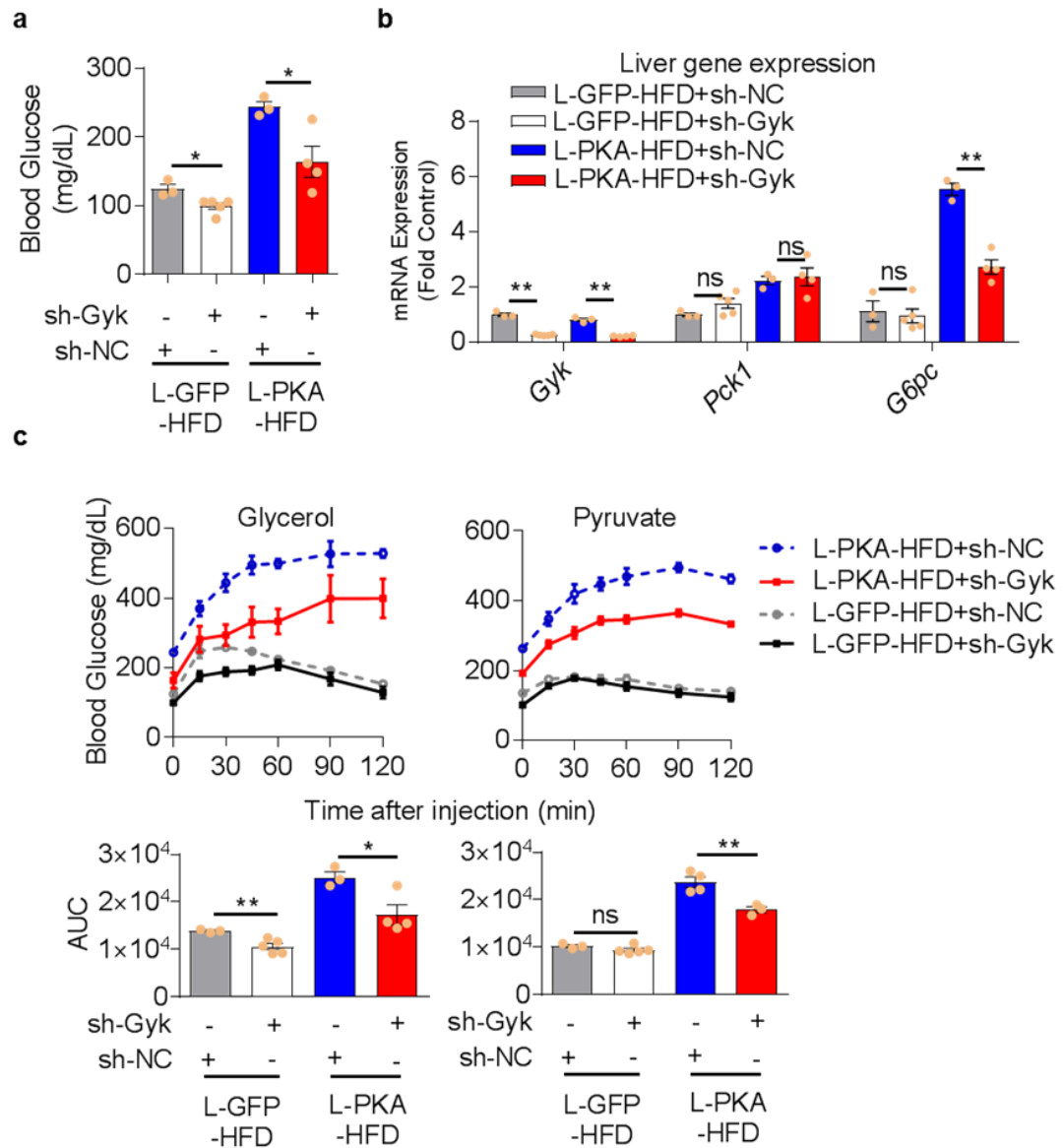
Figure 4.7 | *Gyk* knockdown alleviated the diabetic phenotype in L-GFP-HFD and L-PKA-HFD mice. a, Glucose level after 12-hour fasting. **b,** Fasting gene expression of *Gyk, Pck1* and *G6pc*; Expression levels are normalized to beta actin and expressed as fold change to L-GFP-HFD+sh-NC controls. **c,** Glucose level after bolus injection of pyruvate or glycerol (i.p., 9.1 mmole/kg); total area under the curve (AUC) are used to compare among groups. In all figures, n = 3-4. Data are mean ± s.e.m.;**P<0.01; *P<0.05; ns, not significant between sh-NC and sh-*Gyk* in corresponding groups by two-sided Student's t-test

Discussion

A critical contributor to hyperglycemia in diabetes is dysregulated hepatic gluconeogenesis. These patients exhibit both hyperglucagonemia and hepatosteatosis, which worsens with poorer metabolic control and/or duration of disease. For these reasons, we investigated the interaction between enhanced hepatic glucagon signaling (modeled by constitutive PKA activation) and high fat diet in hepatic glucose production. Our study demonstrates that glucagon signaling and high fat diet work together to increase hepatic gluconeogenesis.

After prolonged fasting, which depletes liver glycogen, blood glucose levels are maintained through gluconeogenesis. The carbon reservoir for gluconeogenesis can be breakdown of glycogen into lactate in the periphery (e.g. skeletal muscle), gluconeogenic amino acids from muscle protein breakdown, or glycerol from triglyceride degradation. Among all gluconeogenic substrates, lactate, pyruvate, alanine and glycerol are considered the main substrates which together have been suggested to contribute over 97% of the carbons to glucose [32]. Lactate, pyruvate and alanine share the same gluconeogenic pathway where lactate and alanine are first converted to pyruvate and enter gluconeogenesis through pyruvate carboxylase in the mitochondria. In contrast, the gluconeogenic pathway for glycerol is shorter and involves entering the pathway through phosphorylation by glycerol kinase directly into cytosolic glycolytic intermediates [93].

Of all the circulating metabolites, lactate has the highest endogenous production rate [33]. When muscle consumes glucose, lactate is produced and circulated to liver, where it is converted to glucose in a process known as the Cori cycle. The Cori cycle, however, is a net glucose producer only when lactate is derived from substrates other than circulating glucose (e.g. glycogen catabolism, glycerol and amino acid catabolism). Alanine, which can be derived from muscle breakdown, can also be metabolized to lactate in the periphery. Our data show that after overnight fasting, a significant portion of the peripheral pyruvate/lactate originates from glycerol (Fig. 4.4a). The $^{13}C_3$-glycerol infusion experiment also demonstrated that, in this context, the majority of the carbon atoms in circulating glucose are originally from glycerol from triglyceride hydrolysis. The contribution of glycerol to glucose is even greater in the HFD condition. The particular importance of glycerol in HFD/obese mice mirrors findings from seminal glycerol tracer studies in lean and obese humans [94].

After a shorter fasting period, when liver glycogen has yet to be depleted, about half of hepatic glucose output is from glycogenolysis [95]. In this context, the contribution of glycerol to gluconeogenesis is lower (although still the predominant carbon source) than after more extended fasting. Consistent with these findings, the relative contribution of glycerol to gluconeogenesis in fasting rodents has been estimated by previous isotope tracer studies to be in the range of 25% to 70% depending on fasting length and conditions [72, 95, 96]. However to measure gluconeogenesis *in vivo* using

a triose phosphate labeling method, both Peroni et al. and Previs et al. employed fast (perturbative) glycerol infusions [72, 96], which may inflate the apparent glycerol contribution and where data cannot be readily combined with other tracers to gain a broader metabolic perspective. Our experimental design was different in that it focused on the relative contributions of different circulating gluconeogenic substrates by employing non-perturbative infusions of multiple tracers (on different days) into the same mouse. Through this approach, we found that glycerol contributes to gluconeogenesis both directly as a substrate and indirectly via circulating pyruvate/lactate, which are themselves important direct gluconeogenic substrates.

We also showed that lactate derived from glycerol can be generated in mice by two routes (Fig. 4.5d): (1) an indirect pathway through circulating glucose and (2) a direct pathway presumably through the lower half of the glycolysis. Glucagon signaling redirects some of the glycerol from the direct to the indirect pathway as it activates gluconeogenesis in the liver. This is reflected by a reduction of the glycerol→lactate and an increase in the in glycerol→glucose →lactate conversion in both the L-PKA and L-PKA-HFD mice (Fig. 4.5e).

Under conditions of elevated glucagon signaling, glycerol is also able to enhance its own synthesis to glucose as well as other substrates by increasing the expression level of G6PC, a rate-limiting enzyme in gluconeogenesis. It has been reported that in a rat hepatoma cell line, glycerol induces the expression of *G6pc* via a nuclear factor 4α

(HNF4α) binding element in the *G6pc* promoter [97]. In addition, cAMP/PKA signaling enhances the transactivation activity of HNF4α in liver [98]. Our laboratory recently extended this work to mouse primary hepatocytes showing that glycerol, but not pyruvate/lactate induces *G6pc* expression [82]. Our new *in vitro* results illustrate that when the hepatic PKA pathway is activated, the presence of the glycerol synergistically increases *G6pc* expression and enzymatic activity. We also demonstrated that the *in vivo* administration of glycerol in L-PKA mice is sufficient to further increase *G6pc* expression. However, hepatic *Gyk* knockdown blocks both glucose production and increased *G6pc* expression, suggesting it is glycerol metabolism, not glycerol itself that mediates the effect with increased PKA signaling (Fig. 4.7b).

In summary, HFD contributes to higher glycerol levels in the liver, which support gluconeogenesis both as a major carbon source and as a regulator of *G6pc* expression. Hepatic glucagon signaling activates *G6pc* expression. HFD feeding increases the availability of glycerol, which also potentiates *G6pc* activity. The combination of *G6pc* activation and increased glycerol availability leads to fasting hyperglycemia. Given the importance of glycerol as both a substrate and regulator, the glycerol metabolic pathway is a potentially important therapeutic target in diabetes.

Chapter 5 . Effect of Hepatic Insulin Receptor Knock-out and High Fat Diet on Gluconeogenesis

Yujue Wang,[1,3] Huiting Xu,[1,3] Hyokjoon Kwon,[1] Xiaoyang Su,[1,2] and Fredric E. Wondisford[1,2*]

[1]Department of Medicine, Rutgers-Robert Wood Johnson Medical School, New Brunswick, NJ 08901, USA.

[2]Rutgers Cancer Institute of New Jersey, New Brunswick, NJ 08903, USA.

[3]These authors contributed equally: Yujue Wang, Huiting Xu

[*]Correspondence: few11@rwjms.rutgers.edu (F.E.W.)

Keywords: Insulin signaling; High fat diet; Glycerol; Substrate contribution; Gluconeogenesis; Metabolic flux analysis

Abstract

Excessive gluconeogenesis is an important driver of the pathogenesis of diabetes mellitus (DM). Although both high fat diet feeding and hepatic insulin resistance have been shown to increase gluconeogenesis, how they interact *in vivo* remains incompletely understood. To explore this question, mouse models of liver insulin receptor knockout (LIRKO) fed a regular or high fat diet (HFD) were studied. LIRKO mice showed complete loss of hepatic insulin signaling but a mild increase of gluconeogenesis flux from both lactate and glycerol whereas HFD fed mice showed median but whole-body insulin resistance with a robust increase of gluconeogenesis flux from glycerol but not lactate. Interestingly, the LIRKO-HFD mice showed complete loss of hepatic insulin signaling and median insulin resistance in the periphery yet its total gluconeogenesis was reduced compared to HFD control mice. Our data suggest the hepatic insulin resistance and HFD feeding increase gluconeogenesis through different mechanisms.

Introduction

Diabetes mellitus (DM) is a chronic disease that affects about 10% of the global population [58, 59]. The most well-known symptom of DM is hyperglycemia, which causes nearly 2 million direct death each year with a series of complications including stroke, blindness and heart attack [58]. In both type 1 (T1DM) and type 2 (T2DM) diabetes, increased hepatic gluconeogenesis is one major cause of hyperglycemia [26-

29].

Studies have showed that diet induced obesity could increase hepatic gluconeogenesis though the exact mechanism is still unclear [99-101]. Many studies showed that obesity could induce hepatic insulin resistance, which was believed as the major cause of increased gluconeogenesis [102, 103]. However, many recent studies have shown that the direct effect of insulin on liver is largely dispensable [60-63]. For example, O-Sullivan et al. showed liver lacks insulin signaling could still maintain normal function of glucose metabolism in the absence of FoxO1 [104]. Consequently, alternative mechanisms such as increased availability of substrates were proposed [24]. However, due to the coexistence of hepatic insulin resistance and other phenotypic changes, it remains unclear which mechanism plays a major role in enhanced gluconeogenesis.

In this study, we utilized liver insulin receptor knockout (LIRKO) mice [16] to model reduced hepatic inulin signaling plus a classic high fat diet (HFD) approach to model the diet induced obesity. By performing metabolic flux analysis, we show that HFD feeding caused median but whole body insulin resistance with increased gluconeogenic flux from glycerol but not from lactate. In contrast, LIRKO mice showed complete loss of hepatic insulin signaling and normal peripheral insulin signaling with slightly increased gluconeogenesis from both glycerol and lactate. Interestingly, compared to HFD control, LIRKO-HFD mice exhibit reduced gluconeogenesis flux with a shift of

substrate preference from glycerol to lactate. Together, our data suggest hepatic insulin resistance and HFD feeding increases gluconeogenesis through different mechanisms.

Methods

Animals and Diets

All mice were maintained on a C57BL6/J-albino background (Jackson Labs; B6(Cg)-Tyrc-2J/J). The glucose homeostasis varies throughout the estrous cycle in female mice [41]. To avoid the variation caused by estrous cycles, only male mice were used in this study. To generate the RD-LIRKO and the RD-GFP mice, mice homozygous for the floxed *Insr* allele [16] were maintained on a normal chow for 11 weeks after weaning and then injected with either Aav-TBG-CRE or Aav-TBG-GFP (1 x 10^12 GC/mouse; Vector Biolabs) via the tail vein and allowed to recover for 14 days (Supplementary Fig. A4.1a). To generate the HFD-LIRKO and HFD-GFP mice, mice homozygous for the *Insr* allele were maintained on a high fat diet for 11 weeks after weaning and then injected with Aav-TBG-CRE or Aav-TBG-GFP, as described above (Supplementary Fig. A4.1a). All animal studies were approved by the Animal Care and Use Committees of Robert Wood Johnson Medical School.

Protein Extraction and Western Blotting

All protein preparations were conducted using tissue samples that had been immediately snap frozen in liquid nitrogen following the sacrifice of the animal. For

protein preparations, tissues were mechanically homogenized in ice-cold RIPA buffer (Sigma) with 1× protease inhibitor (Roche) and 1× phosphatase inhibitor (Thermo Scientific) using a handheld tissue homogenizer (E-Z Grind; Denville Scientific). The homogenate was then centrifuged at 16,000 × g at 4 degrees and the supernatant was collected. Protein concentrations were measured using the Pierce BCA assay (Thermo Scientific). Western blotting was performed using standard procedures utilizing the standard V3 Western Workflow (Bio-Rad). All standard western blotting reagents were obtained from Bio-Rad. Antibodies were obtained from Cell Signaling Technology (PCK1, AKT, AKT pSer473, HRP-conjugated anti-rabbit IgG), Abcam (GYK) or Santa Cruz (IR-b).

Metabolic Tests

All in vivo metabolic tests presented herein were performed within 3 weeks after the injection of virus. Blood glucose measurements were obtained via a small nick in the lateral tail vein using a glucometer (Bayer Contour). For the pyruvate and glycerol tolerance tests, mice were fasted overnight (12 hours) and then injected i.p. with sodium pyruvate or glycerol (9.1 mmole/kg; Sigma). For the insulin tolerance tests, mice were fasted for 6 hours and then injected i.p. with human insulin (0.5 U/kg; Novo Nordisk).

RNA Analysis

Total RNA was obtained from mouse tissue samples that had been snap frozen in liquid

nitrogen immediately after sacrificing the animal. RNA was extracted using the RNeasy Plus Mini Kit (Qiagen). Complementary DNA (cDNA) was generated from 1 μg total RNA using the iScript cDNA Synthesis kit (Bio-Rad). Primers were designed with NCBI Primer-BLAST [78]. Quantitative PCR (qPCR) reactions were conducted using the SYBR green PCR master mix (Applied Biosystems) in CFX96 Touch Real-Time PCR Detection System (Bio-Rad). CT values were normalized to beta actin (*Actb*) mRNA and interpreted as fold changes to the L-GFP control group.

Insulin Response Test

Mice were fasted for 6 hours and then injected i.p. with human insulin (Novo Nordisk). Ten minutes after the injection, mice were sacrificed by cervical dislocation to harvest livers and other organs. All samples were snap frozen in liquid nitrogen and stored at -80 °C before analyses.

In vivo Isotope Labeling Studies

For continuous infusion experiments, approximately four mice from each group (RD-GFP, HFD-GFP, RD-LIRKO, and HFD-LIRKO) were catheterized on the right jugular vein [42] and recovered for more than 6 days. Catheterized mice were fasted for 12 h and then transferred to new cages without food and infused for 6 hours. During the infusion, a tether and swivel system were used to allow mice free movement in the cage (Instech Laboratories). Water-soluble isotope-labelled metabolites tracers (Cambridge

Isotope Laboratories) were prepared as solutions in sterile normal saline and infused via the catheter at a constant rate (0.1 µl/g body weight/min). 200 mM 6, 6-^{2}H$_2$-glucose, 200 mM ^{13}C$_6$ glucose, 150 mM ^{13}C$_3$ glycerol, 150 mM ^{13}C$_3$-^{2}H$_8$ glycerol or 40 mM ^{13}C$_3$ sodium pyruvate with 360 mM ^{13}C$_3$ lactate were infused. About 30 µl blood were collected by tail vein bleeding at each time point, placed on room temperature in the absence of anticoagulant for 30 minutes and centrifuged at 4 °C to prepare serum. At the end of the last infusion experiment, the mouse was euthanized by cervical dislocation and quickly dissected liver was snap frozen in liquid nitrogen with pre-cooled Wollenberger clamp [79]. Serum and tissue samples were kept at −80 °C until further extraction.

Frozen liver pieces were ground using a Cryomill (Retsch) and stored at -80° C until extraction. Tissue powder (25 mg each) or serum (10 µl each) was mixed with −20 °C 40:40:20 methanol:acetonitrile:water solution with 0.1% formic acid, followed by vortexing for 10 s, incubation at 4 °C for 10 min, and centrifugation at 4 °C and 16,000 × g for 10 min. The volume of the extraction solution (in µl) was 40× the weight of tissue (in mg) or 25× the volume of serum. The supernatant was transferred to a clean tube and neutralized with NH$_4$HCO$_3$ solution. The mixture was centrifuged again at 4 °C and 16,000 × g for 10 min. The supernatant was then transferred to another clean tube for mass spectrometry (LC-MS) analysis.

Hyperinsulinemic-euglycemic clamp

Catheterized mice were fasted for 3 hours and then administered an initial bolus of 6, 6-^{2}H$_2$-glucose (10 mg/kg), followed by continuous infusion of 6, 6-^{2}H$_2$-glucose (728 µg/kg/min) throughout the entire experiment. Isotopic steady state of glucose was achieved 3 hours after the onset of infusion, and the first blood samples were collected at this time (t = 0 hour). Immediately after blood collection, insulin was constantly infused at the rate of 8 mU/kg/min. Glucose (50% w/v) was infused at various rates until the blood glucose concentration reached an euglycemia (100 ± 10 mg/dL). Blood samples were taken at t = 3 hour. Serum was prepared for LC-MS as described above.

Glycerol derivatization for LC-MS Analysis

Due to poor ionization of glycerol, an enzymatic derivatization is required to detect glycerol in LC-MS [43]. Samples containing glycerol were added into 10 × volume of reaction buffer containing 25 mM Tris (pH 8.0), 10 mM Mg^{2+}, 50 mM NaCl, 5 mM ATP and 2 U/ml glycerol kinase (Sigma-Aldrich G6278) and incubated for 10 minutes at room temperature. The reaction was quenched with 40:40:20 methanol:acetonitrile:water solution with 0.1% formic acid, and later neutralized with NH$_4$HCO$_3$ solution. The same reaction was also performed on blank to remove background. The ion counts of glycerol-3-phosphate in blank was subtracted from that of the derivatized sample.

LC-MS Analysis

The LC-MS method used reversed-phase ion-pairing chromatography coupled with negative mode electrospray ionization to a stand-alone orbitrap mass spectrometer (Thermo Scientific) scanning from m/z 85-1,000 at 1 Hz at 100,000 resolution with LC separation on a Synergi Hydro RP column (150 mm × 2 mm, 2.4 μm particle size, Phenomenex) using a gradient of solvent A (97%:3% H2O:MeOH with 10 mM tributylamine and 15 mM acetic acid), and solvent B (100% MeOH). The gradient was 0 min, 0% B; 5 min, 0% B; 7 min, 20% B; 17 min, 80% B; 20 min, 100% B; 23.5 min, 100% B; 24 min, 0% B; 30 min, 0% B. The flow rate was 0 min, 200 μl min^{-1}; 20 min, 200 μl min^{-1}; 20.5 min, 300 μl min^{-1}; 29.5 min, 300 μl min^{-1}; 30 min, 200 μl min^{-1}. Injection volume was 10 μL and column temperature 25 °C. For phosphate-containing gluconeogenic intermediates, the extract was dried down under Nitrogen gas and reconstituted in 100 μL of water for LC-MS analysis. For other metabolites, the extract was directly transferred to LC-MS sample vial for analysis, which involves a quadrupole-orbitrap mass spectrometer (Q Exactive Plus, Thermo Fisher Scientific) operating in negative ion mode coupled to hydrophilic interaction chromatography via electrospray ionization scanning from *m/z* 72 to 1,000 at 2 Hz and 70,000 resolution. LC separation was achieved on a XBridge BEH Amide column (2.1 mm × 150 mm, 2.5 μm particle size, 130 Å pore size; Waters) using a gradient of solvent A (20 mM ammonium acetate + 20mM ammonium hydroxide in 95:5 water:acetonitrile, pH 9.4) and solvent B (20 mM ammonium acetate + 20mM ammonium hydroxide in 20:80

water:acetonitrile, pH 9.4). Flow rate was 300 µl min^{-1}. The gradient was: 0 min, 100%

B; 3 min, 100% B; 3.2 min, 90% B; 6.2 min, 90% B; 6.5 min, 80% B; 10.5 min, 80%

B; 10.7 min, 70% B; 13.5 min, 70% B; 13.7 min, 45% B; 16 min, 45% B; 16.5 min, 100%

B; 22 min, 100% B. Data were analyzed using the MAVEN software [44]. The ^{13}C

isotope natural abundances were corrected using AccuCor [45].

Metabolic Flux Analyses

For the calculation of F_{circ} (turnover rate of metabolites), the calculation is based on the

enrichment of tracers and the infusion rate at steady state using the following equation:

$$F_{circ} = \text{Infusion rate} * \left(\frac{1}{labeled\ fraction\ of\ tracer} - 1 \right) \qquad [\text{Eq.5.1}]$$

The flux modeling is modified from a previously described method [80]. In brief, a flux

network is constructed (Supplementary Fig. A4.2a) with the following assumptions:

1. At steady state, all labeled and non-labeled metabolites are completely mixed.

2. The labeled and unlabeled metabolites react identically (i.e. there is no isotope

   discrimination).

3. All glycerol and lactate that makes glucose are from blood circulation.

4. The state of animal is the same when infused with different tracers.

5. The infusion does not alter the normal physiology of mice.

6. Glycogen, free fatty acid and TCA amino acids are non-recyclable from glucose

   during fasting.

7. TCA amino acids contribute to GNG via a universal pool of TCA intermediates.

8. Due to the high interconversion rate among pyruvate, lactate and alanine in vivo, the total contribution of these three metabolites can be calculated together as lactate contribution.

Fluxes were calculated in the unit of μmol product/kg/min. All fluxes occur in the liver except V_{out}, V_{glc}, V_3, V_5, V_6, V_9 and V_{20} which occur in the periphery. V_2, V_5, V_9, V_{13} and V_{19} are input fluxes from glycogen, glycerol (from triglycerides), lactate (including alanine and pyruvate), free fatty acid (FFA) and amino acids (via TCA cycle) respectively. V_{glc} represents the infusion flux from $^{13}C_6$ glucose tracer. V_{11} is pyruvate carboxylase flux that incorporates carbon dioxide. V_{10}, V_{12}, V_{17} and V_{18} are decarboxylase fluxes that release carbon dioxide. V_{flop} is an infinitely large flux to account for the achirality of metabolites. V_3 represents the glycolysis process in peripheral tissue. V_6 represents glycerol synthesis from glucose. V_{20} represents the direct conversion from glycerol to lactate. V_1 is the endogenous glucose production (EGP) flux which equals to the sum of the glucose recycled via the Cori cycle (V_3), glycerol synthesis (V_6) and the net production of glucose (V_{out} - V_{glc}). Therefore, the absolute value of V_1 can be measured as the steady-state glucose turnover rate (F_{circ}) in circulation.

The contribution of amino acids through TCA cycle consists of three components: 1.

via oxaloacetate (Asp, Asn); 2. via fumarate or succinyl CoA (Phe, Tyr, Ile, Met, Val, Thr); 3. via α-ketoglutarate (Gln, Glu, Pro, His, Arg). The average physiological concentrations of amino acids are 13.5 μM Asp, 35.9 μM Asn, 54.1 μM Phe, 46.7 μM Tyr, 73.1 μM Ile, 52.4 μM Met, 178.7 μM Val, 126.2 μM Thr, 25.1 μM Glu, 397.0 μM Gln, 67.4 μM Pro, 49.6 μM His and 93.4 μM Arg [47]. Therefore, the total substrate concentration in the three possible pathways are 49.4, 531.2 and 632.5 μM respectively. Assuming proportional contribution by the three routes, the three sub-fluxes to oxaloacetate, succinate and α-ketoglutarate are 4%, 44% and 52% of V_{19} respectively.

The metabolite mass balance leads to the following equations:

$$
\begin{aligned}
\text{Glucose:} \quad & V_1 - 0.5V_3 - 0.5V_6 + V_{glc} = V_{out} \\
\text{G6P:} \quad & V_1 - V_4 = V_2 \\
\text{DHAP:} \quad & 2V_4 - V_7 = V_8 \\
\text{Glycerol:} \quad & V_{20} + V_8 - V_6 = V_5 \\
\text{PEP:} \quad & V_7 - V_{10} = 0 \\
\text{Pyr:} \quad & V_{11} + V_{12} - V_3 - V_{20} = V_9 \\
\text{Oxa:} \quad & V_{10} + V_{15} + V_{16} - V_{11} - V_{14} = 0.04V_{19} \\
\text{Ac-CoA:} \quad & V_{16} - V_{12} = V_{13} \\
\text{Suc:} \quad & V_{14} - V_{15} - V_{17} = 0.44V_{19} \\
\text{Cit:} \quad & V_{16} - V_{18} = 0 \\
\text{aKG:} \quad & V_{17} - V_{18} = 0.52V_{19}
\end{aligned}
$$

[Eq.5.2]

Balance of input and output mass leads to the following equation:

$$
\begin{aligned}
6V_{out} = {} & 6V_2 + 6V_{glc} + 3V_5 + 3V_9 + 2V_{13} + 4.52V_{19} \\
& - V_{12} - V_{10} - V_{17} - V_{18} + V_{11}
\end{aligned}
$$

[Eq.5.3]

Ten fluxes are designated free fluxes: V_2, V_5, V_8, V_9, V_{12}, V_{13}, V_{15}, V_{19}, V_{20} and V_{glc}.

All other fluxes can be expressed using the free fluxes or known constants ([Eq. 5.4]).

$$
\begin{aligned}
V_1 &= EGP = F_{circ} \\
V_3 &= 2F_{circ} - 2V_2 - V_9 + V_{12} - V_{19} - V_{20} - V_8 \\
V_4 &= F_{circ} - V_2 \\
V_6 &= V_{20} + V_8 - V_5 \\
V_7 &= 2F_{circ} - 2V_2 - V_8 \\
V_{10} &= V_3 + V_9 - V_{12} + V_{19} + V_{20} \\
V_{11} &= V_3 + V_9 - V_{12} + V_{20} \\
V_{14} &= V_{12} + V_{13} + V_{15} + 0.96V_{19} \\
V_{16} &= V_{12} + V_{13} \\
V_{17} &= V_{12} + V_{13} + 0.52V_{19} \\
V_{18} &= V_{12} + V_{13} \\
V_{out} &= 0.5*(V_5 + V_9 + V_{19} - V_{12}) + V_2 + V_{glc} \\
V_{flop} &= Infinite
\end{aligned}
\qquad \text{[Eq. 5.4]}
$$

Since the labeling patterns of all the input molecules are known (either unlabeled or fully labeled as tracers), the steady-state labeling patterns of all metabolites in the system can be calculated using the EMU approach given any set of the ten fluxes. For $^{13}C_3$-$^2H_8$ glycerol infusion data, only $^{13}C_3$-$^2H_1$ and $^{13}C_3$-$^2H_2$ lactate is calculated using the following equation:

$$
\begin{aligned}
{}^{13}C_3\text{-}^2H_1 \text{ lactate} &= 0.5V_8*V_3 / (V_1 + V_{glc}) \\
{}^{13}C_3\text{-}^2H_2 \text{ lactate} &= 0.5V_8*V_3 / (V_1 + V_{glc}) + V_{20} \\
\text{Fraction of } {}^{13}C_3\text{-}^2H_1 \text{ lactate} &= {}^{13}C_3\text{-}^2H_1 \text{ lactate} / ({}^{13}C_3\text{-}^2H_1 \text{ lactate} + {}^{13}C_3\text{-}^2H_2 \text{ lactate}) \\
\text{Fraction of } {}^{13}C_3\text{-}^2H_2 \text{ lactate} &= {}^{13}C_3\text{-}^2H_2 \text{ lactate} / ({}^{13}C_3\text{-}^2H_1 \text{ lactate} + {}^{13}C_3\text{-}^2H_2 \text{ lactate})
\end{aligned}
\qquad \text{[Eq. 5.5]}
$$

The calculated labeling patterns were compared to the measured ones with equal weight. The best estimated flux set was obtained by minimizing the sum of squared residues

(SSR) between the calculated and measured labeling patterns. The measured labeling patterns of glucose, glycerol and pyruvate under four tracers ($^{13}C_3$ glycerol, $^{13}C_3$-$^2H_8$ glycerol, $^{13}C_3$ lactate and $^{13}C_6$ glucose) were used in this process. The numerical simulation of labeling patterns was achieved in R software and the optimization was achieved with DEoptim package [48]. 95% confidence intervals were calculated by (1) move one target flux away from the best-fit value by a small step; (2) choose a combination of the other fluxes that minimize the increase of SSR; (3) calculate the new SSR and repeat step (1) to (3) until the new SSR reached the cutoff for 95% confidence interval [49]. The goodness of fit was tested by chi-square test, $X^2_{0.05}$ (df = 18) = 28.8693, which is equivalent to an SSR value of 0.00288693. The 18 degrees of freedom are based on 28 measurements (labeling fractions of three metabolites under four tracers) and having 10 unknown fluxes; 28 - 10 = 18.

To illustrate the direct contribution and origin of carbon better, we simplified the pathways into the 5-pool network (Supplementary Fig. A4.2b). For convenience, all units of fluxes were normalized to μmol C/kg/min. U_1 and U_2 are input fluxes from glycerol and lactate respectively. U_5 and U_6 represent fluxes that glucose making the glycerol and lactate respectively. U_7, U_8, U_3 and U_4 represent the fluxes that glycerol, lactate glycogen and TCA amino acids making glucose respectively. U_9 represents the pyruvate dehydrogenase (PDH) flux that consumes lactate in TCA cycle. U_{10} represents the flux glycerol directly making lactate. U_{out} is the glucose output which equals to the

net production of glucose. By definition, all fluxes can be represented by the equivalent

fluxes in the EMU model:

$$
\begin{array}{llllll}
U_1 = 3V_5 & U_2 = 3V_9 & U_3 = 6V_2 & U_4 = 3V_{19} & U_5 = 3V_6 & U_6 = 3V_3 \\
U_7 = 3V_8 & U_8 = 3V_{11} & U_9 = 3V_{12} & U_{10} = 3V_{20} & U_{out} = 6\,(V_{out} - V_{glc}) &
\end{array}
\qquad \text{[Eq. 5.6]}
$$

The direct contribution from glycerol and lactate were calculated as the relative ratio of

U_7, U_8 and U_4 (green arrows; supplementary Fig. A4.2b). The origin of carbon from

glycerol and lactate were calculated as the relative ratio of U_1, U_2 and U_4 (purple arrows;

supplementary Fig. A4.2b).

Statistical Analysis

Statistical analyses were performed using the GraphPad Prism software, version 6.07.

Data and Code availability

All data and computer code are available from the authors upon reasonable request.

Results

Hepatic insulin receptor knockout reduces fating glucose of high fat diet fed mice

To obtain a model of both diet-induced obesity and reduced insulin signaling, we first

placed male *Insr*^fl/fl mice on either a normal chow or a high fat diet (HFD) at 4 weeks

of age. After 11 weeks of these diets, mice were injected with either Aav-TBG-CRE or

control Aav-TBG-GFP virus via tail vein to generate four experimental groups: normal

hepatic insulin signaling with normal chow or HFD (RD-GFP and HFD-GFP respectively) and impaired hepatic insulin signaling with normal chow or HFD (RD-LIRKO and HFD-LIRKO respectively) (Supplementary Fig. A4.1a). Both HFD groups displayed similar increase in body weight (Supplementary Fig. A4.1b). Two weeks after the injection of virus, both RD-LIRKO and HFD-LIRKO mice showed significantly reduced insulin receptor in the liver but not in the skeletal muscle compared to the GFP controls (Supplementary Fig. A4.1c). To understand the impact of liver insulin signaling on glucose homeostasis, we investigated the glucose level after overnight fasting (Fig. 5.1a). The RD-LIRKO mice showed similar fasting glucose level compared to the RD-GFP control. Interestingly, the HFD-LIRKO mice showed decreased fasting glucose level compared to the HFD-GFP group.
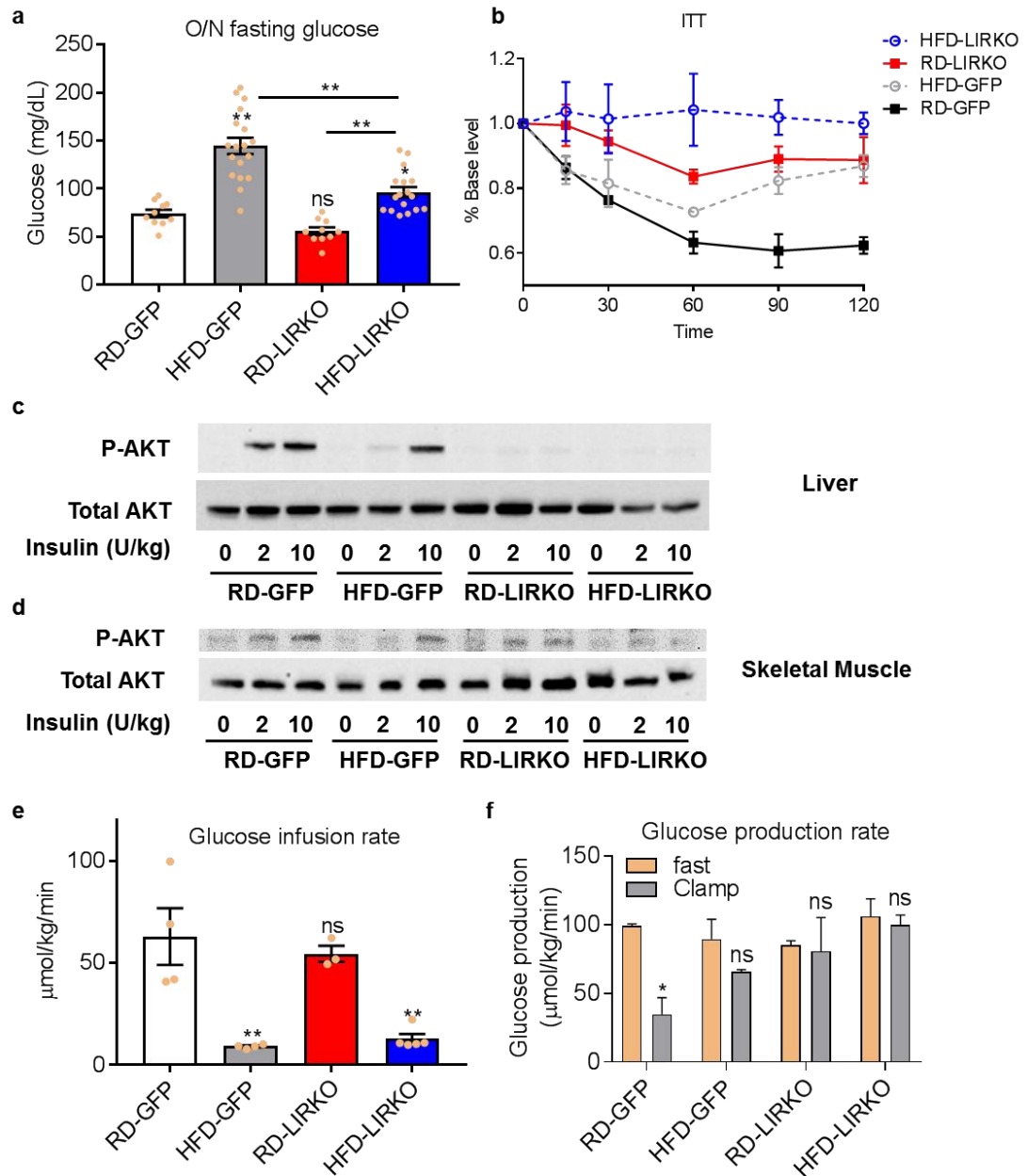
Figure 5.1 | Liver insulin receptor knock-out reduced fasting glucose and caused insulin resistance in the liver but not in the periphery. a, glucose level after overnight fasting. **b,** insulin tolerance test. **c-d,** phosphor-AKT in response to insulin in liver (c) and skeletal muscle (d). **e-f,** hyperinsulinemic-euglycemic clamp. **e,** glucose infusion rate under clamp condition. **f,** glucose production rate under fast and clamp condition. In all figures, data are mean ± s.e.m.; n = number of mice, **$P<0.01$; *$P<0.05$; ns, not significant by one-way ANOVA. All comparisons are against L-GFP unless indicated otherwise.

Hepatic insulin receptor knockout impairs insulin signaling in the liver but not in the periphery.

HFD feeding is known to induce insulin resistance in both liver and periphery tissue [85]. To understand the interactions between HFD feeding and liver insulin signaling, we investigated insulin signaling in all four groups of mice. In the insulin tolerance test, both HFD-GFP and RD-LIRKO mice showed insulin resistance compared to the RD-GFP control (Fig. 5.1b). Interestingly, the HFD-LIRKO mice showed the most severe insulin resistance among all the four groups. To distinguish the location of insulin resistance, we tested the phospho-AKT level in the liver and skeletal muscle after injection of insulin (Fig. 5.1c and 5.1d). HFD-GFP mice showed median insulin resistance in both liver and skeletal muscle as only high dosage of insulin (10 U/kg) can induce AKT phosphorylation. In contrast, RD-LIRKO mice showed complete loss of insulin signaling in the liver but intact insulin signaling in skeletal muscle. As expected, the HFD-LIRKO mice combined both effect with complete insulin resistance in the liver but median insulin resistance in skeletal muscle. To further confirm these findings, we performed a hyperinsulinemic-euglycemic clamp with 6,6-^{2}H$_2$-glucose infused simultaneously [86, 87]. The RD-LIRKO mice showed similar glucose infusion rate compared to RD-GFP group, suggesting an intact insulin sensitivity in the periphery (Fig. 5.1e). In contrast, both HFD-GFP and HFD-LIRKO mice showed decreased glucose infusion rate compared to RD-GFP group, suggesting insulin resistance in the periphery. By analyzing the fraction of ^{2}H-labeled glucose, we

calculated the change of glucose production rate in response to high insulin (Fig. 5.1f).

Among all the four groups, only RD-GFP mice showed suppressed glucose production in response to insulin. All the other three groups showed unsuppressed glucose production, indicating insulin resistance in the liver. Together, these findings suggest HFD feeding causes median but whole-body insulin resistance whereas LIRKO causes complete insulin resistance in the liver without altering the peripheral insulin signaling.

Hepatic insulin receptor knockout shifts the gluconeogenic substrate utilization from glycerol to lactate in HFD fed mice

Hepatic insulin signaling has been shown to play important roles in regulating gluconeogenesis [103]. To investigate the effect of HFD and LIRKO on gluconeogenesis, we injected four groups of mice with equal molarity of glycerol and pyruvate after overnight fasting and measured the glucose excursion after the injection (Fig. 5.2). RD-LIRKO mice showed similar glucose excursion profile compared to RD-GFP mice. In contrast, HFD-LIRKO mice showed reduced glucose excursion from glycerol but increased excursion from pyruvate compared to HFD-GFP mice. Together, these data suggest in mice fed on HFD, hepatic insulin receptor knock-out has a strong impact on the preference of gluconeogenic substrate, which favors lactate over glycerol.
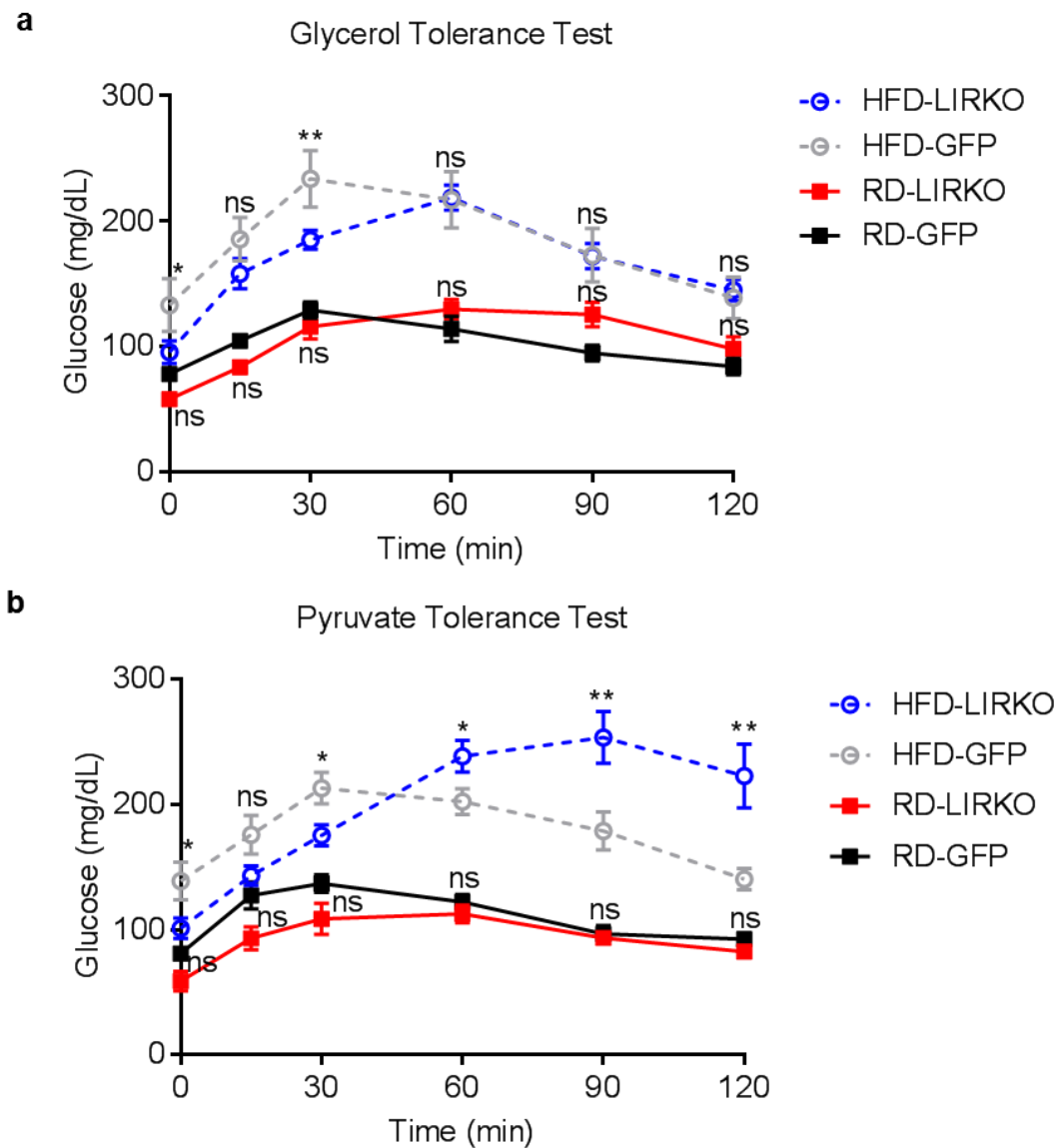
Figure 5.2 | Glycerol and pyruvate tolerance tests. Mice were fasted for 12 hours and injected with equal molarity of pyruvate (a) or glycerol (b). In all figures, data are mean ± s.e.m.; **P<0.01; *P<0.05; ns, not significant by one-way ANOVA. Comparisons are RD-LIRKO against RD-GFP and HFD-LIRKO against HFD-GFP

Hepatic insulin receptor knockout decreases the turnover rate of glycerol and glucose but increases that of lactate in HFD fed mice

To investigate the utilization of glycerol and lactate further, we studied the metabolism of glycerol, lactate and glucose *in vivo* using non-perturbative $^{13}C_3$-glycerol, $^{13}C_3$-sodium lactate (mixed with $^{13}C_3$-sodium pyruvate in physiological ratio to maintain

NAD/NADH balance) and $^{13}C_6$-glucose infusion [80] in mice after a 12-hour fast (Fig. 5.3). At steady-state, the production and consumption rate of metabolites are at equilibrium and can be presented as the turnover rate (Fcirc) [33]. RD-LIRKO mice showed similar turnover rate of glycerol (Fig. 5.3b), lactate (Fig. 5.3d) and glucose (Fig. 5.3f) compared to RD-GFP mice. In contrast, HFD-GFP mice showed increased glycerol turnover compared to RD-GFP mice but this increase is rescued by the knockout of hepatic insulin receptor as shown in HFD-LIRKO mice (Fig. 5.3b). Moreover, HFD-LIRKO mice showed the highest lactate turnover among all groups (Fig. 5.3d), suggesting an increased production and consumption of lactate. In the similar trend as glycerol, the glucose turnover is increased in HFD-GFP mice compared to RD-GFP mice, but this increase is rescued by the knockout of hepatic insulin receptor as shown in HFD-LIRKO mice (Fig. 5.3f).

Hepatic insulin receptor knockout decreases the contribution from glycerol to lactate in the context of HFD feeding

We next studied the gluconeogenic contribution from glycerol and lactate. Because only one ^{13}C tracer was used at a time, the fractional contribution from the tracer metabolite can be roughly estimated by the average carbon enrichment ratio of glucose over the tracer [80]. For example, in the $^{13}C_3$ lactate infusion, the relative gluconeogenic contribution from lactate can be estimated by the enrichment ratio of glucose versus lactate (Fig. 5.3a and Fig. 5.4a). The gluconeogenic contribution from lactate were

found similar among all the groups (Fig. 5.4a), suggesting neither HFD feeding nor insulin receptor knockout affects the relative contribution from lactate. In contrast, the relative contribution from glycerol was significantly increased in both the HFD-GFP and HFD-LIRKO compared to the normal chow controls (Fig. 5.4a), suggesting HFD feeding increases glycerol contribution to glucose. RD-LIRKO and RD-GFP mice showed similar contribution from glycerol (Fig. 5.4a), suggesting insulin signaling has little impact on the glycerol contribution. There is also a trend of reduced contribution from glycerol in HFD-LIRKO mice compared to HFD-GFP mice.

It should be noticed that the enrichment ratio method is only a rough estimation because it assumes all substrates except the tracer are non-labeled. In reality, glycerol may indirectly contribute to gluconeogenesis by converting to lactate first [80]. For this reason, we next investigated the interconversion between glycerol and lactate. By comparing the enrichment ratio between glycerol and lactate, we found in all groups, lactate is not a significant carbon source of glycerol ($< 10\%$) but glycerol is a significant carbon source of lactate (40-70%) (Fig. 5.4b). Glycerol contributed about 40% of lactate carbon in RD-GFP and RD-LIRKO mice and this contribution increased to 70% in HFD-GFP mice. Interestingly, this contribution in HFD-GFP mice was significantly lower than that in HFD-GFP mice, suggesting the knockout of liver insulin receptor reduced glycerol conversion to lactate in the context of HFD feeding.
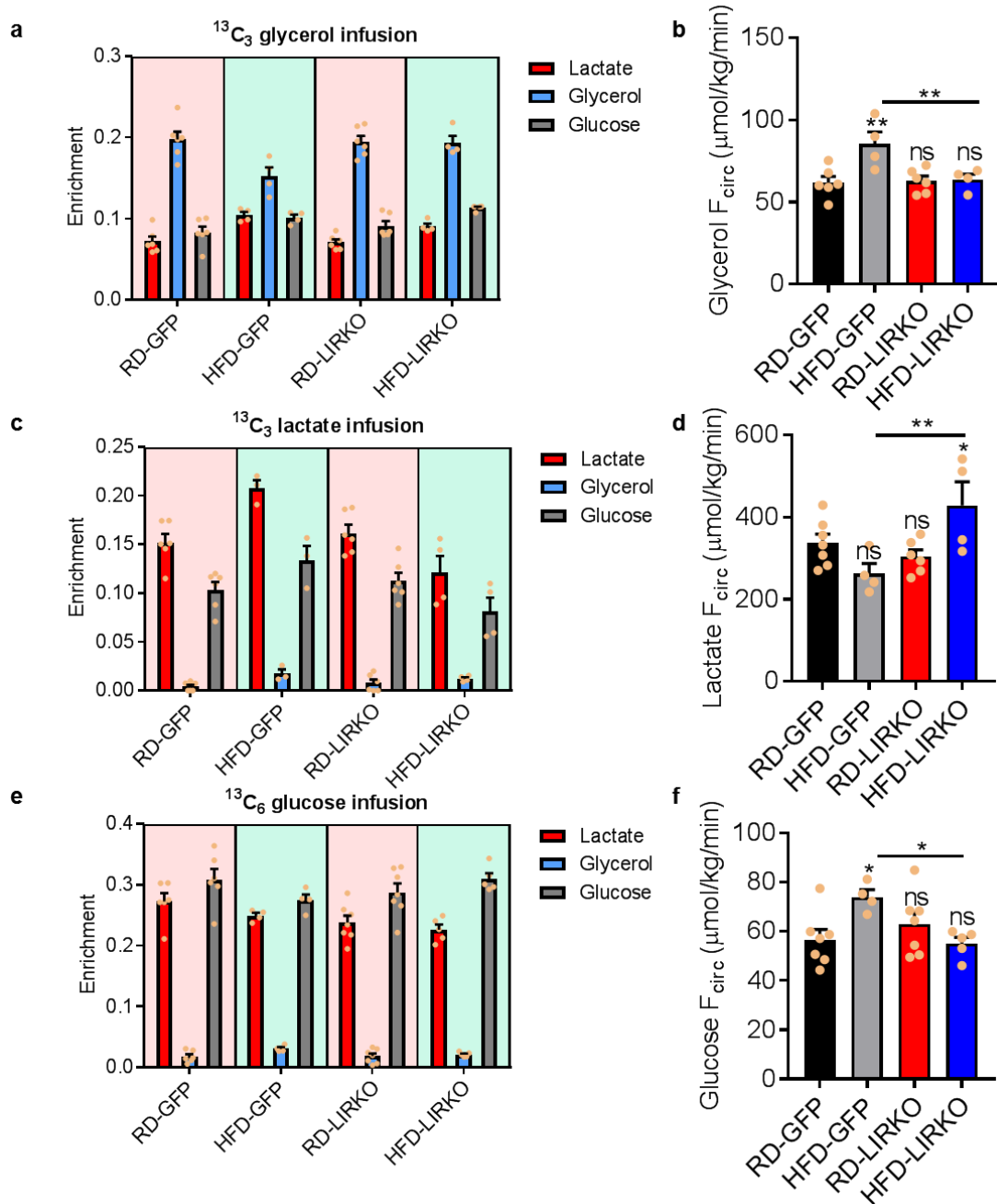
Figure 5.3 | Infusion of ^{13}C labeled glycerol, lactate and glucose. a-b, infusion of ^{13}C$_3$ glycerol. **a,** ^{13}C enrichment of serum metabolites at steady state. **b,** Turnover rate of circulating glycerol (F_{circ}). **c-d,** infusion of ^{13}C$_3$ lactate **c,** ^{13}C enrichment of serum metabolites at steady state. **d,** Turnover rate of circulating lactate (F_{circ}). **e-f,** infusion of ^{13}C$_6$ glucose. **e,** ^{13}C enrichment of serum metabolites at steady state. **f,** Turnover rate of circulating glucose (F_{circ}). In all figures, data are mean ± s.e.m.; **P<0.01; *P<0.05; ns, not significant by one-way ANOVA. All comparisons are against RD-GFP
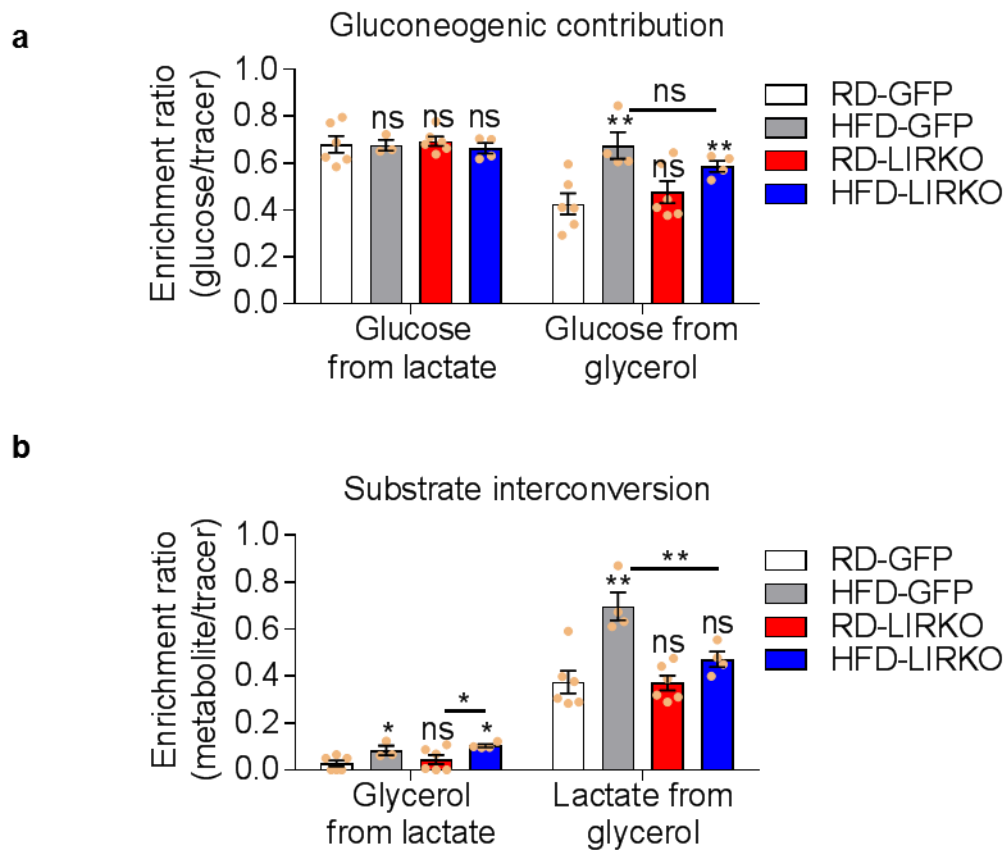
Figure 5.4 | Interconversion between glycerol, lactate and glucose. a, Fraction of carbon in glucose come from lactate or glycerol tracer. **b,** Fraction of carbon in glycerol come from lactate and fraction of carbon in lactate come from glycerol. In all figures, data are mean ± s.e.m.; **P<0.01; *P<0.05; ns, not significant by one-way ANOVA. All comparisons are against RD-GFP unless indicated otherwise.

Hepatic insulin receptor knockout decreases the gluconeogenic input flux from glycerol but increases that from lactate in the context of HFD feeding

To accurately evaluate the gluconeogenic flux from glycerol and lactate, we applied a recently developed mathematical model (Supplementary Fig. A4.2a) [80] which enumerates different flux combinations and simulates the labeling pattern of metabolites associated with each combination (Supplementary Fig. A4.3). The best-fit flux is the one associated with the least residue between simulated and observed

labelling patterns. Using this method, we are able to estimate all the essential fluxes in gluconeogenic pathway (Fig. 5.5). Both RD-LIRKO and HFD-LIRKO mice showed increased gluconeogenic fluxes from both glycerol and lactate compared to RD-GFP mice, suggesting hepatic insulin receptor knockout increased gluconeogenesis from both substrates. In the context of HFD feeding, HFD-GFP mice showed a robust increase in the flux from glycerol but not from lactate. However, this trend was impaired by the knockout of hepatic insulin receptor as the HFD-LIRKO mice showed less flux from glycerol compared to HFD-GFP mice (Fig. 5.5). Beyond the glycerol flux, HFD-LIRKO mice also showed a decreased flux from free fatty acid (FFA) and an increased flux in pyruvate dehydrogenase (PDH) pathway compared to HFD-GFP mice (Fig. 5.5).
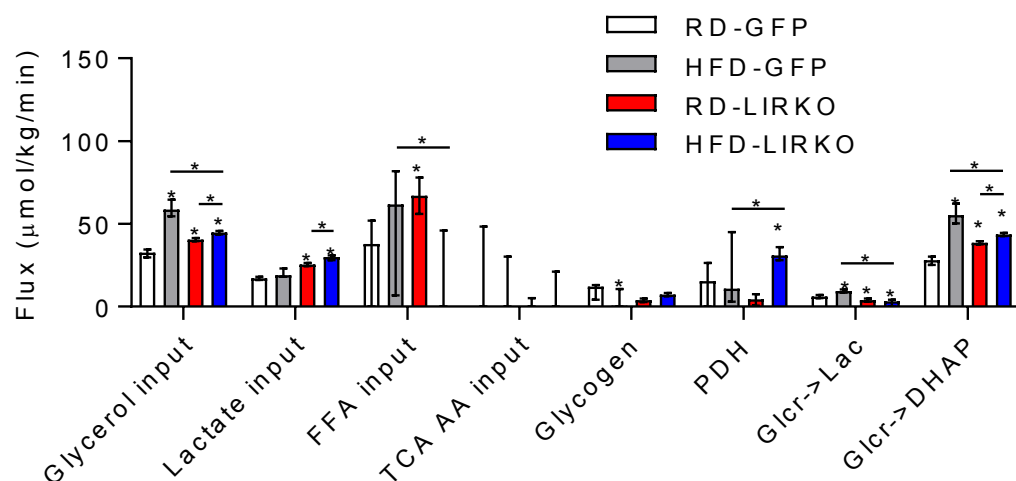
Figure 5.5 | Estimated fluxes in gluconeogenesis pathway. PDH, pyruvate dehydrogenase; DHAP, dihydroxyacetone phosphate. In all figures, data are mean ± 95% confidence interval; *P<0.05. All comparisons are against RD-GFP unless indicated otherwise.

To illustrate the gluconeogenic contribution better, we summarized all the fluxes into a 5-pool network (Fig. 5.6a-d; Supplementary Fig. A4.2b) and calculated the direct contribution and the origin of carbon for glucose production (Fig. 5.6e and 5.6f). To calculate gluconeogenesis only, the contribution from glycogen was excluded from the calculation. The direct contribution is the relative ratio of the fluxes directly making glucose (green arrows, Fig. 5.6a-d) while the overall contribution is the relative ratio of the overall input fluxes (purple arrows, Fig. 5.6a-d). In terms of the direct contribution, HFD-GFP mice showed about 100% increase in glycerol flux and 50% increase in lactate compared to RD-GFP mice (Fig. 5.6a and 5.6b) and consequently, glycerol became more preferred substrate in HFD-GFP mice (Fig. 5.6e). In contrast, RD-LIRKO mice increased glycerol and lactate flux in the same proportion compared to RD-GFP mice (Fig. 5.6a and 5.6c) and as a result, the direct contribution remained unchanged (Fig. 5.6e). Interestingly, HFD-LIRKO mice showed increased glycerol flux but decreased lactate flux compared to RD-GFP (Fig. 5.6a and 6d) and as a result, HFD-LIRKO mice showed the highest preference for glycerol over lactate in the direct contribution to gluconeogenesis (Fig. 5.6e).

In terms of the origin of carbon in gluconeogenesis, HFD-GFP mice showed higher input flux from glycerol with similar input flux from lactate compared to RD-GFP mice (Fig. 5.6a and 5.6b) and as a result, more carbon in gluconeogenesis originates from glycerol compared to RD-GFP mice (Fig. 5.6f). In contrast, RD-LIRKO mice showed

25% increase in glycerol input flux and 50% increase in lactate input flux (Fig. 5.6a and 5.6c). As a result, the origin of carbon slightly favored lactate compared to RD-GFP mice (Fig. 5.6f). Similarly, HFD-LIRKO mice showed 40% increase in glycerol input flux and 75% increase in lactate input flux (Fig. 5.6a and 5.6d). Therefore, the origin of carbon also slightly favored lactate in HFD-LIRKO mice compared to RD-GFP mice (Fig. 5.6f).

Hepatic insulin receptor knockout decreases gene expression of *Gyk* but increases that of *Pck1* and *G6pc* in the context of HFD feeding

HFD-LIRKO mice showed decreased input flux from glycerol and increased input flux from lactate compared to HFD-GFP mice (Fig. 5.6b and 5.6d). To further investigate the possible mechanism that affects the preference of substrate, we compared the liver gene expression of all the key enzymes in gluconeogenesis pathway (Fig. 5.7a). Interestingly, HFD-LIRKO mice showed reduced expression of glycerol specific gene (*Gyk*) but increased expression of lactate specific gene (*Pck1*). These observations were further confirmed at the protein level that the HFD-LIRKO mice showed reduced GYK with slightly increased PCK1 (Fig. 5.7c) compared to the HFD-GFP mice. Together, these data provide further evidence that hepatic insulin receptor knockout affects the substrate preference by regulating the expression of GYK and PCK1.
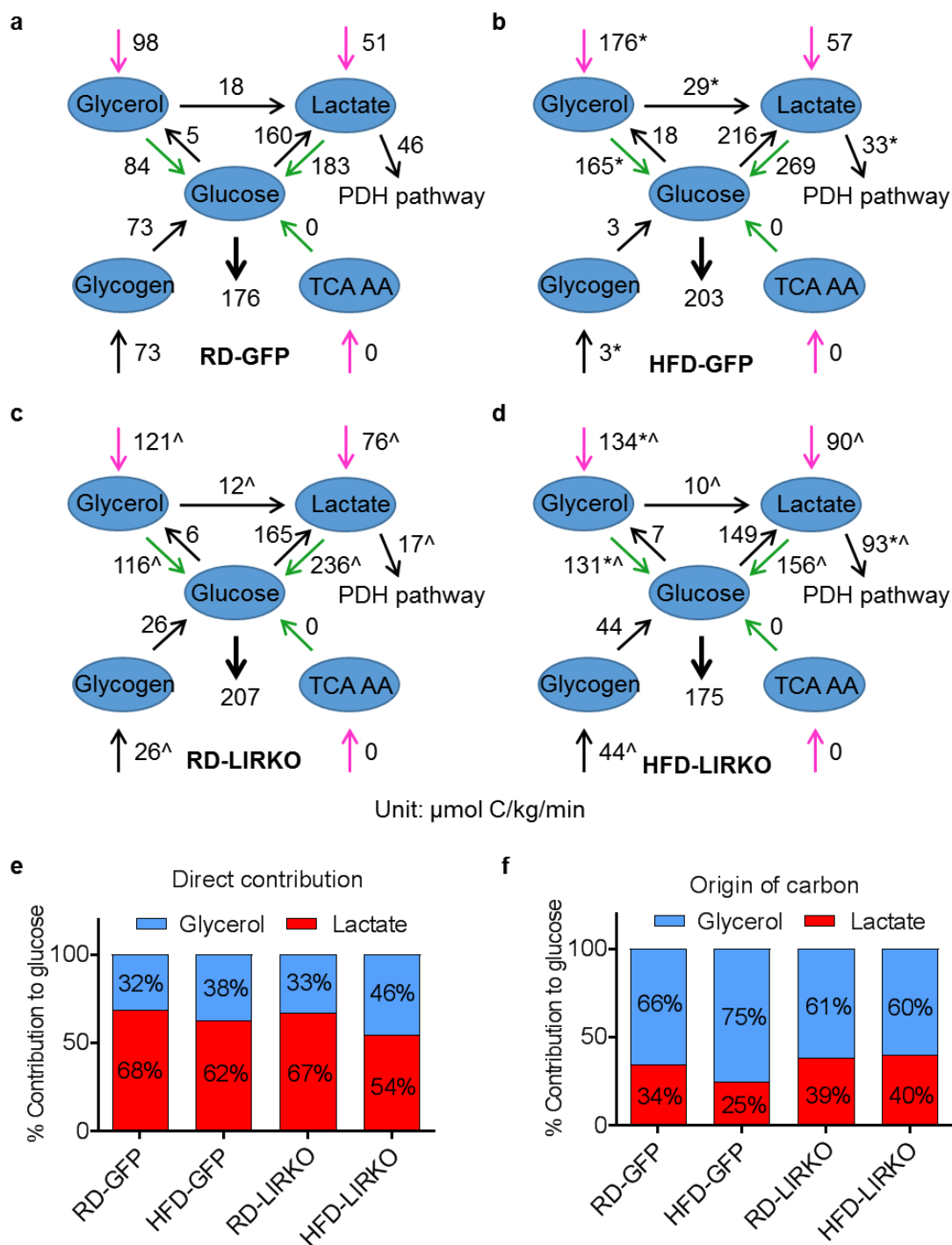
Figure 5.6 | Direct contribution and origin of carbon in gluconeogenesis. a-d, summarized flux network of RD-GFP, HFD-GFP, RD-LIRKO, HFD-LIRKO mice; the direct contribution and origin of carbon flux are shown in green and purple arrows respectively;* significant difference caused by HFD; ^ significant difference caused by LIRKO. **e,** direct contribution of glucose. **f,** origin of carbon.
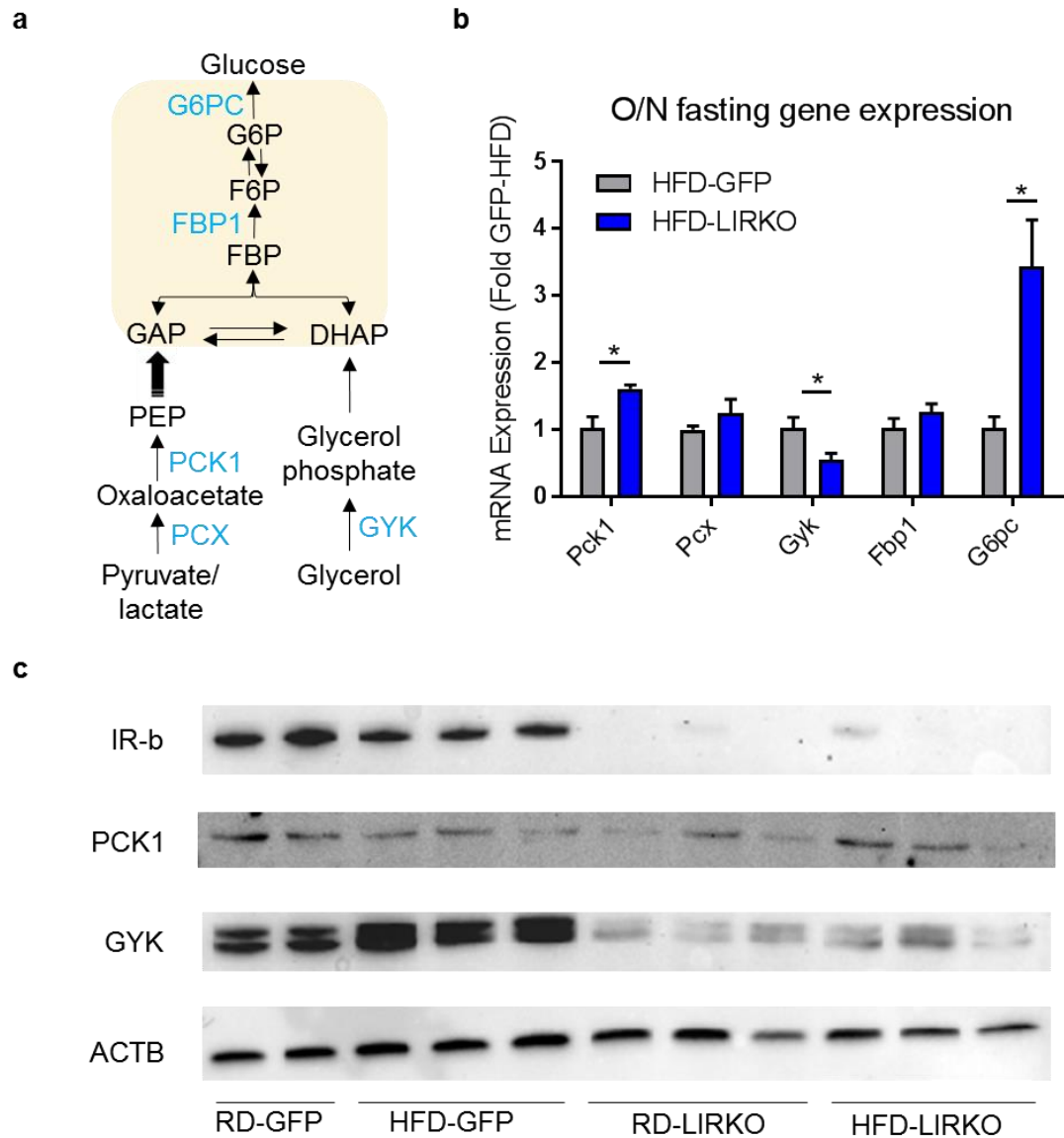
Figure 5.7 | Glycerol kinase is down-regulated in LIRKO mice. a, Gluconeogenic pathway using pyruvate and glycerol as substrates. Enzymes are shown in blue. The shared pathways of the two substrates are highlighted in yellow. **b,** Gluconeogenic gene expression of HFD-GFP and HFD-LIRKO mice. **c,** Western blot images showing levels of insulin receptor beta (IR-b) and glycerol kinase (Gyk). In all figures, data are mean ± s.e.m.; *P<0.05 by student's t-test.

Discussion

This study investigated the interactions between liver insulin signaling and HFD feeding. We showed that HFD feeding caused median but whole body insulin resistance and significantly enhanced gluconeogenic flux from glycerol but not lactate. In contrast, LIRKO caused complete hepatic insulin resistance and a mild increase of gluconeogenic flux from both glycerol and lactate. Interestingly, HFD-LIRKO mice showed reduced total gluconeogenesis with a shift of substrate preference from glycerol to lactate compared to the HFD-GFP mice. Together, these results suggest hepatic insulin resistance and HFD feeding increases gluconeogenesis through different mechanisms.

Lactate and glycerol require different enzymes to enter gluconeogenesis pathway (Fig. 5.7a). Lactate requires pyruvate carboxylase (PCX) and Phosphoenolpyruvate Carboxykinase 1 (PCK1) while glycerol requires glycerol kinase (GYK). Our data showed that when hepatic insulin receptor is knocked out, a shift of substrate preference from glycerol to lactate is observed in the HFD fed animal but not in the normal chow fed animal (Fig. 5.2). In consistence with these findings, HFD-LIRKO mice showed a reduction in GYK expression but not in PCX or PCK1 expression, suggesting a restriction of the usage of glycerol in LIRKO mice. However, although both RD-LIRKO and HFD-LIRKO mice showed reduced GYK expression, the shift of substrate preference was only observed in HFD fed mice (Fig. 5.2). One explanation is that GYK

is rate limiting only when the usage of glycerol is increased in HFD-fed mice. Further studies should investigate the mechanism of LIRKO reducing GYK expression.

In conclusion, HFD and LIRKO have different effects on gluconeogenesis. HFD feeding significantly increases gluconeogenic flux from glycerol whereas LIRKO slightly increases gluconeogenic flux from both glycerol and lactate. When two effects are combined in HFD-LIRKO mice, a reduction of gluconeogenesis and a shift of substrate preference from glycerol to lactate is observed compared to HFD-GFP mice. Therefore, we conclude HFD feeding and hepatic insulin resistance are two different mechanisms that increases gluconeogenesis.

Chapter 6 . GENERAL DISCUSSION

Review of major findings

In this dissertation, we developed a mathematical model for the flux analysis of gluconeogenesis (GNG). After verified its performance in primary hepatocytes, we performed metabolic flux analysis (MFA) in 6 different mouse models: wild type control fed on normal chow (GFP) or high fat diet (GFP-HFD), mice with activated liver glucagon signaling fed on normal chow (PKA) or high fat diet (PKA-HFD) and mice with liver insulin resistance fed on normal chow (LIRKO) or high fat diet (LIRKO-HFD).

In wild type control mice, we investigated the relative contribution of glycogen, lactate and glycerol in glucose production after 6, 12 and 18 hours of fasting (Chapter 3). By performing non-perturbative infusions of $^{13}C_3$ lactate, $^{13}C_3$ glycerol and $^{13}C_6$ glucose, we found both lactate and glycerol significantly labeled about 60% and 30%-50% glucose carbon but glucose labeled much more lactate (~90%) than glycerol carbon (~10%). Using the newly developed flux model, we showed that lactate, but not glycerol is largely recycled during all fasting periods such that lactate is the largest direct contributor to GNG via the Cori cycle but a minor source of new glucose carbon. In contrast, glycerol is not only a significant direct contributor to GNG but also the largest overall contributor to GNG regardless of fasting length. Prolonged fasting decreased both the whole-body turnover rate of glucose and lactate but increased that

of glycerol, indicating that the usage of glycerol in GNG became more significant with longer fasting.

In GFP-HFD, PKA and PKA-HFD mice, we investigated the interactions between HFD feeding and liver glucagon signaling in GNG. We found both HFD and glucagon signaling individually enhanced gluconeogenesis by presumably different mechanisms. HFD increased GNG flux from glycerol but not from lactate. In contrast, glucagon signaling increased GNG flux from both glycerol and lactate. The most interesting phenotype was found in the HFD-PKA model where the two factors are combined. HFD-PKA mice exhibited a synergistic increase of GNG compared to HFD or PKA activation alone. Further investigations suggested this effect was facilitated by increased expression of *G6pc*, which was regulated by both enhanced glycerol and PKA activation. Through this study, we emphasized the dual roles of glycerol that it not only provided the majority of new carbon in GNG, but also an important regulator of *G6pc*.

Similarly, in GFP-HFD, LIRKO and LIRKO-HFD mice, we investigated the effect and interactions between HFD and liver insulin resistance in GNG. LIRKO mice which have complete liver insulin resistance but normal peripheral insulin signaling showed a mild increase of GNG flux from both lactate and glycerol. In contrast, GFP-HFD mice which have median insulin resistance in both liver and periphery showed a robust increase of GNG flux from glycerol but not lactate. Interestingly, the LIRKO-HFD mice

which have both complete liver insulin resistance and median peripheral insulin resistance, showed a switch of substrate preference from glycerol to lactate compared to HFD-GFP mice. Further investigations suggested this switch was related to the downregulation of glycerol kinase in LIRKO-HFD mice. Together, these data suggest the hepatic insulin resistance and HFD increase GNG through different mechanisms.

This dissertation illustrated how metabolic flux models are constructed and help to analyze a relatively complicated pathway like GNG. By performing flux analysis in multiple diabetic mouse models, we demonstrated metabolic flux analysis (MFA) as a useful, powerful and unique tool to investigate the metabolism *in vivo*. Our result suggest neither enzyme level nor substrate concentration alone is sufficient to quantify a metabolic flux. For example, the expression of glycerol kinase was down-regulated in the RD-LIRKO mice compared to RD-GFP mice (Fig. 5.7c) yet we did not observe a decrease of glycerol flux associated with it (Fig. 5.5). This is because when the availability of substrate is restricted, the reaction rate is determined by the substrate concentration instead of the enzyme level. Similarly, the glycerol concentration was decreased in PKA mice compared to RD-GFP mice (Fig. 4.3d), yet the glycerol flux was found increased (Fig. 4.5e). Therefore, to accurately quantify the metabolism *in vivo* and distinguish its changes under different conditions, MFA seems to be the only reliable solution so far.

<u>Future directions</u>

Although we illustrated MFA as a powerful tool to study metabolism, MFA is still not a popular technique that is widely used, especially in clinical studies. To more easily apply MFA in clinical studies, several obstacles must be resolved. First, MFA experiments require the infusion of multiple isotopic tracers at the same steady-state to ensure the accuracy of flux measurement. In mouse studies, this is normally achieved by infusing the same mouse with different tracers one at a time and each time requires the same fasting condition. Consequently, the whole experiment may take several weeks to complete. However, this strategy is usually impractical in clinical studies since human subjects may hesitate to visit multiple times and fast for a long period of time before each visit. Therefore, better experimental strategies must be applied for clinical studies. For example, multiple tracers may be infused together to minimize the total number of visits. However, further investigations are required to verify such strategies.

Another obstacle need to be resolved is the difficulty to construct MFA models and perform flux analysis. Although in Chapter 2 we described how the GNG flux model is constructed and worked in detail, MFA in general is still out of reach for most investigators without necessary training of programming. To solve this problem, flux analysis software with more user friendly and intuitive human-computer interface must be developed. The ultimate goal would be to allow investigators to construct their own flux network and perform flux analysis without any coding process.

Lastly, current MFA experiments rely on analyzing the blood sample to illustrate the whole body metabolism. Consequently, specific flux from individual organs cannot be illustrated. For example, in terms of GNG, although the whole body GNG flux can be calculated, it does not provide any information about the location of GNG. Previous studies suggest both live and kidney are capable of making glucose, but the exact contribution from these two organs are controversial [105]. Therefore, to better understand the function and contribution of individual organ, new experimental strategies such as organ specific tracer perfusion must be developed.

<u>Conclusions</u>

In conclusion, MFA is a useful, powerful and unique tool to investigate the metabolism in gluconeogenesis. Using MFA, we illustrated the individual effect of fasting, glucagon signaling, HFD and hepatic insulin resistance on gluconeogenesis fluxes from different substrates. Moreover, by combining different mouse models, we also illustrated that glucagon signaling and HFD synergistically increase GNG whereas hepatic insulin receptor knock-out switches the substrate preference of GNG in the context of HFD. Further studies should focus on simplify the procedure of MFA experiments and analysis to make it more accessible and suitable for clinical studies.

Appendix 1: Supplemental Materials for Chapter 2: Construction of Flux Models for Gluconeogenesis

Supplementary Fig. A1. 1: R code for generating atom transition matrices

```
#Code adapted from Xiaoyang Su

EMU_S1_Input <- read.csv("EMU_GlcNeo_1.csv",header = FALSE,stringsAsFactors=FALSE)

EMU_S2_Input <- read.csv("EMU_GlcNeo_2.csv",header = FALSE,stringsAsFactors=FALSE)

EMU_S3_Input <- read.csv("EMU_GlcNeo_3.csv",header = FALSE,stringsAsFactors=FALSE)

EMU_S4_Input <- read.csv("EMU_GlcNeo_4.csv",header = FALSE,stringsAsFactors=FALSE)

EMU_S5_Input <- read.csv("EMU_GlcNeo_5.csv",header = FALSE,stringsAsFactors=FALSE)

EMU_S6_Input <- read.csv("EMU_GlcNeo_6.csv",header = FALSE,stringsAsFactors=FALSE)

EMU_S1_List <- EMU_S1_Input[1:31,4]

EMU_S2_List <- EMU_S2_Input[1:33,4]

EMU_S3_List <- EMU_S3_Input[1:23,4]

EMU_S4_List <- EMU_S4_Input[1:8,4]

EMU_S5_List <- EMU_S5_Input[1:5,4]

EMU_S6_List <- EMU_S6_Input[1:6,4]

EMU_FluxList <- EMU_S1_Input[1:23,5]

EMU_S1_Substrate <- as.numeric(factor(EMU_S1_Input[,1],levels = EMU_S1_List))

EMU_S1_Product <- as.numeric(factor(EMU_S1_Input[,2],levels = EMU_S1_List))

EMU_S1_Flux <- as.numeric(factor(EMU_S1_Input[,3],levels = EMU_FluxList))

EMU_S2_Substrate <- as.numeric(factor(EMU_S2_Input[,1],levels = EMU_S2_List))
```

```
EMU_S2_Product <- as.numeric(factor(EMU_S2_Input[,2],levels = EMU_S2_List))

EMU_S2_Flux <- as.numeric(factor(EMU_S2_Input[,3],levels = EMU_FluxList))

EMU_S3_Substrate <- as.numeric(factor(EMU_S3_Input[,1],levels = EMU_S3_List))

EMU_S3_Product <- as.numeric(factor(EMU_S3_Input[,2],levels = EMU_S3_List))

EMU_S3_Flux <- as.numeric(factor(EMU_S3_Input[,3],levels = EMU_FluxList))

EMU_S4_Substrate <- as.numeric(factor(EMU_S4_Input[,1],levels = EMU_S4_List))

EMU_S4_Product <- as.numeric(factor(EMU_S4_Input[,2],levels = EMU_S4_List))

EMU_S4_Flux <- as.numeric(factor(EMU_S4_Input[,3],levels = EMU_FluxList))

EMU_S5_Substrate <- as.numeric(factor(EMU_S5_Input[1:3,1],levels = EMU_S5_List))

EMU_S5_Product <- as.numeric(factor(EMU_S5_Input[1:3,2],levels = EMU_S5_List))

EMU_S5_Flux <- as.numeric(factor(EMU_S5_Input[1:3,3],levels = EMU_FluxList))

EMU_S6_Substrate <- as.numeric(factor(EMU_S6_Input[1:4,1],levels = EMU_S6_List))

EMU_S6_Product <- as.numeric(factor(EMU_S6_Input[1:4,2],levels = EMU_S6_List))

EMU_S6_Flux <- as.numeric(factor(EMU_S6_Input[1:4,3],levels = EMU_FluxList))

EMUfy <- function(product, substrate, flux, EMU_number,EMU_number_total) {

  LeftMatrix <- matrix(0,nrow=EMU_number,ncol=EMU_number)

  RightMatrix <- matrix(0,nrow=EMU_number,ncol=EMU_number_total-EMU_number)

  for (i in 1:length(flux)) {

    a <- product[i]

    b <- substrate[i]

    c <- flux[i]
```

```
    if (b > EMU_number) {

      RightMatrix[a,b-EMU_number] <- c

    }

    else {

      LeftMatrix[a,b] <- c

    }

  }

  return(list(Left=LeftMatrix, Right=RightMatrix))

}

EMU <- list()

EMU[[1]]  <-  EMUfy(substrate  =  EMU_S1_Substrate,product  =  EMU_S1_Product,flux  =
EMU_S1_Flux,EMU_number = 23,EMU_number_total = 31)

EMU[[2]]  <-  EMUfy(substrate  =  EMU_S2_Substrate,product  =  EMU_S2_Product,flux  =
EMU_S2_Flux,EMU_number = 23,EMU_number_total = 33)

EMU[[3]]  <-  EMUfy(substrate  =  EMU_S3_Substrate,product  =  EMU_S3_Product,flux  =
EMU_S3_Flux,EMU_number = 15,EMU_number_total = 23)

EMU[[4]]  <-  EMUfy(substrate  =  EMU_S4_Substrate,product  =  EMU_S4_Product,flux  =
EMU_S4_Flux,EMU_number = 4,EMU_number_total = 8)

EMU[[5]]  <-  EMUfy(substrate  =  EMU_S5_Substrate,product  =  EMU_S5_Product,flux  =
EMU_S5_Flux,EMU_number = 2,EMU_number_total = 5)

EMU[[6]]  <-  EMUfy(substrate  =  EMU_S6_Substrate,product  =  EMU_S6_Product,flux  =
```

```
EMU_S6_Flux,EMU_number = 3,EMU_number_total = 6)

for (i in 1:6) {

  write.csv(EMU[[i]][[1]],file=paste("EMU_GlcNeo_",i,"L.csv",sep=""),row.names=FALSE)

  write.csv(EMU[[i]][[2]],file=paste("EMU_GlcNeo_",i,"R.csv",sep=""),row.names=FALSE)

}
```

Supplementary Fig. A1. 2: R code for obtaining best-fit fluxes and confidence intervals

```
#Code adapted from Xiaoyang Su

EMU_Model <- list()

require(DEoptim)

require(nloptr)

require(nloptr)

require(MASS)

require(pracma)

require(numDeriv)

for (i in c(1:6)) {

  for (j in c("L","R")) {

    index <- paste(i,j,sep="")

    EMU_Model[[index]]  <-  read.csv(paste("EMU_GlcNeo_",index,".csv",sep=""),header  =

TRUE,stringsAsFactors=FALSE)

  }
```

```
}

Test.Labeling <- read.csv(file="Kasia's data.csv")

Test.Glucose.lac <- Test.Labeling[1:7,4]

Test.G6P.lac <- Test.Labeling[8:14,4]

Test.PEP.lac <- Test.Labeling[15:18,4]

Test.Pyruvate.lac <- Test.Labeling[19:22,4]

Test.Malate.lac <- Test.Labeling[23:27,4]

Test.Citrate.lac <- Test.Labeling[28:34,4]

Test.aKG.lac <- Test.Labeling[35:40,4]

Test.Glucose.glcr <- Test.Labeling[1:7,5]

Test.G6P.glcr <- Test.Labeling[8:14,5]

Test.PEP.glcr <- Test.Labeling[15:18,5]

Test.Pyruvate.glcr <- Test.Labeling[19:22,5]

Test.Malate.glcr <- Test.Labeling[23:27,5]

Test.Citrate.glcr <- Test.Labeling[28:34,5]

Test.aKG.glcr <- Test.Labeling[35:40,5]

E_glcr <- 1

E_lac <- 1

######################

Lactate_Input_U <- list(

  cbind(c(1,1),c(0,0)),
```

```
  cbind(c(1,1),c(0,0),c(0,0)),

  c(1,0,0,0)

)

Lactate_Input_L <- list(

  cbind(c(1-E_lac,1-E_lac),c(E_lac,E_lac)),

  rbind(c(1-E_lac,0,E_lac),c(1-E_lac,0,E_lac)),

  c(1-E_lac,0,0,E_lac)

)

Glycerol_Input_U <- list(

  cbind(c(1,1),c(0,0)),

  cbind(c(1,1),c(0,0),c(0,0)),

  c(1,0,0,0)

)

Glycerol_Input_L <- list(

  cbind(c(1-E_glcr,1-E_glcr),c(E_glcr,E_glcr)),

  rbind(c(1-E_glcr,0,E_glcr),c(1-E_glcr,0,E_glcr)),

  c(1-E_glcr,0,0,E_glcr)

)

Protein_Input <- list(

  c(1,0),

  c(1,0,0),
```

```
    c(1,0,0,0),

    c(1,0,0,0,0),

    c(1,0,0,0,0,0),

    c(1,0,0,0,0,0,0)

)

FFA_Input <- list(

    c(1,0),

    c(1,0,0)

)

Glycogen_Input <- list(

    c(1,0),

    c(1,0,0),

    c(1,0,0,0),

    c(1,0,0,0,0),

    c(1,0,0,0,0,0),

    c(1,0,0,0,0,0,0)

)

Glutamine_Input_U <- list(

    c(1,0),

    c(1,0,0),

    c(1,0,0,0),
```

```r
  c(1,0,0,0,0),

  c(1,0,0,0,0,0)

)

Glutamine_Input_L <- list(

  c(0,1),

  c(0,0,1),

  c(0,0,0,1),

  c(0,0,0,0,1),

  c(0,0,0,0,0,1)

)

CO2_Input_U <- c(1,0)

CO2_Input_L <- c(0,1)

Lactate_Input <- Lactate_Input_U

Glycerol_Input <- Glycerol_Input_L

Glutamine_Input <- Glutamine_Input_U

CO2_Input <- CO2_Input_U

CP <- function(x,y) {

  nx <- length(x)

  ny <- length(y)

  n <- nx+ny-1

  Tx <- matrix(0,ncol=ny,nrow=n)
```

```
    Product <- rep(0,n)

    for (i in 1:ny) {

        Tx[i:(i+nx-1),i] <- x

    }

    Product <- Tx %*% y

    return(t(Product))

}

Fluxify <- function(f) {

    Glycogen <- f[1]

    Glycerol <- f[2]

    Lactate <- f[3]

    FFA <- f[4]

    Protein <- f[5]

    Enolase <- f[6]

    PCX <- f[7]

    PDH <- f[8]

    Suc_DH <- f[9]

    Flop <- 5000

    v <- rep(0,23)

    #In vivo(0.18/0.45/0.37) #In vitro(0/0.55/0.45)

    v[3] <- 30
```

v[19] <- Protein

v[20] <- 0*Protein

v[21] <- 0.55*Protein

v[22] <- 0.45*Protein

v[23] <- Flop

v[1] <- 0.5*(v[3]-PDH+Lactate+Glycerol+Protein+2*Glycogen)

v[2] <- Glycogen

v[4] <- v[1]-Glycogen

v[5] <- Glycerol

v[6] <- Enolase+PDH-Lactate-Protein

v[7] <- Enolase

v[8] <- PCX+PDH-Lactate #v[11]+v[12]-v[9]

v[9] <- Lactate

v[10] <- Protein+PCX

v[11] <- PCX

v[12] <- PDH

v[13] <- FFA

v[14] <- Suc_DH+PDH+FFA+v[21]+v[22]

v[15] <- Suc_DH

v[16] <- PDH+FFA

v[17] <- PDH+FFA+v[22]

```
    v[18] <- PDH+FFA

    return(v)

}

#########

MID <- function(f) {#Basic function

    v <- Fluxify(f)

    v[3] <- v[3]/2 # Glucose [2] and [5] all gives DHAP[2], therefore the flux is used twice here, should
use half of the flux.

    EMU_Matrices <- EMU_Model
#convert flux name into actural values

    for (i in 1:length(EMU_Matrices)) {

        for (j in 1:23) {

            EMU_Matrices[[i]][EMU_Model[[i]]==j] <- v[j]

        }

        EMU_Matrices[[i]] <- as.matrix(EMU_Matrices[[i]])

    }
#fill in the diagnal of each left matrix

    for (i in c(1:6)) {

        for (j in 1:ncol(EMU_Matrices[[2*i-1]])) {

            EMU_Matrices[[2*i-1]][j,j]                <-                -(sum(EMU_Matrices[[2*i-
1]][j,])+sum(EMU_Matrices[[2*i]][j,]))
```

```
    }

  }

#solve matrices from level 1 to level 6

  EMU_S1_Label <- solve(EMU_Matrices$'1L') %*% -EMU_Matrices$'1R' %*%

    rbind(Glycerol_Input[[1]][1,],

        Glycerol_Input[[1]][2,],

        Glycogen_Input[[1]],

        Lactate_Input[[1]][1,],

        Lactate_Input[[1]][2,],

        Protein_Input[[1]],

        FFA_Input[[1]],

        Glutamine_Input[[1]])

  Right_Input_2 <- rbind(CP(EMU_S1_Label[1,],EMU_S1_Label[16,]),

            CP(EMU_S1_Label[16,],EMU_S1_Label[1,]),

            Glycerol_Input[[2]][1,],

            Glycerol_Input[[2]][2,],

            Glycogen_Input[[2]],

            Lactate_Input[[2]][1,],

            Lactate_Input[[2]][2,],

            FFA_Input[[2]],

            Protein_Input[[2]],
```

```
                              Glutamine_Input[[2]])

EMU_S2_Label <- solve(EMU_Matrices$'2L') %*% -EMU_Matrices$'2R' %*% Right_Input_2

Right_Input_3 <- rbind(CP(EMU_S2_Label[1,],EMU_S1_Label[16,]),

                       CP(EMU_S2_Label[17,],EMU_S1_Label[1,]),

                       CP(CO2_Input,EMU_S2_Label[21,]),

                       Glycerol_Input[[3]],

                       Glycogen_Input[[3]],

                       Lactate_Input[[3]],

                       Protein_Input[[3]],

                       Glutamine_Input[[3]])

EMU_S3_Label <- solve(EMU_Matrices$'3L') %*% -EMU_Matrices$'3R' %*% Right_Input_3

Right_Input_4 <- rbind(Protein_Input[[4]],

                       CP(EMU_S2_Label[1,],EMU_S2_Label[16,]),

                       CP(EMU_S3_Label[15,],CO2_Input),

                       Glutamine_Input[[4]]

                       )

EMU_S4_Label <- solve(EMU_Matrices$'4L') %*% -EMU_Matrices$'4R' %*% Right_Input_4

Right_Input_5 <- rbind(Protein_Input[[5]],

                       CP(EMU_S3_Label[11,],EMU_S2_Label[1,]),

                       Glutamine_Input[[5]]

                       )

)
```

```r
EMU_S5_Label <- solve(EMU_Matrices$'5L') %*% -EMU_Matrices$'5R' %*% Right_Input_5

Right_Input_6 <- rbind(CP(EMU_S3_Label[5,],EMU_S3_Label[5,]),

                       Glycogen_Input[[6]],

                       CP(EMU_S4_Label[4,],EMU_S2_Label[1,])

)

EMU_S6_Label <- solve(EMU_Matrices$'6L') %*% -EMU_Matrices$'6R' %*% Right_Input_6

ResultMatrix <- matrix(0,nrow=7,ncol=7)

ResultMatrix[1:7,1] <- EMU_S6_Label[1,]#Glucose

ResultMatrix[1:4,2] <- EMU_S3_Label[5,]#DHAP

ResultMatrix[1:4,3] <- EMU_S3_Label[12,]#PEP

ResultMatrix[1:4,4] <- EMU_S3_Label[15,]#Pyruvate

ResultMatrix[1:5,5] <- EMU_S4_Label[1,]#Succinate

ResultMatrix[1:6,6] <- EMU_S5_Label[1,]#aKG

ResultMatrix[1:7,7] <- EMU_S6_Label[3,]#Citrate

colnames(ResultMatrix) <- c("Glucose","DHAP","PEP","Pyruvate","Succinate","aKG","Citrate")

rownames(ResultMatrix) <- c("M+0","M+1","M+2","M+3","M+4","M+5","M+6")

return(ResultMatrix)
}

MID2 <- function(f) {#Function that used for labeled balance

v <- Fluxify(f)
```

v[3] <- v[3]/2 # Glucose [2] and [5] all gives DHAP[2], therefore the flux is used twice here, should use half of the flux.

```
EMU_Matrices <- EMU_Model

#convert flux name into actural values

for (i in 1:length(EMU_Matrices)) {

  for (j in 1:23) {

    EMU_Matrices[[i]][EMU_Model[[i]]==j] <- v[j]

  }

  EMU_Matrices[[i]] <- as.matrix(EMU_Matrices[[i]])

}

#fill in the diagnal of each left matrix

for (i in c(1:6)) {

  for (j in 1:ncol(EMU_Matrices[[2*i-1]])) {

    EMU_Matrices[[2*i-1]][j,j]                    <-                    -(sum(EMU_Matrices[[2*i-1]][j,])+sum(EMU_Matrices[[2*i]][j,]))

  }

}

#solve matrices from level 1 to level 6

EMU_S1_Label <- solve(EMU_Matrices$'1L') %*% -EMU_Matrices$'1R' %*%

  rbind(Glycerol_Input[[1]][1,],

        Glycerol_Input[[1]][2,],
```

```
                Glycogen_Input[[1]],

                Lactate_Input[[1]][1,],

                Lactate_Input[[1]][2,],

                Protein_Input[[1]],

                FFA_Input[[1]],

                Glutamine_Input[[1]])

Right_Input_2 <- rbind(CP(EMU_S1_Label[1,],EMU_S1_Label[16,]),

                CP(EMU_S1_Label[16,],EMU_S1_Label[1,]),

                Glycerol_Input[[2]][1,],

                Glycerol_Input[[2]][2,],

                Glycogen_Input[[2]],

                Lactate_Input[[2]][1,],

                Lactate_Input[[2]][2,],

                FFA_Input[[2]],

                Protein_Input[[2]],

                Glutamine_Input[[2]])

EMU_S2_Label <- solve(EMU_Matrices$'2L') %*% -EMU_Matrices$'2R' %*% Right_Input_2

Right_Input_3 <- rbind(CP(EMU_S2_Label[1,],EMU_S1_Label[16,]),

                CP(EMU_S2_Label[17,],EMU_S1_Label[1,]),

                CP(CO2_Input,EMU_S2_Label[21,]),

                Glycerol_Input[[3]],
```

```
                            Glycogen_Input[[3]],

                            Lactate_Input[[3]],

                            Protein_Input[[3]],

                            Glutamine_Input[[3]])

EMU_S3_Label <- solve(EMU_Matrices$'3L') %*% -EMU_Matrices$'3R' %*% Right_Input_3

Right_Input_4 <- rbind(Protein_Input[[4]],

                            CP(EMU_S2_Label[1,],EMU_S2_Label[16,]),

                            CP(EMU_S3_Label[15,],CO2_Input),

                            Glutamine_Input[[4]]

)

EMU_S4_Label <- solve(EMU_Matrices$'4L') %*% -EMU_Matrices$'4R' %*% Right_Input_4

Right_Input_5 <- rbind(Protein_Input[[5]],

                            CP(EMU_S3_Label[11,],EMU_S2_Label[1,]),

                            Glutamine_Input[[5]]

)

EMU_S5_Label <- solve(EMU_Matrices$'5L') %*% -EMU_Matrices$'5R' %*% Right_Input_5

Right_Input_6 <- rbind(CP(EMU_S3_Label[5,],EMU_S3_Label[5,]),

                            Glycogen_Input[[6]],

                            CP(EMU_S4_Label[4,],EMU_S2_Label[1,])

)

EMU_S6_Label <- solve(EMU_Matrices$'6L') %*% -EMU_Matrices$'6R' %*% Right_Input_6
```

```r
ResultMatrix <- matrix(0,nrow=7,ncol=5)

ResultMatrix[1:7,1] <- EMU_S6_Label[1,]#Glucose

ResultMatrix[1:4,2] <- EMU_S3_Label[5,]#DHAP

ResultMatrix[1:4,3] <- EMU_S3_Label[12,]#PEP

ResultMatrix[1:4,4] <- EMU_S3_Label[15,]#Pyruvate

ResultMatrix[1:5,5] <- EMU_S4_Label[1,]#Succinate

colnames(ResultMatrix) <- c("Glucose","DHAP","PEP","Pyruvate","Succinate")

rownames(ResultMatrix) <- c("M+0","M+1","M+2","M+3","M+4","M+5","M+6")

return(list(Levle1=EMU_S1_Label,

            Levle2=EMU_S2_Label,

            Levle3=EMU_S3_Label,

            Levle4=EMU_S4_Label,

            Levle5=EMU_S5_Label,

            Levle6=EMU_S6_Label,

            v))

}

MID_glcr <- function(f) {# function use glycerol tracer

   Lactate_Input <- Lactate_Input_U

   Glycerol_Input <- Glycerol_Input_L

   Glutamine_Input <- Glutamine_Input_U

   return(MID(f))
```

```r
}

MID_lac <- function(f) {# function use lactate tracer

  Lactate_Input <- Lactate_Input_L

  Glycerol_Input <- Glycerol_Input_U

  Glutamine_Input <- Glutamine_Input_U

  return(MID(f))

}

Res <- function(f) {

  Label_lac <- MID_lac(f)

  Label_glcr <- MID_glcr(f)

  Residual <- sum(c(

    (Test.Glucose.lac - Label_lac[1:7,1])^2,

    (Test.G6P.lac - Label_lac[1:7,1])^2,

    (Test.PEP.lac - Label_lac[1:4,3])^2,

    (Test.Pyruvate.lac - Label_lac[1:4,4])^2,

    (Test.Glucose.glcr - Label_glcr[1:7,1])^2,

    (Test.G6P.glcr - Label_glcr[1:7,1])^2,

    (Test.PEP.glcr - Label_glcr[1:4,3])^2,

    (Test.Pyruvate.glcr - Label_glcr[1:4,4])^2

  ))

  return(Residual)
```

```r
}

CI<-function(fluxset,threshold,fluxnumber){

  #upper boundary

  fluxlength<-length(fluxset)

  FluxPath <- matrix(0,nrow=1000,ncol=fluxlength+2)

  FluxPath[1,1:fluxlength] <- fluxset

  FluxPath[1,fluxlength+1] <- Res(fluxset)

  FluxPath[1,fluxlength+2] <- threshold

  CurrentFlux <- fluxset

  goodcount<-0

  highlimit<-0

  lowlimit<-0

  changingset<-CurrentFlux>0

  changingset[fluxnumber]<-FALSE

  for (i in 1:500) {

    J <- grad(Res,CurrentFlux)

    H <- hessian(Res,CurrentFlux)

    if(CurrentFlux[fluxnumber]<1){

      h <- 2*CurrentFlux[fluxnumber]

    } else {

      h <- 1
```

```
}

b <- -J[changingset]-H[changingset,fluxnumber]*h

A <- H[changingset,changingset]

u <- ginv(A,tol=1e-5) %*% b

update <- rep(0,fluxlength)

update[fluxnumber]<-h

update[changingset]<-u[1:sum(changingset)]

CurrentFlux <- CurrentFlux + update

while(!prod(CurrentFlux>0)){

  changingset<-changingset*CurrentFlux>0

  CurrentFlux <- CurrentFlux - update

  b <- -J[changingset]-H[changingset,fluxnumber]*h

  A <- H[changingset,changingset]

  u <- ginv(A,tol=1e-5) %*% b

  update <- rep(0,fluxlength)

  update[fluxnumber]<-h

  update[changingset]<-u[1:sum(changingset)]

  CurrentFlux <- CurrentFlux + update

}

FluxPath[1+i,1:fluxlength] <- CurrentFlux

FluxPath[1+i,fluxlength+1] <- Res(CurrentFlux)
```

```
  if(Res(CurrentFlux)>=threshold){

    goodcount <- goodcount + 1

  }

  if(Res(CurrentFlux)<threshold){

    goodcount <- 0

    highlimit <- CurrentFlux[fluxnumber]

  }

  flush.console()

  if(i%%1==0) print(paste(FluxPath[1+i,]))

  if(goodcount == 5) break

}

highPath<-FluxPath[1:(i+2),]

#lower boundary

FluxPath <- matrix(0,nrow=400,ncol=fluxlength+2)

FluxPath[1,1:fluxlength] <- fluxset

FluxPath[1,fluxlength+1] <- Res(fluxset)

FluxPath[1,fluxlength+2] <- threshold

CurrentFlux <- fluxset

goodcount<-0

changingset<-CurrentFlux>0

changingset[fluxnumber]<-FALSE
```

```
for (i in 1:500) {

  J <- grad(Res,CurrentFlux)

  H <- hessian(Res,CurrentFlux)

  if(CurrentFlux[fluxnumber]<1){

    break

  }

  else{

    h <- -1

  }

  b <- -J[changingset]-H[changingset,fluxnumber]*h

  A <- H[changingset,changingset]

  u <- ginv(A,tol=1e-5) %*% b

  update <- rep(0,fluxlength)

  update[fluxnumber]<-h

  update[changingset]<-u[1:sum(changingset)]

  CurrentFlux <- CurrentFlux + update

  while(!prod(CurrentFlux>0)){

    changingset<-changingset*CurrentFlux>0

    CurrentFlux <- CurrentFlux - update

    b <- -J[changingset]-H[changingset,fluxnumber]*h

    A <- H[changingset,changingset]
```

```r
    u <- ginv(A,tol=1e-5) %*% b

    update <- rep(0,fluxlength)

    update[fluxnumber]<-h

    update[changingset]<-u[1:sum(changingset)]

    CurrentFlux <- CurrentFlux + update

  }

  FluxPath[1+i,1:fluxlength] <- CurrentFlux

  FluxPath[1+i,fluxlength+1] <- Res(CurrentFlux)

  if(Res(CurrentFlux)>=threshold){

    goodcount <- goodcount + 1

  }

  if(Res(CurrentFlux)<threshold){

    goodcount <- 0

    lowlimit <- CurrentFlux[fluxnumber]

  }

  flush.console()

  if(i%%1==0) print(paste(FluxPath[1+i,]))

  if(goodcount == 5) break

}

lowPath<-FluxPath[1:(i+1),]

resultPath <- rbind(highPath,lowPath,c(highlimit,lowlimit,rep(0,fluxlength)))
```

```
    return(resultPath)

}

fluxsDE <- DEoptim(fn = Res,lower=rep(0.0001,9),upper= rep(5000,9),control=list(itermax=2000))

write.csv(c(fluxsDE$optim$bestval,fluxsDE$optim$bestmem),file=paste(group,"_flux_17df",".csv",se

p=""),row.names=TRUE)

bestflux<-fluxsDE$optim$bestmem

for (i in 1:5){

fluxes<-bobyqa(bestflux, lower=rep(0.0001,9),upper= rep(5000,9),fn=Res)

    bestflux<-fluxes$par

}

write.csv(c(Res(bestflux),bestflux),file=paste(group,"_flux_17df",".csv",sep=""),row.names=TRUE)

threshold<-Res(bestflux)+0.0001*qchisq(c(0.8,0.9,0.95),1)[3]#Chi square threshold

for(fluxnumber in c(1:9)){

write.csv(CI(bestflux,threshold,fluxnumber),file=paste("group",group,"_v",fluxnumber,".csv",sep=""))

}
```

Appendix 2: Supplemental Materials for Chapter 3: Effect of Fasting on Substrate Contribution in Gluconeogenesis

a

b

$$U_1 = 3V_5$$
$$U_2 = 3V_9$$
$$U_3 = 6V_2$$
$$U_4 = 3V_{19}$$
$$U_5 = 3V_6$$
$$U_6 = 3V_3$$
$$U_7 = 3V_8$$
$$U_8 = 3V_{11}$$
$$U_9 = 3V_{12}$$
$$U_{out} = 6(V_{out} - V_{glc})$$

Unit: nmol C /g/min
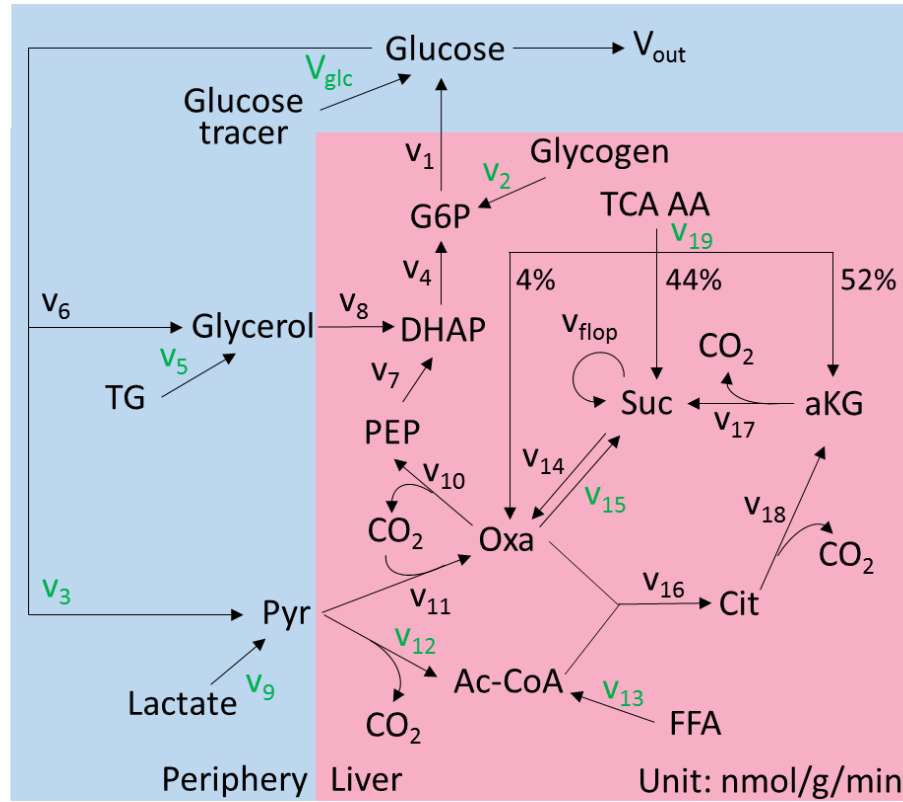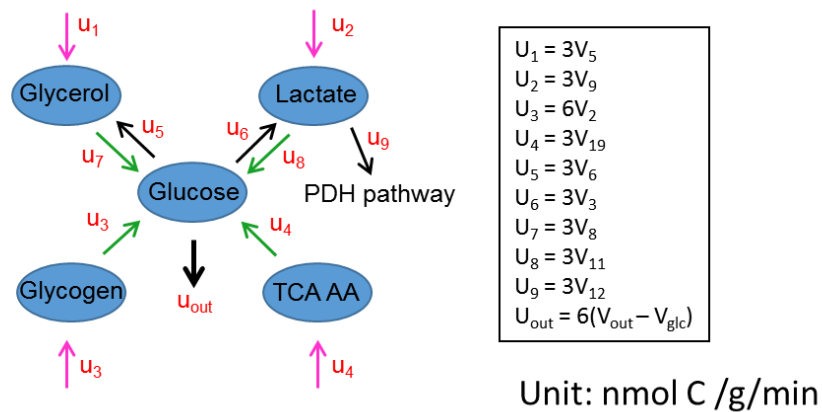
Supplementary Figure A2. 1 | Flux models. Related to Methods. a, EMU model with detailed gluconeogenic pathway. Reactions occur in the periphery and liver are shown under blue and red background respectively. Free fluxes are shown in green. **b,** Summarized gluconeogenic network and the equivalent fluxes. G6P, glucose-6-phosphate; TG, triglycerides; TCA, tricarboxylic acid; AA, amino acids; PEP, phosphoenolpyruvate; DHAP, dihydroxyacetone phosphate; Pyr, pyruvate; Ac-CoA, acetyl CoA; Oxa, oxaloacetate; Suc, succinate; Cit, citrate; aKG, α-ketoglutarate; FFA, free fatty acids.

Supplementary Table A2.1 | EMU atom transition. Related to Chapter 3 Methods. Refer to Supplementary Figure A2. 2 for atom transition information

| EMU size	Substrate	Product	Flux	EMU size	Substrate	Product	Flux
2+4=6	Ac-CoA[1-2]+Oxa[1-4]	Cit[1-6]	V16	2=2	PEP[2-3]	DHAP[2-3]	V7
6=6	Glycogen[1-6]	G6P[1-6]	V2	2=2	TG[2-3]	Glycerol[2-3]	V5
3+3=6	DHAP[1-3]+DHAP[1-3]	G6P[1-6]	V4	2=2	Glucose[2-3]	Glycerol[2-3]	V6
6=6	G6P[1-6]	Glucose[1-6]	V1	2=2	Oxa[2-3]	PEP[2-3]	V10
6=6	Glc-tracer[1-6]	Glucose[1-6]	Vglc	2=2	Pyr[2-3]	Oxa[2-3]	V11
5=5	Cit[1-5]	aKG[1-5]	V18	2=2	Suc[2-3]	Oxa[2-3]	V14
5=5	TCA-AA[1-5]	aKG[1-5]	V19c	2=2	TCA-AA[2-3]	Oxa[2-3]	V19a
2+3=5	Ac-CoA[1-2]+Oxa[2-4]	Cit[1-5]	V16	2=2	Oxa[2-3]	Suc[2-3]	V15
4=4	Cit[1-4]	aKG[1-4]	V18	2=2	aKG[2-3]	Suc[2-3]	V17
4=4	TCA-AA[1-4]	aKG[1-4]	V19c	2=2	TCA-AA[2-3]	Suc[2-3]	V19b
2+2=4	Ac-CoA[1-2]+Oxa[2-3]	Cit[1-4]	V16	2=2	Cit[2-3]	aKG[2-3]	V18
1+3=4	Pyr[1-3]+CO2	Oxa[1-4]	V11	2=2	TCA-AA[2-3]	aKG[2-3]	V19c
4=4	Suc[1-4]	Oxa[1-4]	V14	1+1=2	Ac-CoA[2]+Oxa[2]	Cit[2-3]	V16
4=4	TCA-AA[1-4]	Oxa[1-4]	V19a	1=1	Pyr[3]	Ac-CoA[2]	V12
4=4	Oxa[1-4]	Suc[1-4]	V15	1=1	FFA[2]	Ac-CoA[2]	V13
4=4	aKG[1-4]	Suc[1-4]	V17	1=1	Pyr[2]	Oxa[2]	V11
4=4	TCA-AA[1-4]	Suc[1-4]	V19b	1=1	Suc[2]	Oxa[2]	V14
3=3	Glycerol[1-3]	DHAP[1-3]	V8	1=1	TCA-AA[2]	Oxa[2]	V19a
3=3	PEP[1-3]	DHAP[1-3]	V7	1=1	Glucose[2]	Pyr[2]	V3
3=3	TG[1-3]	Glycerol[1-3]	V5	1=1	Lactate[2]	Pyr[2]	V9
3=3	Glucose[1-3]	Glycerol[1-3]	V6	1=1	G6P[2]	Glucose[2]	V1
3=3	G6P[1-3]	Glucose[1-3]	V1	1=1	Glc-tracer[2]	Glucose[2]	Vglc
3=3	Glu-tracer[1-3]	Glucose[1-3]	Vglc	1=1	Glycogen[2]	G6P[2]	V2
3=3	Glycogen[1-3]	G6P[1-3]	V2	1=1	DHAP[2]	G6P[2]	V4
3=3	DHAP[1-3]	G6P[1-3]	V4	1=1	Glycerol[2]	DHAP[2]	V8
3=3	Oxa[1-3]	PEP[1-3]	V10	1=1	PEP[2]	DHAP[2]	V7
3=3	Pyr[1-3]	Oxa[1-3]	V11	1=1	TG[2]	Glycerol[2]	V5
3=3	Suc[1-3]	Oxa[1-3]	V14	1=1	Glucose[2]	Glycerol[2]	V6
3=3	TCA-AA[1-3]	Oxa[1-3]	V19a	1=1	Oxa[2]	PEP[2]	V10
2+1=3	Pyr[2-3]+CO2	Oxa[2-4]	V11	1=1	Suc[3]	Suc[2]	Vflop
3=3	Suc[2-4]	Oxa[2-4]	V14	1=1	Oxa[2]	Suc[2]	V15
3=3	TCA-AA[2-4]	Oxa[2-4]	V19a	1=1	aKG[2]	Suc[2]	V17
3=3	Glucose[1-3]	Pyr[1-3]	V3	1=1	TCA-AA[2]	Suc[2]	V19b
3=3	Lactate[1-3]	Pyr[1-3]	V9	1=1	Suc[2]	Suc[3]	Vflop
3=3	Suc[2-4]	Suc[1-3]	Vflop	1=1	Oxa[3]	Suc[3]	V15
3=3	Oxa[1-3]	Suc[1-3]	V15	1=1	aKG[3]	Suc[3]	V17
3=3	aKG[1-3]	Suc[1-3]	V17	1=1	TCA-AA[3]	Suc[3]	V19b
3=3	TCA-AA[1-3]	Suc[1-3]	V19b	1=1	Pyr[3]	Oxa[3]	V11
3=3	Suc[1-3]	Suc[2-4]	Vflop	1=1	Suc[3]	Oxa[3]	V14
3=3	Oxa[2-4]	Suc[2-4]	V15	1=1	TCA-AA[3]	Oxa[3]	V19a
3=3	aKG[2-4]	Suc[2-4]	V17	1=1	Glucose[1]	Pyr[3]	V3
3=3	TCA-AA[2-4]	Suc[2-4]	V19b	1=1	Lactate[3]	Pyr[3]	V9
3=3	Cit[1-3]	aKG[1-3]	V18	1=1	G6P[1]	Glucose[1]	V1
3=3	TCA-AA[1-3]	aKG[1-3]	V19c	1=1	Glc-tracer[1]	Glucose[1]	Vglc
3=3	Cit[2-4]	aKG[2-4]	V18	1=1	Glycogen[1]	G6P[1]	V2
3=3	TCA-AA[2-4]	aKG[2-4]	V19c	1=1	DHAP[3]	G6P[1]	V4
2+1=3	Ac-CoA[1-2]+Oxa[2]	Cit[1-3]	V16	1=1	Glycerol[3]	DHAP[3]	V8
1+2=3	Ac-CoA[2]+Oxa[2-3]	Cit[2-4]	V16	1=1	PEP[3]	DHAP[3]	V7
2=2	FFA[1-2]	Ac-CoA[1-2]	V13	1=1	TG[3]	Glycerol[3]	V5
2=2	Pyr[2-3]	Ac-CoA[1-2]	V12	1=1	Glucose[3]	Glycerol[3]	V6
2=2	Glucose[1-2]	Pyr[2-3]	V3	1=1	Oxa[3]	PEP[3]	V10
2=2	Lactate[2-3]	Pyr[2-3]	V9	1=1	Cit[2]	aKG[2]	V18
2=2	G6P[1-2]	Glucose[1-2]	V1	1=1	TCA-AA[2]	aKG[2]	V19c
2=2	Glc-tracer[1-2]	Glucose[1-2]	Vglc	1=1	Cit[3]	aKG[3]	V18
2=2	Glycogen[1-2]	G6P[1-2]	V2	1=1	TCA-AA[3]	aKG[3]	V19c
2=2	DHAP[2-3]	G6P[1-2]	V4	1=1	Ac-CoA[2]	Cit[2]	V16
2=2	Glycerol[2-3]	DHAP[2-3]	V8	1=1	Oxa[2]	Cit[3]	V16
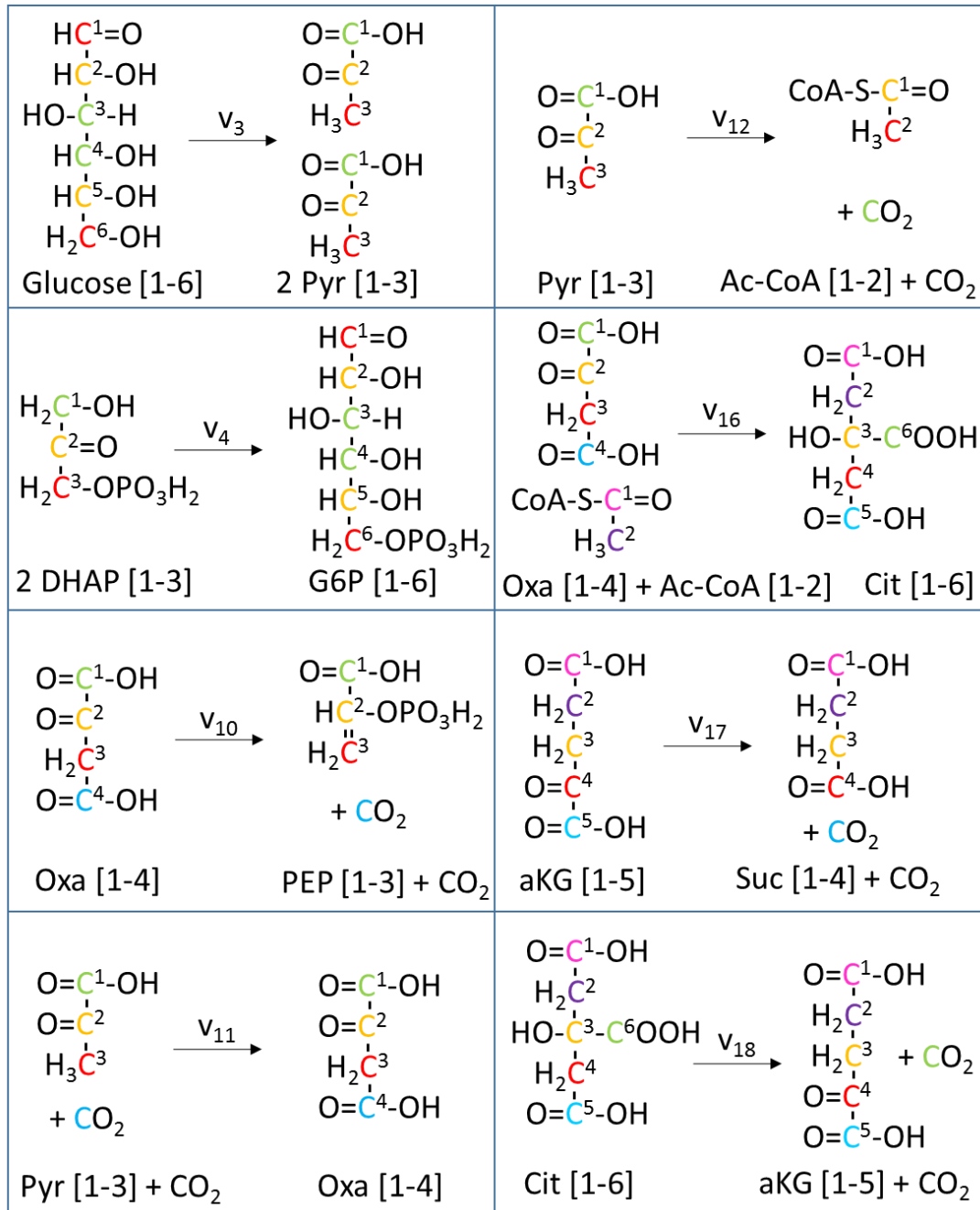
Supplementary Figure A2. 2 | Carbon rearrangement in EMU model. G6P, glucose-6-phosphate; PEP, phosphoenolpyruvate; DHAP, dihydroxyacetone phosphate; Ac-CoA, acetyl CoA; Oxa, oxaloacetate; Suc, succinate; Cit, citrate; aKG, α-ketoglutarate; Pyr, pyruvate.

Supplementary Table A2. 2 | Metabolomic changes 18-hour over 6-hour fasting. Related to Figure 3. 1.

| Name	Fold change	p-value	Name	Fold change	p-value
Acetyl leucine	1.53	0.89	Lyxose	2.47	0.50
Acetyl proline	2.51	0.98	Malate	1.37	0.10
Aconitate	1.41	0.23	Maleic acid	4.78	0.06
Adipic acid	12.39	0.07	Malonic acid	6.72	0.00
Arginine	0.99	1.00	Methionine	1.07	1.00
Ascorbic acid	4.49	0.47	Methionine sulfoxide	4.83	0.06
Aspartate	1.76	0.47	Methylcrotonic acid	26.73	0.00
Carnosine	3.67	1.00	Ketoleucine	1.12	1.00
Cholesteryl sulfate	1.00	1.00	Methylsuccinic acid	2.44	0.07
Citrate	0.54	0.98	N-Acetylaspartate	1.51	0.74
Citrulline	2.75	0.09	N-acetyl-glutamine	0.15	0.93
Creatine	1.77	0.63	N-Acetyl-L-alanine	0.00	1.00
Creatine Phosphate	0.48	0.73	N-acetyl-L-ornithine	0.44	0.96
Cresol	1.94	0.93	N-carbomoyl-L-aspartate	infinite	0.01
Cystine	0.00	0.67	N-octanoylglycine	3.03	0.04
Cytidine	1.80	0.93	o-acetyl-L-serine	2.28	0.07
Deoxycholic acid	4.28	0.54	Pantothenate	0.39	0.02
D-erythrose-4-phosphate	0.50	0.47	Phenylacetylglycine	1.87	0.01
dGDP	0.90	1.00	Phenylalanine	0.99	1.00
dGMP	1.20	1.00	Proline	1.23	1.00
Dihydroxyacetone phosphate	2.58	0.95	Pyridoxic acid	1.33	1.00
Glycerol	1.10	1.00	Pyroglutamate	1.47	0.40
Galactaric acid	1.62	1.00	Pyruvate	2.00	0.10
gamma-amino butyrate	2.60	0.21	Ribitol	1.34	1.00
Glucosamine	0.00	1.00	Ribonolactone	4.40	0.00
Glucose-1-phosphate	0.67	0.29	Sarcosine	1.42	0.74
Glucose	0.48	0.01	Serine	1.24	1.00
Glutamine	0.69	0.09	Sorbitol	0.93	1.00
Glyceric acid	54.44	0.00	Stearic acid	2.19	0.29
Glycine	2.30	1.00	Succinate	2.19	0.01
Gly-Gly	0.81	0.98	Sucrose	0.00	1.00
GTP	0.00	0.99	Tartaric acid	17.32	0.10
Hippuric acid	0.05	0.13	Taurine	1.01	1.00
Hisidine	1.14	1.00	Thiamine pyrophosphate	1.17	1.00
Homocysteic acid	8.27	0.00	Threonic acid	3.26	0.00
Homovanillic acid	0.12	0.63	Threonine	1.13	0.93
Hypoxanthine	0.00	0.96	Tryptophan	0.90	0.99
IMP	1.04	1.00	Tyrosine	0.65	0.81
Indolelactic acid	2.11	0.98	UMP	infinite	0.05
Indoxyl sulfate	0.88	1.00	Uracil	2.12	1.00
Inosine	0.02	0.78	Uric acid	1.80	0.05
Isovalerylglycine	8.37	0.00	Urocanic acid	0.00	1.00
Itaconic acid	1.18	1.00	Valine	0.92	0.99
Lactate	1.05	1.00	Xanthine	0.00	0.89
Leucine	1.07	0.99	Xylose-5-phosphate	0.43	0.24
Levulinic Acid	0.88	1.00			
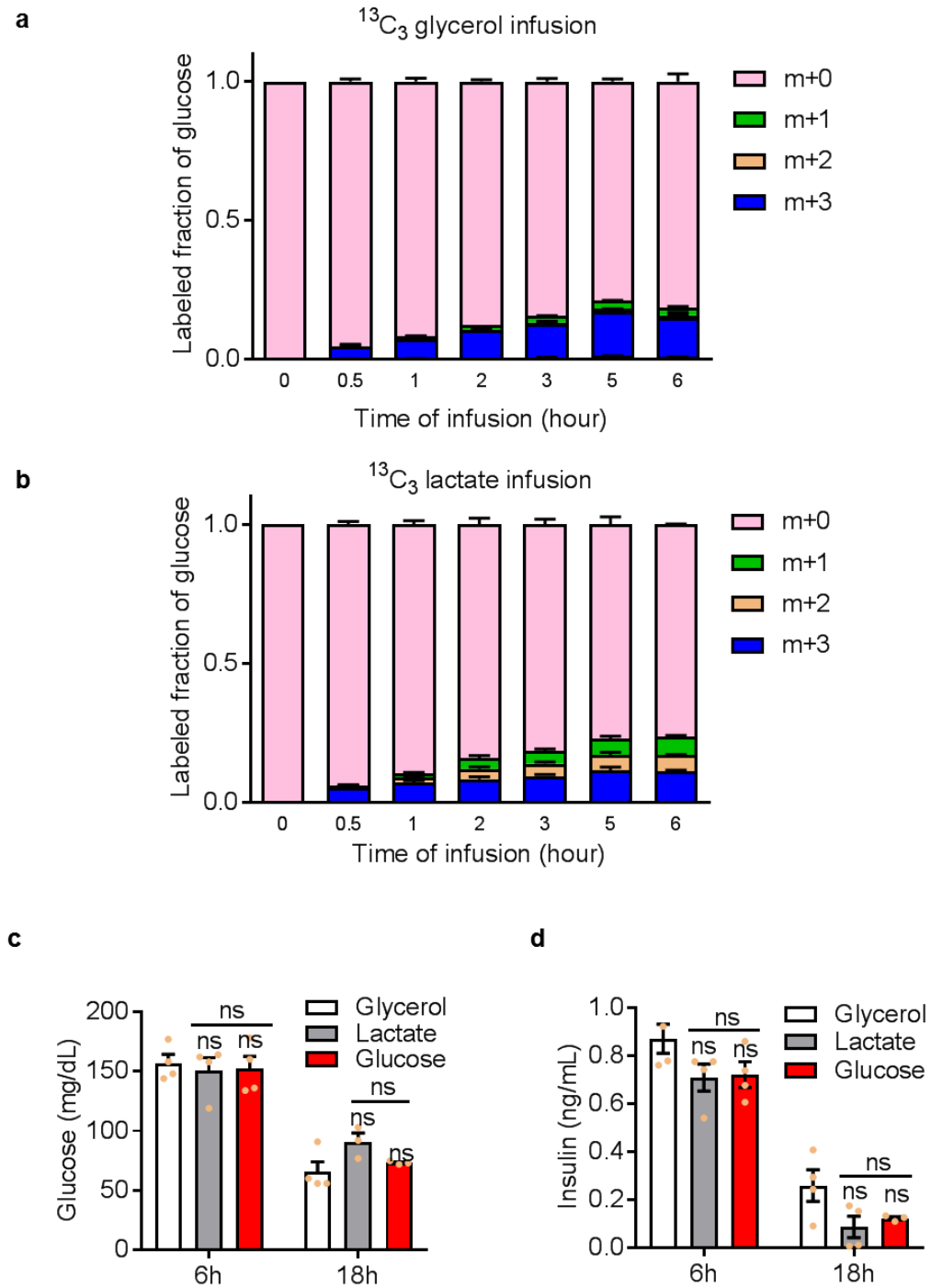
Supplementary Figure A2. 3 | Tracer infusions. a-b, Labeled fraction of glucose during 6-hour infusion of $^{13}C_3$ glycerol (**a**) and $^{13}C_3$ sodium lactate with $^{13}C_3$ sodium pyruvate in physiological ratio (**b**). Mice were fasted for 12 hours before infusion. **c-d,** Serum glucose (c) and insulin (d) levels of mice fasted for 0 and 12 hours followed by 6 hour infusion of ^{13}C tracers without food. For all experiment, n = 3 or 4 for each group. All data are expressed as mean ± s.e.m. ns = not significant by one-way ANOVA. All comparisons are against 6 h data unless indicated otherwise.
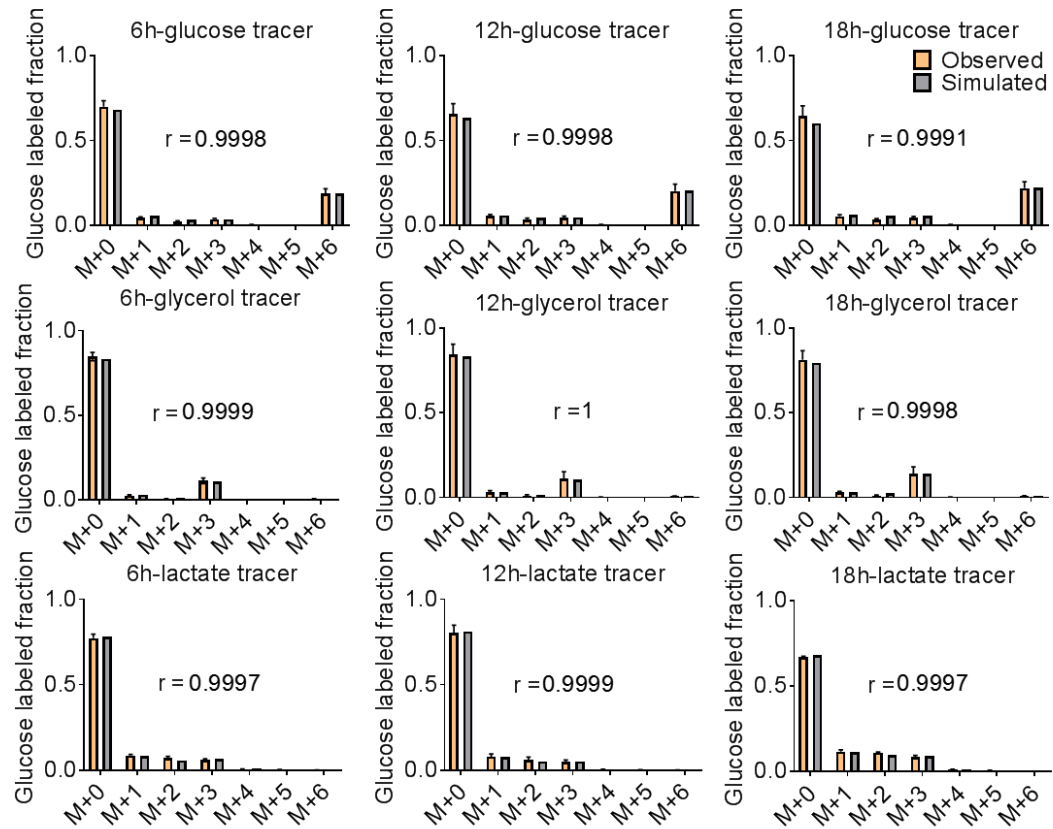
Supplementary Figure A2. 4 | EMU model with simulated and observed labeling pattern of glucose. Related to Figure 3. 3. Comparison of observed labeling pattern of glucose and the simulation from the best-fit values of fluxes. All observed data are expressed as mean ± s.e.m. The Pearson correlation coefficient (r) is shown.

a
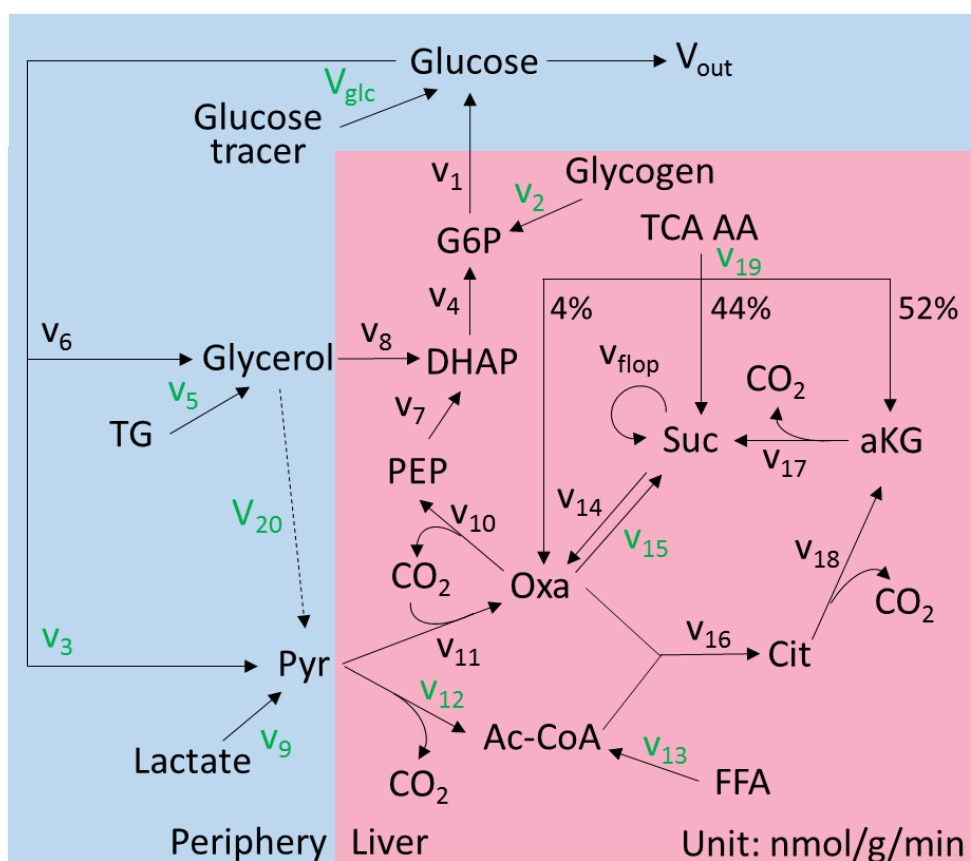
b

|	Fast time	Best-fit value (nmole/g/min)	95% CI upper limit (nmole/g/min)	95% CI lower limit (nmole/g/min)
Glcr->Lac (V_{20})	6h	0.0	13.4	0.0
	12h	0.0	11.8	0.0
	18h	0.0	16.3	0.0

Supplementary Figure A2. 5 | Testing a proposed pathway. a, EMU model with a proposed pathway (V_{20}) added. Reactions occur in the periphery and liver are shown under blue and red background respectively. Free fluxes are shown in green. **b,** Best-fit value with 95% confidence interval of V_{20}. G6P, glucose-6-phosphate; TG, triglycerides; TCA, tricarboxylic acid; AA, amino acids; PEP, phosphoenolpyruvate; DHAP, dihydroxyacetone phosphate; Pyr, pyruvate; Ac-CoA, acetyl CoA; Oxa, oxaloacetate; Suc, succinate; Cit, citrate; aKG, α-ketoglutarate; FFA, free fatty acids; Glcr, glycerol; Lac, lactate.

Supplementary Table A2. 3 | Gluconeogenic fluxes and 95% confidence interval. Related to Figure 3. 4.

|	Fast time	Best-fit value (nmole C/g/min)	95% CI upper limit (nmole C/g/min)	95% CI lower limit (nmole C/g/min)
Glycerol Input (U_1)	6h	114.5	120.5	105.5
	12h	92.7	98.7	83.7
	18h	114.5	117.5	105.5
Lactate Input (U_2)	6h	86.4	101.4	62.4
	12h	61.5	67.5	55.5
	18h	52.4	55.4	43.4
Glycogen Input (U_3)	6h	219.0	237.0	213.0
	12h	198.0	203.9	191.9
	18h	62.9	68.9	0.0
TCA AA Input (U_4)	6h	0.0	0.0	0.0
	12h	0.0	0.0	0.0
	18h	4.4	112.4	0.0
Glycolysis (U_6)	6h	219.8	237.8	207.8
	12h	220.0	232.0	208.0
	18h	143.9	149.9	131.9
PDH (U_9)	6h	136.7	196.7	118.7
	12h	152.9	203.9	116.9
	18h	46.0	52.0	31.0

Appendix 3: Supplemental Materials for Chapter 4: Effect of Hepatic Glucagon Signaling and High Fat Diet Feeding on Gluconeogenesis
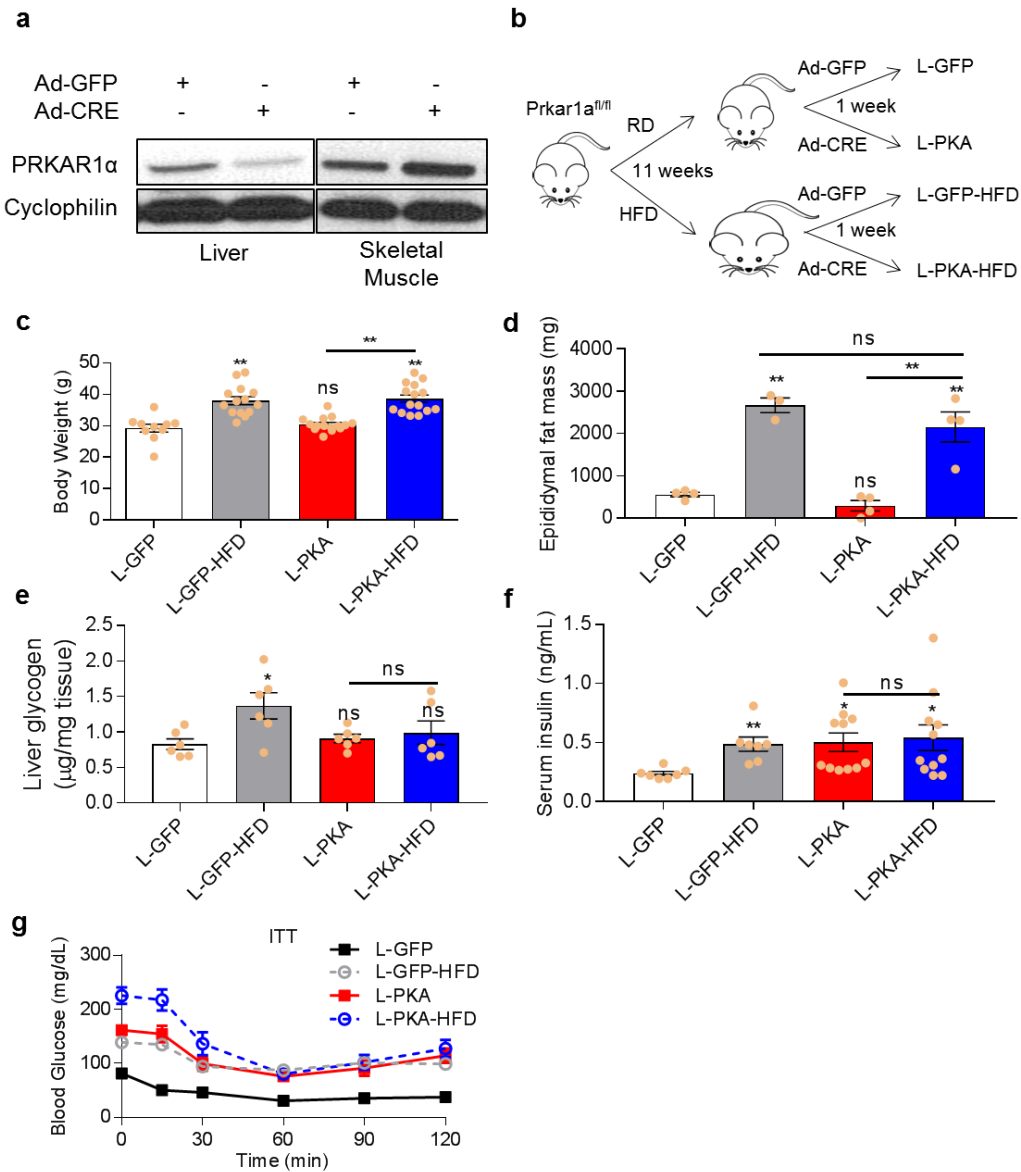

Supplementary Fig. A3.1 | Mice fed on regular and high fat diet. Related to Fig. 4.1. a, Western blot images of PRKAR1α levels in liver and skeletal muscle samples from PKArs^{fl/fl} mice injected with adenovirus coding for CRE recombinase (Ad-CRE) or GFP (Ad-GFP). **b,** Experimental design to obtain four different mouse groups. **c,** Body weight of mice; n = 10-15. **d.** Epididymal fat mass n = 3-4. **e.** Liver glycogen level; n= 6. **f.** Serum insulin level n = 7-11. **g.** Insulin tolerance test with actual glucose values; n = 4-7. All mice were fasted for 12 hours (c-f) or 6 hours (g) before experiments. All data are expressed as mean ± s.e.m. **p < 0.01; *p < 0.05; ns = not significant. Statistical analysis was performed using one-way ANOVA corrected for multiple comparisons using the Holm-Sidak method.
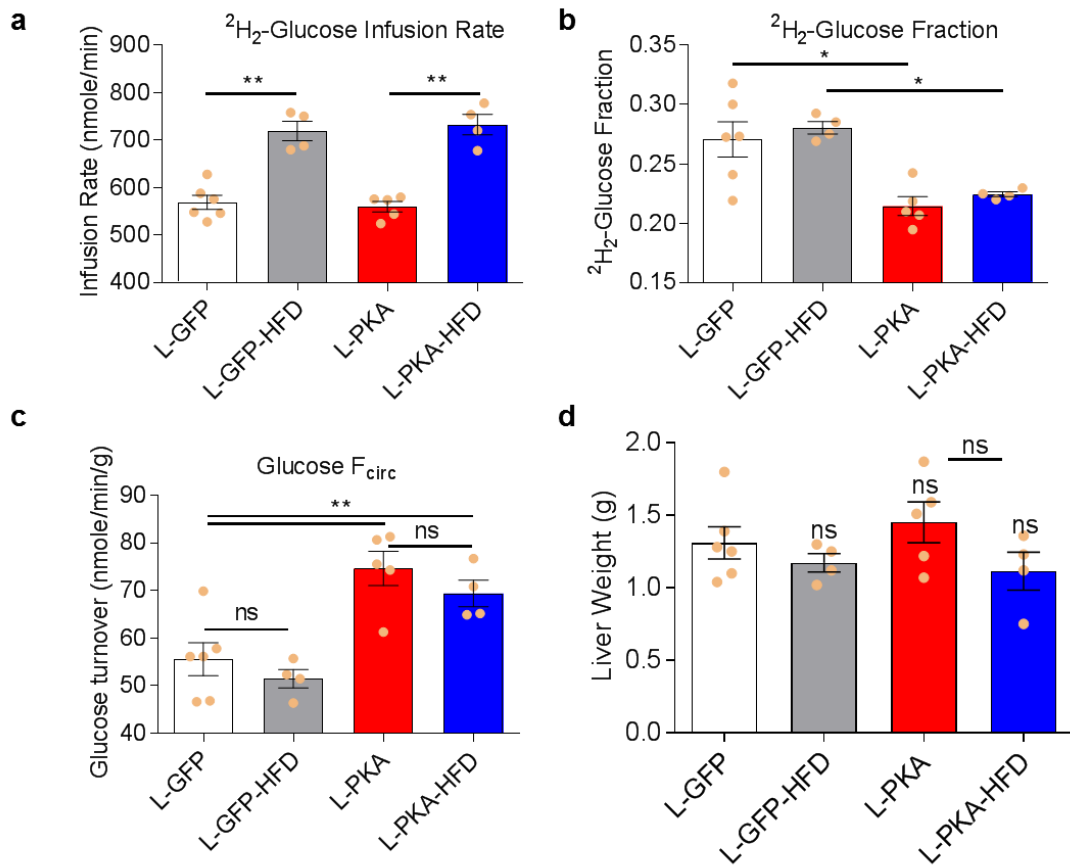
Supplementary Fig. A3.2 | 6, 6-^{2}H$_2$ glucose infusion data. Related to Fig. 4.1. a. Absolute infusion rate of 6, 6-^{2}H$_2$ glucose. **b.** Fraction of 6, 6-^{2}H$_2$ glucose at steady state. **c.** Glucose flux normalized to body weight. **d.** Total liver weight. n = 4-6. All data are expressed as mean ± s.e.m. **p < 0.01; *p < 0.05; ns = not significant. Statistical analysis was performed using one-way ANOVA corrected for multiple comparisons using the Holm-Sidak method.
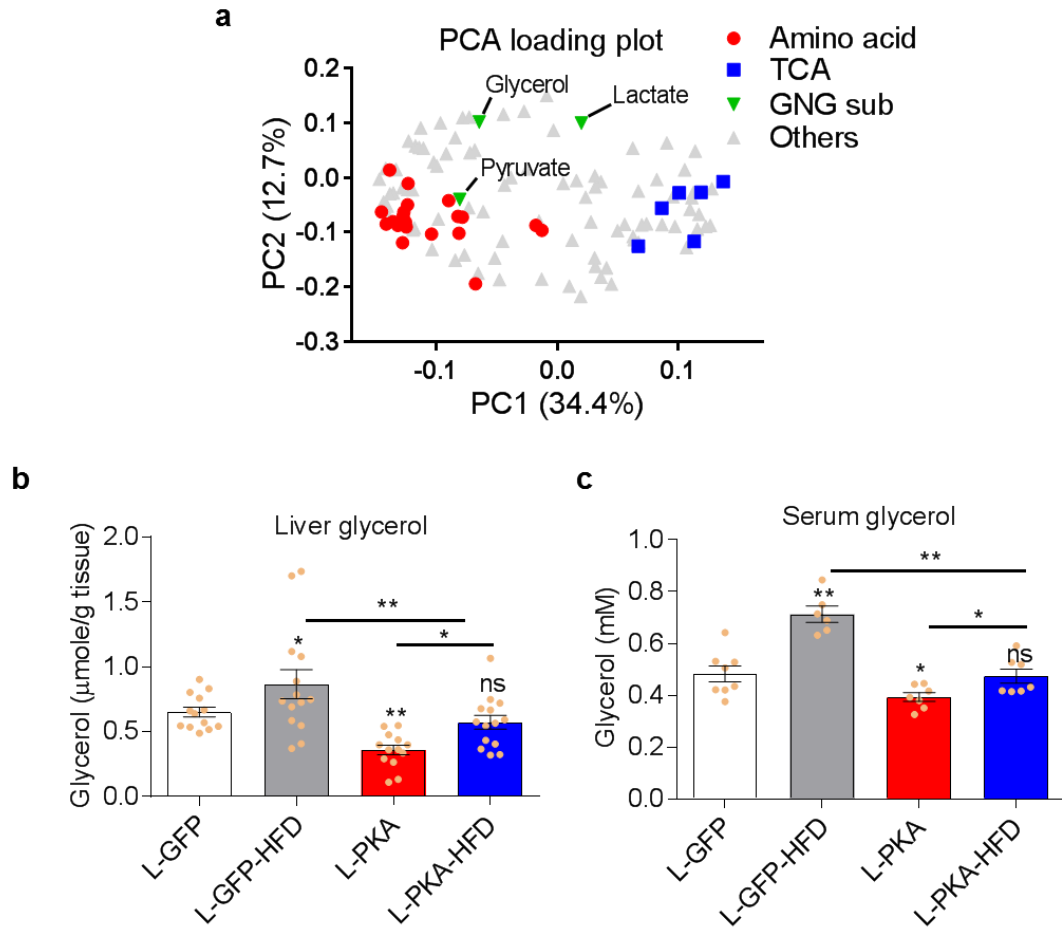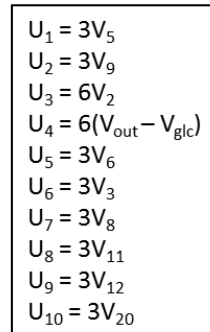
Supplementary Fig. A3.3 | Metabolomics and glycerol level. Related to Fig. 4.3. a, PCA loading plot; each dot represents one metabolite. n = 3-5 mice, 2-3 liver samples per mice. **b**, Liver glycerol measurements of mice fasted for 12 hours n = 13-14 . **c.** Serum glycerol measurements of mice fasted for 12 hours n = 6-8. All data are expressed as mean ± s.e.m. **p < 0.01; *p < 0.05; ns = not significant by one-way ANOVA. TCA, tricarboxylic acid intermediates; GNG sub, non-amino acid gluconeogenic substrates.
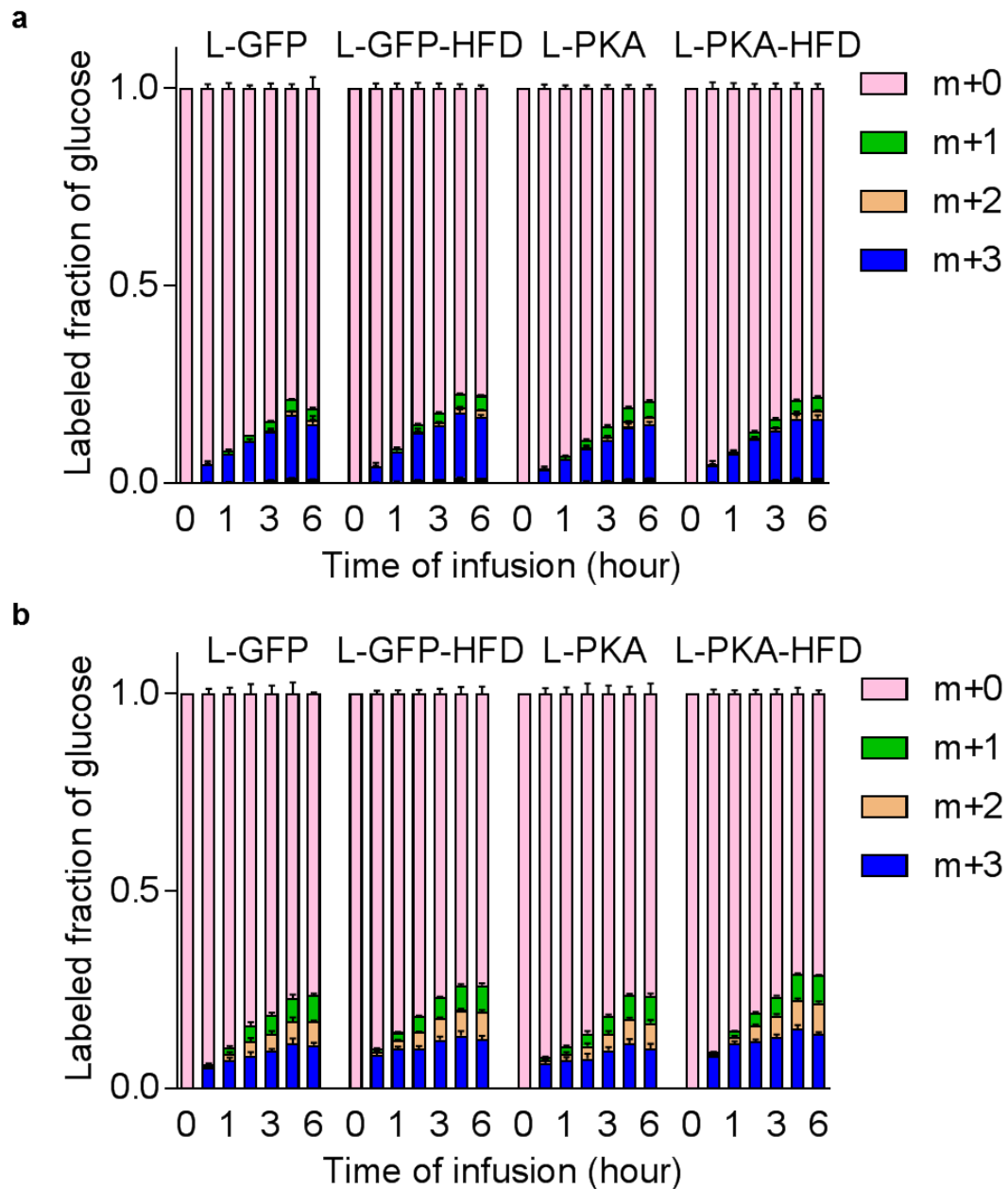
Supplementary Fig. A3.4 | Time course of tracer infusion. Related to Fig. 4.4. a, Labeled fraction of glucose during 6-hour infusion (0.1 ul/g body weight/min) of $^{13}C_3$ glycerol (150 mM). **b,** Labeled fraction of glucose during 6-hour infusion (0.1 ul/g body weight/min) of $^{13}C_3$ sodium pyruvate (40 mM) and $^{13}C_3$ sodium lactate (360 mM). All mice were fasted for 12 hours before experiments (n=4). All data are expressed as mean ± s.e.m. Serum samples were collected at 0, 0.5, 1, 2, 3, 5 and 6 hours of infusion.

a

b

$$U_1 = 3V_5$$
$$U_2 = 3V_9$$
$$U_3 = 6V_2$$
$$U_4 = 6(V_{out} - V_{glc})$$
$$U_5 = 3V_6$$
$$U_6 = 3V_3$$
$$U_7 = 3V_8$$
$$U_8 = 3V_{11}$$
$$U_9 = 3V_{12}$$
$$U_{10} = 3V_{20}$$

Unit: 10^{-2} nmol C /min

Supplementary Fig. A3.5 | Flux models. Related to Fig. 4.5. a, EMU model with detailed gluconeogenic pathway. Reactions occur in the periphery and liver are shown under blue and red background respectively. Free fluxes are shown in green. **b,** Summarized gluconeogenic network and the equivalent fluxes. G6P, glucose-6-phosphate; TG, triglycerides; TCA, tricarboxylic acid; AA, amino acids; PEP, phosphoenolpyruvate; DHAP, dihydroxyacetone phosphate; Pyr, pyruvate; Ac-CoA, acetyl CoA; Oxa, oxaloacetate; Suc, succinate; Cit, citrate; aKG, α-ketoglutarate; FFA, free fatty acids.
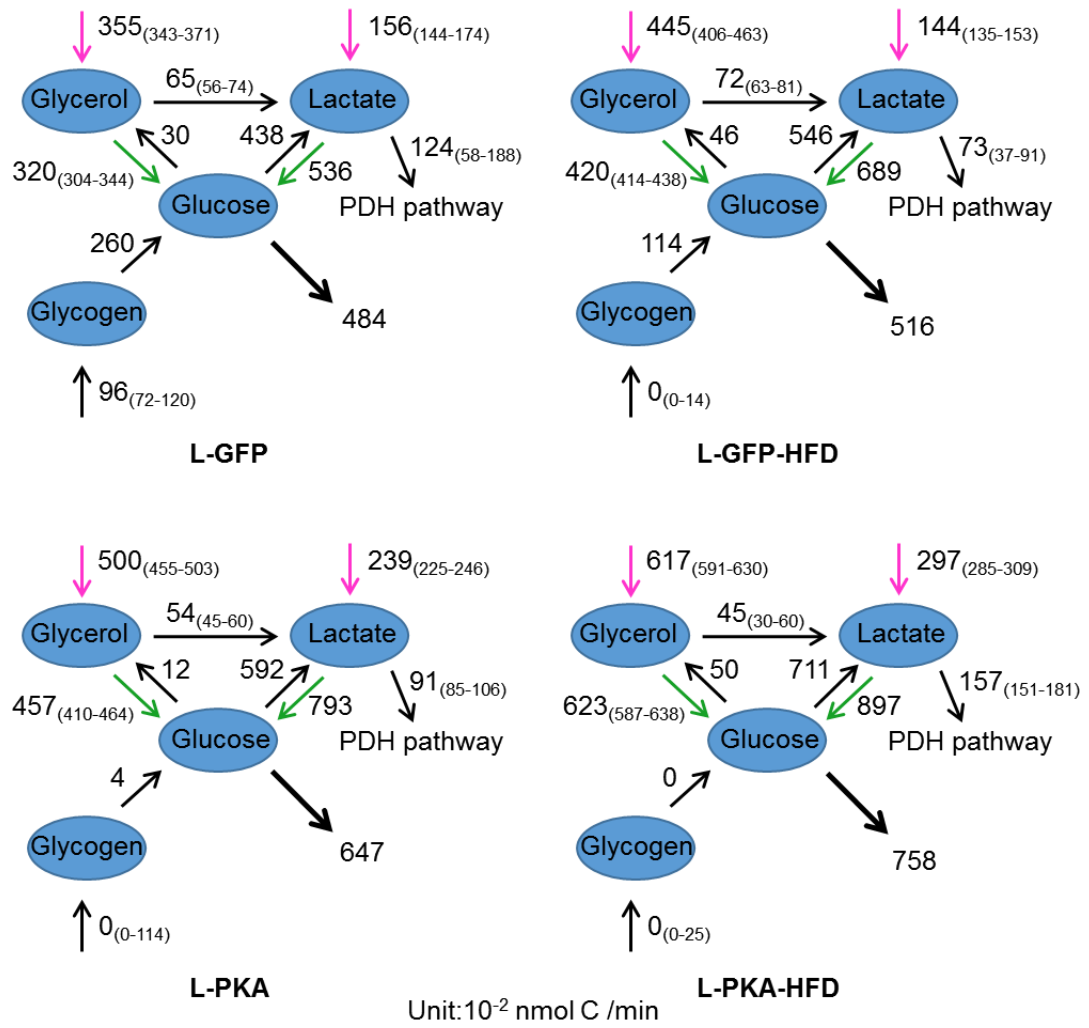
Supplementary Fig. A3.6 | Gluconeogenic flux of L-GFP, L-GFP-HFD, L-PKA and L-PKA-HFD mice. Related to figure 4.5. All fluxes are normalized to the 10^{-2} nmole carbon per minute; All data are shown as best-fit value (95% confidence interval); PDH, pyruvate dehydrogenase. See also Supplementary Table 4 for confidence intervals of fluxes.
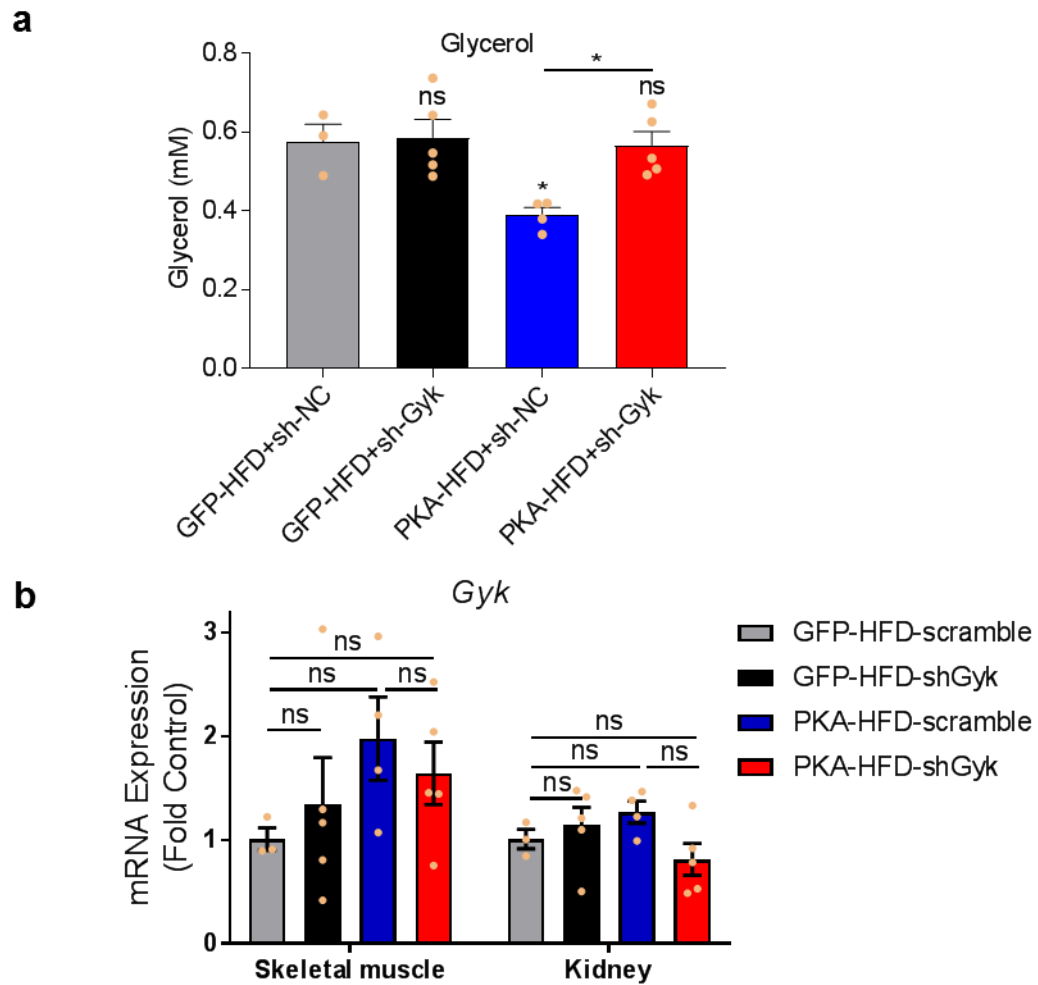
Supplementary Fig. A3.7 | Serum glycerol and *Gyk* expression. Related to Fig. 4.7. a, Serum glycerol level of mice after 12 hour fasting. **b,** *Gyk* expression levels normalized to beta actin and expressed as fold change to L-GFP-HFD+sh-NC controls; For all data, n = 3-5. Data are mean ± s.e.m.; ns, not significant compared to L-GFP-HFD+sh-NC group by one-way ANOVA corrected for multiple comparisons using the Holm-Sidak method.

Appendix 4: Supplemental Materials for Chapter 5: Effect of Hepatic Insulin Receptor Knock-out on Gluconeogenesis

a

b

c
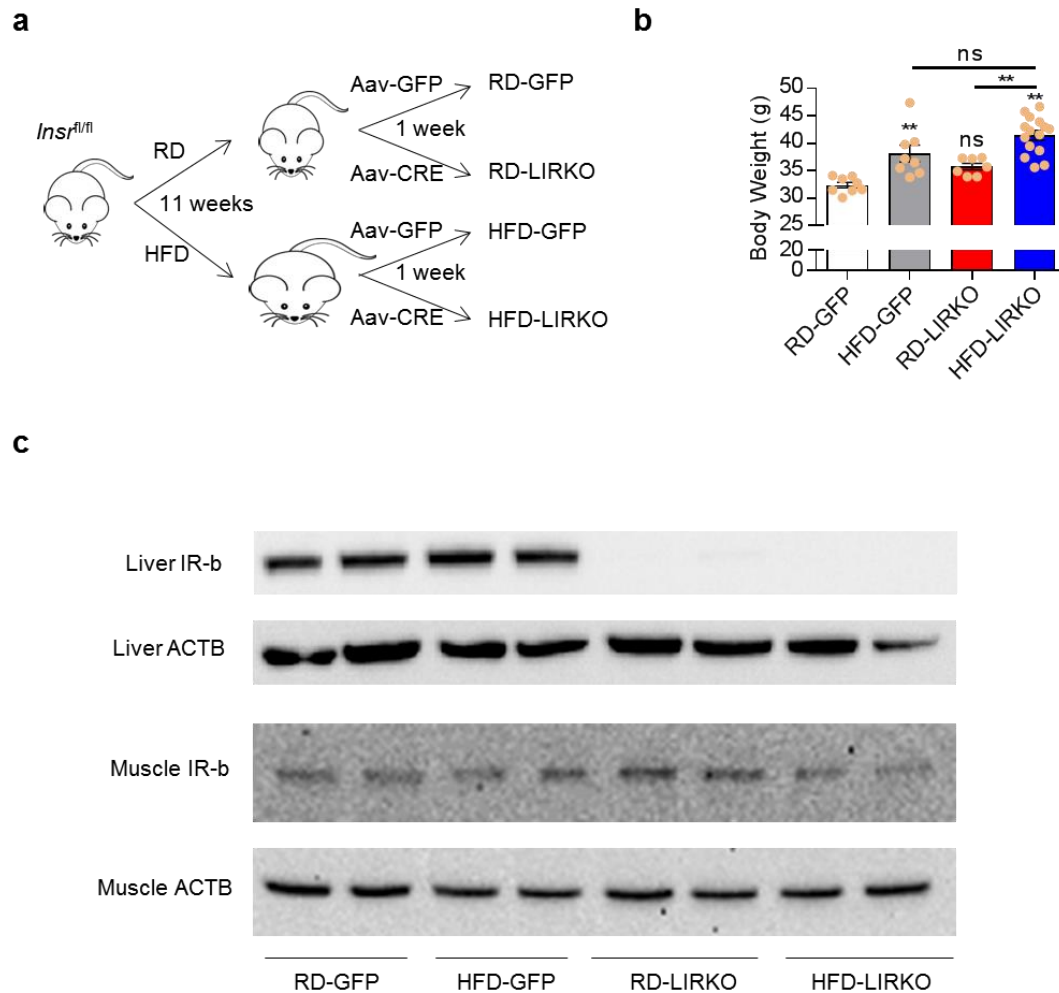
Supplementary Fig. A4.1 | Development of mouse models. a, Experimental design to obtain four different mouse groups. **b,** Body weight of mice; **c,** Western blot images showing the knockout of insulin receptor in the liver and skeletal muscle.
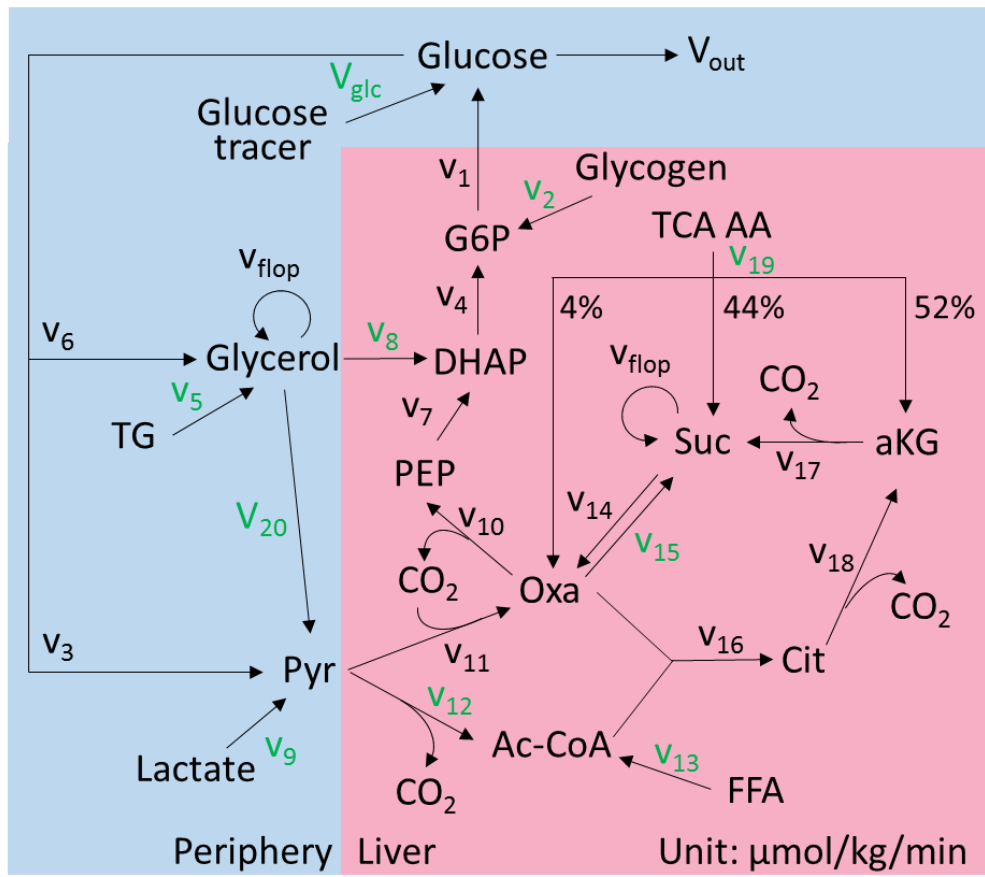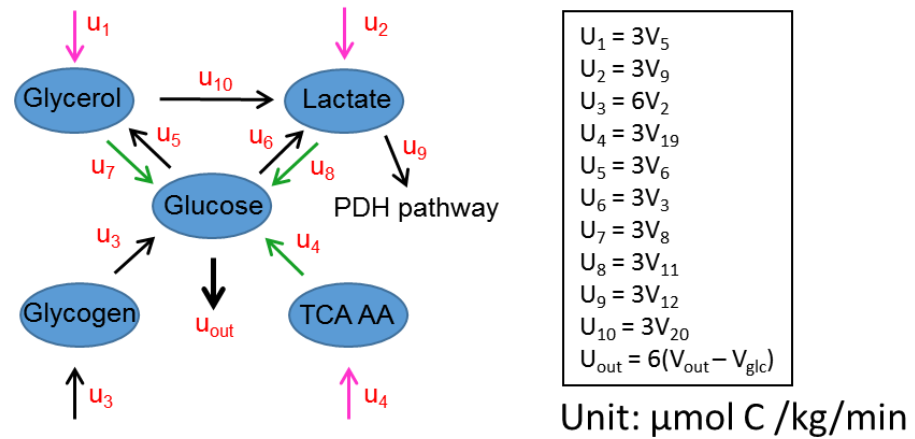
Supplementary Fig. A4.2 | Flux models. a, EMU model with detailed gluconeogenic pathway. Reactions occur in the periphery and liver are shown under blue and red background respectively. Free fluxes are shown in green. **b,** Summarized gluconeogenic network and the equivalent fluxes. G6P, glucose-6-phosphate; TG, triglycerides; TCA, tricarboxylic acid; AA, amino acids; PEP, phosphoenolpyruvate; DHAP, dihydroxyacetone phosphate; Pyr, pyruvate; Ac-CoA, acetyl CoA; Oxa, oxaloacetate; Suc, succinate; Cit, citrate; aKG, α-ketoglutarate; FFA, free fatty acids.
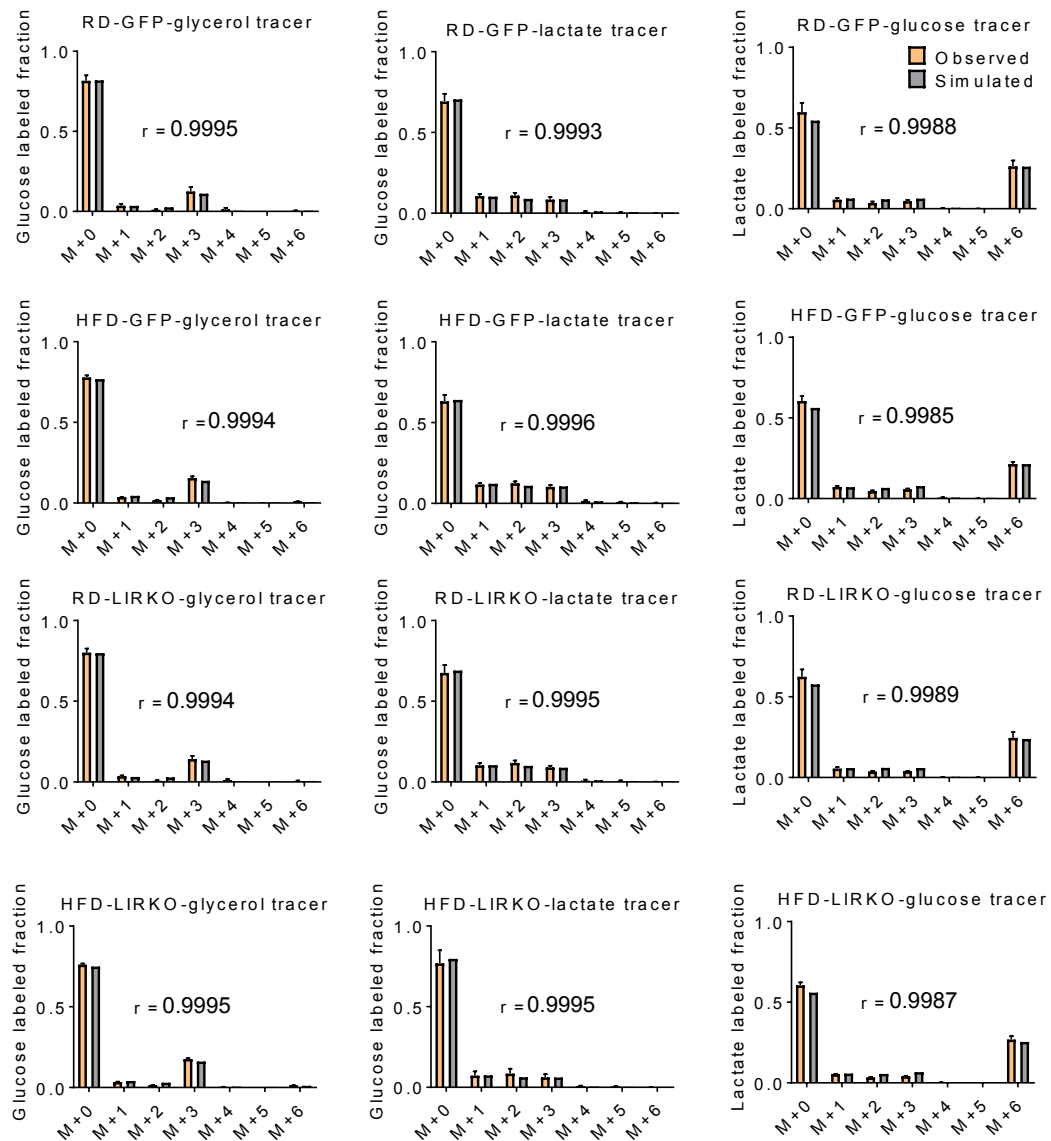
Supplementary Figure A4.3 | EMU model with simulated and observed labelling pattern of glucose and lactate. Comparison of observed labelling pattern of glucose and the simulation from the best-fit values of fluxes. All observed data are expressed as mean ± s.d; n= 4-7. The Pearson correlation coefficient (r) is shown.

Supplementary Table A4.1 | Gluconeogenic fluxes and 95% confidence interval.

	Group	Best-fit value (μmole C/kg/min)	95% CI upper limit (μmole C/kg/min)	95% CI lower limit (μmole C/kg/min)
Glycerol Input (U1)	L-GFP	97.9	103.9	88.9
	L-GFP-HFD	175.8	193.8	163.8
	L-PKA	121.4	124.4	118.4
	L-PKA-HFD	134.1	137.1	131.1
Lactate Input (U2)	L-GFP	51.0	54.0	48.0
	L-GFP-HFD	57.1	69.1	54.1
	L-PKA	76.1	79.1	73.1
	L-PKA-HFD	90.1	93.1	84.1
Glycogen Input (U3)	L-GFP	72.9	78.9	24.9
	L-GFP-HFD	3.2	63.7	0.0
	L-PKA	23.0	29.0	17.0
	L-PKA-HFD	43.6	49.6	37.6
TCA AA Input (U4)	L-GFP	0.0	145.2	0.0
	L-GFP-HFD	0.0	90.3	0.0
	L-PKA	0.0	15.4	0.0
	L-PKA-HFD	0.0	63.3	0.0
Glycerol→DHAP (U7)	L-GFP	84.4	90.4	75.4
	L-GFP-HFD	165.7	186.7	150.7
	L-PKA	115.6	118.6	112.6
	L-PKA-HFD	130.9	133.9	127.9
PDH (U9)	L-GFP	46.3	79.3	0.0
	L-GFP-HFD	32.9	134.9	8.9
	L-PKA	13.5	22.5	1.5
	L-PKA-HFD	92.9	107.9	83.9
Glycerol→Lactate (U10)	L-GFP	18.4	21.4	15.4
	L-GFP-HFD	28.4	31.4	25.4
	L-PKA	11.7	14.7	8.7
	L-PKA-HFD	9.8	12.8	0.0

References

1. Organization, W.H., *GLOBAL REPORT ON DIABETES*. 2016, World Health Organization: Geneva, Switzerland.

2. Laios, K., et al., *Aretaeus of Cappadocia and the first description of diabetes.* Hormones (Athens, Greece), 2012. **11**(1): p. 109-113.

3. Ahmed, A.M., *History of diabetes mellitus.* Saudi medical journal, 2002. **23**(4): p. 373-378.

4. Leroy, C., et al., *Diabetes insipidus.* Annales d'endocrinologie, 2013. **74**(5-6): p. 496-507.

5. Cho, N.H., et al., *IDF Diabetes Atlas: Global estimates of diabetes prevalence for 2017 and projections for 2045.* Diabetes research and clinical practice, 2018. **138**: p. 271-281.

6. Prevention, C.f.D.C.a., *National Diabetes Statistics Report: Estimates of Diabetes and Its Burden in the United States.* 2017, US Department of Health and Human Services: Atlanta, GA.

7. Brownlee, M., *Biochemistry and molecular cell biology of diabetic complications.* Nature, 2001. **414**(6865): p. 813-20.

8. Rodríguez-Saldaña, J., et al., *Diabetes mellitus in a subgroup of older Mexicans: Prevalence, association with cardiovascular risk factors, functional and cognitive impairment, and mortality.* Journal of the American Geriatrics Society, 2002. **50**(1): p. 111-116.

9. Sinclair, A.J., S.P. Conroy, and A.J. Bayer, *Impact of Diabetes on Physical Function in Older People.* Diabetes Care, 2008. **31**(2): p. 233.

10. Chung, S.T., et al., *Increased gluconeogenesis in youth with newly diagnosed type 2 diabetes.* Diabetologia, 2015. **58**(3): p. 596-603.

11. Unger, R.H., *Glucagon and the insulin: glucagon ratio in diabetes and other catabolic illnesses.* Diabetes, 1971. **20**(12): p. 834-8.

12. Unger, R.H., et al., *Studies of pancreatic alpha cell function in normal and diabetic subjects.* J Clin Invest, 1970. **49**(4): p. 837-48.

13. Daneman, D., *Type 1 diabetes.* Lancet, 2006. **367**(9513): p. 847-58.

14. Jin, E.S., et al., *Hepatic glucose production pathways after three days of a high-fat diet.* Metabolism, 2013. **62**(1): p. 152-62.

15. Ramnanan, C.J., et al., *Physiologic action of glucagon on liver glucose metabolism.* Diabetes Obes Metab, 2011. **13**(Suppl 1): p. 118-25.

16. Michael, M.D., et al., *Loss of insulin signaling in hepatocytes leads to severe insulin resistance and progressive hepatic dysfunction.* Mol Cell, 2000. **6**(1): p. 87-97.

17. Michaelis, L., et al., *The original Michaelis constant: translation of the 1913 Michaelis-Menten paper.* Biochemistry, 2011. **50**(39): p. 8264-9.

18. Hughey, C.C., et al., *Approach to assessing determinants of glucose homeostasis in the conscious mouse.* Mammalian genome : official journal of the International Mammalian Genome Society, 2014. **25**(9-10): p. 522-538.

19. Riekeberg, E. and R. Powers, *New frontiers in metabolomics: from measurement to insight.* F1000Research, 2017. **6**: p. 1148-1148.

20. Wiechert, W., *13C Metabolic Flux Analysis.* Metabolic Engineering, 2001. **3**(3): p. 195-206.

21. Antoniewicz, M.R., *Methods and advances in metabolic flux analysis: a mini-review.* J Ind Microbiol Biotechnol, 2015. **42**(3): p. 317-25.

22. Orth, J.D., I. Thiele, and B.Ø. Palsson, *What is flux balance analysis?* Nature biotechnology, 2010. **28**(3): p. 245-248.

23. Murphy, T.A. and J.D. Young, *ETA: robust software for determination of cell specific rates from extracellular time courses.* Biotechnol Bioeng, 2013. **110**(6): p. 1748-58.

24. Rui, L., *Energy metabolism in the liver.* Comprehensive Physiology, 2014. **4**(1): p. 177-197.

25. American Diabetes Association, *Standards of medical care in diabetes--2010.* Diabetes care, 2010. **33 Suppl 1**(Suppl 1): p. S11-S61.

26. Hundal, R.S., et al., *Mechanism by which metformin reduces glucose production in type 2 diabetes.* Diabetes, 2000. **49**(12): p. 2063-9.

27. Magnusson, I., et al., *Increased rate of gluconeogenesis in type II diabetes mellitus. A ^{13}C nuclear magnetic resonance study.* J Clin Invest, 1992. **90**(4): p. 1323-7.

28. Petersen, K.F., T.B. Price, and R. Bergeron, *Regulation of net hepatic glycogenolysis and gluconeogenesis during exercise: impact of type 1 diabetes.* J Clin Endocrinol Metab, 2004. **89**(9): p. 4656-64.

29. Petersen, M.C., D.F. Vatner, and G.I. Shulman, *Regulation of hepatic glucose metabolism in health and disease.* Nat Rev Endocrinol, 2017. **13**(10): p. 572-587.

30. Wajngot, A., et al., *Quantitative contributions of gluconeogenesis to glucose production during fasting in type 2 diabetes mellitus.* Metabolism, 2001. **50**(1): p. 47-52.

31. Katz, J. and J.A. Tayek, *Gluconeogenesis and the Cori cycle in 12-, 20-, and 40-h-fasted humans.* Am. J. Physiol, 1998. **275**(3 Pt 1): p. E537-42.

32. Kida, K., et al., *The circadian change of gluconeogenesis in the liver in vivo in fed rats.* J Biochem, 1980. **88**(4): p. 1009-13.

33. Hui, S., et al., *Glucose feeds the TCA cycle via circulating lactate.* Nature, 2017. **551**(7678): p. 115-118.

34. Ross, B.D., R. Hems, and H.A. Krebs, *The rate of gluconeogenesis from various precursors in the perfused rat liver.* The Biochemical journal, 1967. **102**(3): p. 942-951.

35. Kaloyianni, M. and R.A. Freedland, *Contribution of several amino acids and lactate to gluconeogenesis in hepatocytes isolated from rats fed various diets.* J Nutr, 1990. **120**(1): p. 116-22.

36. Jensen, M.D., et al., *Sources of blood glycerol during fasting.* American Journal of Physiology-Endocrinology and Metabolism, 2001. **281**(5): p. E998-E1004.

37. Owen, O.E., et al., *Energy metabolism in feasting and fasting.* Adv Exp Med Biol, 1979. **111**: p. 169-88.

38. Stumvoll, M., et al., *Role of glutamine in human carbohydrate metabolism in kidney and other tissues.* Kidney Int, 1999. **55**(3): p. 778-92.

39. Hankard, R.G., M.W. Haymond, and D. Darmaun, *Role of glutamine as a glucose precursor in fasting humans.* Diabetes, 1997. **46**(10): p. 1535-41.

40. Newsholme, P., L. Brennan, and K. Bender, *Amino Acid Metabolism, β-Cell Function, and Diabetes.* Diabetes, 2006. **55**(Supplement 2): p. S39.

41. Santiago, A.M., D.J. Clegg, and V.H. Routh, *Ventromedial hypothalamic glucose sensing and glucose homeostasis vary throughout the estrous cycle.* Physiology & behavior, 2016. **167**: p. 248-254.

42. Bardelmeijer, H.A., et al., *Cannulation of the jugular vein in mice: a method for serial withdrawal of blood samples.* Lab Anim, 2003. **37**(3): p. 181-7.

43. Chiles, E., et al., *Fast LC-MS quantitation of glucose and glycerol via enzymatic derivatization.* Anal Biochem, 2019. **575**: p. 40-43.

44. Clasquin, M.F., E. Melamud, and J.D. Rabinowitz, *LC-MS Data Processing with MAVEN: A Metabolomic Analysis and Visualization Engine*, in *Current Protocols in Bioinformatics*. 2002, John Wiley & Sons, Inc.

45. Su, X., W. Lu, and J.D. Rabinowitz, *Metabolite spectral accuracy on orbitraps.* Anal Chem, 2017. **89**(11): p. 5940-5948.

46. Antoniewicz, M.R., J.K. Kelleher, and G. Stephanopoulos, *Elementary metabolite units (EMU): a novel framework for modeling isotopic distributions.* Metab Eng, 2007. **9**(1): p. 68-86.

47. Sugimoto, M., et al., *MMMDB: Mouse Multiple Tissue Metabolome Database.* Nucleic Acids Res, 2012. **40**(Database issue): p. D809-14.

48. Mullen, K.M., et al., *DEoptim: An R Package for Global Optimization by Differential Evolution.* Journal of Statistical Software; Vol 1, Issue 6 (2011), 2011.

49. Antoniewicz, M.R., J.K. Kelleher, and G. Stephanopoulos, *Determination of confidence intervals of metabolic fluxes estimated from stable isotope measurements.* Metab Eng, 2006. **8**(4): p. 324-37.

50. Mao, C.S., et al., *Underestimation of gluconeogenesis by the [U-13C6]glucose method: effect of lack of isotope equilibrium.* American Journal of Physiology-Endocrinology and Metabolism, 2002. **282**(2): p. E376-E385.

51. Agoston, D.V., *How to Translate Time? The Temporal Aspect of Human and Rodent Biology.* Frontiers in Neurology, 2017. **8**: p. 92.

52. Rothman, D.L., et al., *Quantitation of hepatic glycogenolysis and gluconeogenesis in fasting humans with 13C NMR.* Science, 1991. **254**(5031): p. 573.

53. Peroni, O., et al., *Glucose production and gluconeogenesis in postabsorptive and starved normal and streptozotocin-diabetic rats.* Metabolism, 1997. **46**(11): p. 1358-63.

54. Perry, R.J., et al., *Non-invasive assessment of hepatic mitochondrial metabolism by positional isotopomer NMR tracer analysis (PINTA).* Nat Commun, 2017. **8**(1): p. 798.

55. Nunes, P.M. and J.G. Jones, *Quantifying endogenous glucose production and contributing source fluxes from a single 2H NMR spectrum.* Magn Reson Med, 2009. **62**(3): p. 802-7.

56. Mahendran, Y., et al., *Glycerol and fatty acids in serum predict the development of hyperglycemia and type 2 diabetes in Finnish men.* Diabetes Care, 2013. **36**(11): p. 3732-8.

57. Nurjhan, N., A. Consoli, and J. Gerich, *Increased lipolysis and its consequences on gluconeogenesis in non-insulin-dependent diabetes mellitus.* J Clin Invest, 1992. **89**(1): p. 169-75.

58. World Health Organization, *Global report on diabetes.* 2016, World Health Organization: Geneva, Switzerland.

59. Centers for Disease Control and Prevention, *National diabetes statistics report: estimates of diabetes and its burden in the United States.* 2017, US department of health and human services: Atlanta, GA.

60. Samuel, V.T. and G.I. Shulman, *The pathogenesis of insulin resistance: integrating signaling pathways and substrate flux.* J Clin Invest, 2016. **126**(1): p. 12-22.

61. Perry, R.J., et al., *Hepatic acetyl CoA links adipose tissue inflammation to hepatic insulin resistance and type 2 diabetes.* Cell, 2015. **160**(4): p. 745-58.

62. Buettner, C., et al., *Severe impairment in liver insulin signaling fails to alter hepatic insulin action in conscious mice.* J Clin Invest, 2005. **115**(5): p. 1306-13.

63. Okamoto, H., et al., *Restoration of liver insulin signaling in Insr knockout mice fails to normalize hepatic insulin action.* J Clin Invest, 2005. **115**(5): p. 1314-22.

64. Lee, Y.H., et al., *Glucagon is the key factor in the development of diabetes.* Diabetologia, 2016. **59**(7): p. 1372-5.

65. Gaisano, H.Y., P.E. Macdonald, and M. Vranic, *Glucagon secretion and signaling in the development of diabetes.* Front Physiol, 2012. **3**: p. 349.

66. Pearson, M.J., R.H. Unger, and W.L. Holland, *Clinical trials, triumphs, and tribulations of glucagon receptor antagonists.* Diabetes Care, 2016. **39**(7): p. 1075.

67.   Dunning, B.E. and J.E. Gerich, *The role of alpha-cell dysregulation in fasting and postprandial hyperglycemia in type 2 diabetes and therapeutic implications.* Endocr Rev, 2007. **28**(3): p. 253-83.

68.   Muller, W.A., G.R. Faloona, and R.H. Unger, *Hyperglucagonemia in diabetic ketoacidosis. Its prevalence and significance.* Am J Med, 1973. **54**(1): p. 52-7.

69.   Exton, J.H. and C.R. Park, *Control of gluconeogenesis in liver. II. Effects of glucagon, catecholamines, and adenosine 3',5'-monophosphate on gluconeogenesis in the perfused rat liver.* J Biol Chem, 1968. **243**(16): p. 4189-96.

70.   He, L., et al., *Metformin and insulin suppress hepatic gluconeogenesis through phosphorylation of CREB binding protein.* Cell, 2009. **137**(4): p. 635-46.

71.   Konopka, A.R., et al., *Hyperglucagonemia mitigates the effect of metformin on glucose production in prediabetes.* Cell Rep, 2016. **15**(7): p. 1394-1400.

72.   Previs, S.F., G.W. Cline, and G.I. Shulman, *A critical evaluation of mass isotopomer distribution analysis of gluconeogenesis in vivo.* Am J Physiol, 1999. **277**(1): p. E154-60.

73.   Musil, F., et al., *Effects of body weight reduction on plasma leptin and adiponectin/leptin ratio in obese patients with type 1 diabetes mellitus.* Physiol Res, 2015. **64**(2): p. 221-8.

74.   Zhang, L., et al., *Dapagliflozin treatment in patients with different stages of type 2 diabetes mellitus: effects on glycaemic control and body weight.* Diabetes Obes Metab, 2010. **12**(6): p. 510-6.

75.   Ceriello, A., et al., *Glucagon and heart in type 2 diabetes: new perspectives.* Cardiovascular Diabetology, 2016. **15**(1): p. 123.

76.   Farhy, L.S. and A.L. McCall, *Optimizing reduction in basal hyperglucagonaemia to repair defective glucagon counterregulation in insulin deficiency.* Diabetes Obes Metab, 2011. **13 Suppl 1**: p. 133-43.

77.   Kirschner, L.S., et al., *A mouse model for the Carney complex tumor syndrome develops neoplasia in cyclic AMP-responsive tissues.* Cancer Res, 2005. **65**(11): p. 4506-14.

78.   Ye, J., et al., *Primer-BLAST: A tool to design target-specific primers for polymerase chain reaction.* BMC Bioinformatics, 2012. **13**: p. 134-134.

79.   Easom, R.A. and V.A. Zammit, *A cold-clamping technique for the rapid sampling of rat liver for studies on enzymes in separate cell fractions. Suitability for the study of enzymes regulated by reversible phosphorylation-dephosphorylation.* Biochem J, 1984. **220**(3): p. 733-8.

80.   Wang, Y., et al., *Glycerol not lactate is the major net carbon source for gluconeogenesis in mice during both short and prolonged fasting.* Molecular Metabolism, 2020. **31**: p. 36-44.

81.   Mithieux, G., et al., *Induction of control genes in intestinal gluconeogenesis is sequential during fasting and maximal in diabetes.* Am J Physiol Endocrinol Metab, 2004. **286**(3): p. E370-5.

82. Kalemba, K.M., et al., *Glycerol induces G6pc in primary mouse hepatocytes and is the preferred substrate for gluconeogenesis both in vitro and in vivo.* J Biol Chem, 2019. **294**(48): p. 18017-18028.

83. Song, W.J., et al., *Glucagon regulates hepatic kisspeptin to impair insulin secretion.* Cell Metab, 2014. **19**(4): p. 667-81.

84. Bier, D.M., et al., *Measurement of "true" glucose production rates in infancy and childhood with 6,6-dideuteroglucose.* Diabetes, 1977. **26**(11): p. 1016-23.

85. Qi, L., et al., *Adipocyte CREB promotes insulin resistance in obesity.* Cell metabolism, 2009. **9**(3): p. 277-286.

86. Zhang, Y., et al., *Evaluation of insulin sensitivity by hyperinsulinemic-euglycemic clamps using stable isotope-labeled glucose.* Cell discovery, 2018. **4**: p. 17-17.

87. Li, E., et al., *OLFR734 Mediates Glucose Metabolism as a Receptor of Asprosin.* Cell Metabolism, 2019. **30**(2): p. 319-328.e8.

88. Consoli, A., et al., *Determination of Krebs cycle metabolic carbon exchange in vivo and its use to estimate the individual contributions of gluconeogenesis and glycogenolysis to overall glucose output in man.* J Clin Invest, 1987. **80**(5): p. 1303-10.

89. Chan, C., et al., *Metabolic flux analysis of cultured hepatocytes exposed to plasma.* Biotechnol Bioeng, 2003. **81**(1): p. 33-49.

90. Hasenour, C.M., et al., *Liver AMP-Activated Protein Kinase Is Unnecessary for Gluconeogenesis but Protects Energy State during Nutrient Deprivation.* PLoS One, 2017. **12**(1): p. e0170382.

91. Antoniewicz, M.R., *A guide to (13)C metabolic flux analysis for the cancer biologist.* Exp Mol Med, 2018. **50**(4): p. 19.

92. Salgado, M.C., et al., *Transcriptional regulation of glucose-6-phosphatase catalytic subunit promoter by insulin and glucose in the carnivorous fish, Sparus aurata.* J Mol Endocrinol, 2004. **33**(3): p. 783-95.

93. Rui, L., *Energy Metabolism in the Liver.* Compr Physiol, 2014. **4**(1): p. 177-97.

94. Bortz, W.M., et al., *Glycerol turnover and oxidation in man.* J Clin Invest, 1972. **51**(6): p. 1537-46.

95. Burgess, S.C., et al., *Impaired tricarboxylic acid cycle activity in mouse livers lacking cytosolic phosphoenolpyruvate carboxykinase.* J Biol Chem, 2004. **279**(47): p. 48941-9.

96. Peroni, O., et al., *Measuring glycerol turnover, gluconeogenesis from glycerol, and total gluconeogenesis with [2-^{13}C] glycerol: role of the infusion-sampling mode.* Metabolism, 1996. **45**(7): p. 897-901.

97. Yoshida, M., et al., *Importance of hepatocyte nuclear factor 4alpha in glycerol-induced glucose-6-phosphatase expression in liver.* Biomed Res, 2016. **37**(2): p. 85-93.

98.   Dankel, S.N., et al., *cAMP-mediated regulation of HNF-4alpha depends on the level of coactivator PGC-1alpha.* Biochim Biophys Acta, 2010. **1803**(9): p. 1013-9.

99.   Al-Goblan, A.S., M.A. Al-Alfi, and M.Z. Khan, *Mechanism linking diabetes mellitus and obesity.* Diabetes, metabolic syndrome and obesity : targets and therapy, 2014. **7**: p. 587-591.

100.   Chevalier, S., et al., *The greater contribution of gluconeogenesis to glucose production in obesity is related to increased whole-body protein catabolism.* Diabetes, 2006. **55**(3): p. 675-81.

101.   Gastaldelli, A., et al., *Influence of obesity and type 2 diabetes on gluconeogenesis and glucose output in humans: a quantitative study.* Diabetes, 2000. **49**(8): p. 1367-73.

102.   Kahn, B.B. and J.S. Flier, *Obesity and insulin resistance.* The Journal of clinical investigation, 2000. **106**(4): p. 473-481.

103.   Hatting, M., et al., *Insulin regulation of gluconeogenesis.* Annals of the New York Academy of Sciences, 2018. **1411**(1): p. 21-35.

104.   O-Sullivan, I., et al., *FoxO1 integrates direct and indirect effects of insulin on hepatic glucose production and glucose utilization.* Nature communications, 2015. **6**: p. 7079-7079.

105.   Gerich, J.E., et al., *Renal Gluconeogenesis.* Diabetes Care, 2001. **24**(2): p. 382.